ISTANBUL TECHNICAL UNIVERSITY ★ GRADUATE SCHOOL

FUSED FILAMENT FABRICATION OF PETG: INVESTIGATION OF THE MECHANICAL PROPERTIES THROUGH THE PARAMETER OPTIMIZATION

M.Sc. THESIS

Buket PARLAK

Department of Aeronautics and Astronautics Engineering

Aeronautics and Astronautics Engineering Programme

JUNE 2022

ISTANBUL TECHNICAL UNIVERSITY ★ GRADUATE SCHOOL

FUSED FILAMENT FABRICATION OF PETG: INVESTIGATION OF THE MECHANICAL PROPERTIES THROUGH THE PARAMETER OPTIMIZATION

M.Sc. THESIS

Buket PARLAK
(511171104)

Department of Aeronautics and Astronautics Engineering

Aeronautics and Astronautics Engineering Programme

Thesis Advisor: Assoc. Prof. Dr. Hülya CEBECİ

JUNE 2022

İSTANBUL TEKNİK ÜNİVERSİTESİ ★ LİSANSÜSTÜ EĞİTİM ENSTİTÜSÜ

PETG'NİN ERGİYİK YIĞMA MODELLEMESİ: MEKANİK ÖZELLİKLERİNİN PARAMETRE OPTİMİZASYONU İLE İNCELENMESİ

YÜKSEK LİSANS TEZİ

Buket PARLAK
(511171104)

Uçak ve Uzay Mühendisliği Anabilim Dalı

Uçak ve Uzay Mühendisliği Programı

Tez Danışmanı: Doç. Dr. Hülya CEBECİ

HAZİRAN 2022

Buket PARLAK, a M.Sc. student of ITU Graduate School student ID 511171104, successfully defended the thesis entitled "FUSED FILAMENT FABRICATION OF PETG: INVESTIGATION OF THE MECHANICAL PROPERTIES THROUGH THE PARAMETER OPTIMIZATION", which she prepared after fulfilling the requirements specified in the associated legislations, before the jury whose signatures are below.

Thesis Advisor:	**Assoc. Prof. Dr. Hülya CEBECİ** Istanbul Technical University	.....
Jury Members:	**Assoc. Prof. Dr. Mesut KIRCA** Istanbul Technical University	.....
	Assist. Prof. Dr. Özgür DEMİR Yildiz Technical University	.....

Date of Submission : 03 June 2022
Date of Defense : 23 June 2022

To everyone who has a passion for aviation,

FOREWORD

This thesis study aimed to increase the strength of the part with a parametric study where additive manufacturing gains importance every year in the world. It is expected that the studies will create a vision of the effect of parameters on the strength of polymer parts to be produced with additive manufacturing, especially in aviation, which has high strength requirements, and it is expected to contribute to the literature in this direction today, where the sample standard to be used has not been generalized yet.

I would like to express my deepest gratitude to my advisor, Assoc.Prof.Dr. Hülya CEBECI for her guidance, encouragement, and support throughout this study. I also would like to thank Mrs. Rabia GÜNAY and Mr. Emre DİLEKTAŞLI at the Department of Materials and Process Development Engineering, TEI Tusas Engine Industries Inc., for giving me the opportunity to complete this project. Thanks to our colleagues Mr. Asım Efe ARSAL, Techn. İlker ADALI, Techn. Ramazan ALTAŞ, Techn. Cengiz KOCALAR, Techn. Ethem ŞENOL, Techn. Mustafa KELEŞ, for giving me an opportunity to use devices for production and testing. Thanks to Ms. Zeliha İdil KARA, Ms. Aslınur ATAKLI, Mr. Anıl UZER and Mrs. Pınar Fatoş EKŞİ for their supports.

Finally, a very special thanks to my dear husband Gökhan PARLAK for giving support with his presence throughout my thesis, my master's degree and my life. I want to express my sincere thanks to my one and only grandmother Fatma TAŞPINAR who taught me all the values to become a strong and successful woman throughout my life and grandfather Mehmet TAŞPINAR who has passed away to eternity, and to all my teachers who have contributed to me throughout my education life.

June 2022

Buket PARLAK
(Metallurgical and Materials Engineer)

TABLE OF CONTENTS

Page

ABBREVIATIONS

3D **:** Three Dimensional

ABS **:** Acrylonitrile Butadiene Styrene

AGM **:** A: Angled Failure Type G: Gage Failure Area T: Top Failure Location

AM **:** Additive Manufacturing

ASTM **:** The American Society for Testing and Materials

BJ **:** Binder Jetting

CAD/CAM **:** Computer Aided Design/Computer Aided Manufacturing

DED **:** Direct Energy Deposition

DED **:** Directed Energy Deposition

E **:** Elastic Modulus

EBM **:** Electron Beam Melting

EBM **:** Electron Beam Melting

FDM **:** Fused Deposition Modeling

FFF **:** Fused Filament Fabrication

GAT **:** G: Grip/tab Failure Type A: At grip/tab Failure Area T: Top Failure Location

GE **:** General Electric

IGV **:** Inlet Guide Vane

IM **:** Injection Molded Samples

ISO **:** International Standards Organization

LGM **:** L: Lateral Failure Type G: Gage Failure Area T: Top Failure Location

ME **:** Material Extrusion

MJ **:** Material Jetting

NASA **:** National Aeronautics and Space Administration

NX **:** Unigraphics

PAI **:** Polyamideimide

PBF **:** Powder Bed Fusion

PBF **:** Powder bed fusion

PC **:** Polycarbonate

PE **:** Polyethylene

PEEK **:** Polyether Ether Ketone

PEI **:** Polyetherimide

PET **:** Polyethylene Tetraphthalate

PETG **:** Polyethylene Tetraphthalate Glycol-Modified

PLA **:** Polylactic Acid

PP **:** Polypropylene

SEM **:** Scanning Electron Microscope

SL **:** Sheet Lamination

SLA **:** Stereolithography

SLM **:** Selective Laser Melting

SLM **:** Selective Laser Melting

SLS **:** Selective Laser Sintering

SLS **:** Selective Laser Sintering

STL **:** Standard Triangle Language

Tg **:** Glass Transition Temperature

UAV **:** Unmanned Aerial Vehicle

UTS **:** Ultimate Tensile Strength

VP **:** Vat Photopolymerization

SYMBOLS

C **:** Celcius

LIST OF TABLES

Page

LIST OF FIGURES

Page

FUSED FILAMENT FABRICATION OF PETG: INVESTIGATION OF THE MECHANICAL PROPERTIES THROUGH THE PARAMETER OPTIMIZATION

SUMMARY

Additive manufacturing methods are in increasing demand every year due to their low cost, production of complex parts, rapid prototyping possibilities, and accessibility, and they can be preferred over other traditional methods (casting, forging).

Additive manufacturing; is used effectively in many fields, especially in aviation. In addition, it is available in the literature that wax patterns (wax-patterns) used in precision casting, with its rapid prototyping feature, are obtained by the Fused Filament Fabrication (FFF) method. However, it is seen that the choice of polymer used here is very important. The polymer having high strength, low thermal expansion coefficient, and no causing shrinkage and warping during production are the desired properties. There are wax models produced with PLA and ABS in the literature. It is seen that parts produced with FFF are used not only in prototyping, but also in unmanned aerial vehicles.

Additive manufacturing methods are classified according to the type of material as metal, ceramic and polymer-based. According to the ISO/ASTM 52900:2015 standard, material types are also divided into their sub-headings. The basic working principle of additive manufacturing is based on the principle that the feeder (it can be a powder or polymer filament) is melted with the help of a melting source and reassembled on a table at the desired dimensions. First of all, the CAD (Computer Aided Design) models of the part are created as .STL (Standard Triangle Language) file format and it is combined with the parameter information to be used in the printer with the help of a slicer and the g-code is created. This generated g-code is uploaded to the printer and the processes are started. Parameter selections play an important role in determining the mechanical properties of the polymer parts. The most important parameters used in the FFF method are as follows; the infill ratio, the layer height, the layer thickness, the width of the raster, the infill pattern, the air gap ratio, the raster orientation, the build direction, the printer speed, the printer temperature and the nozzle diameter.

The choice of polymer type is another important parameter. In this study, PETG polymer was used because of its high resistance to chemicals, fatigue resistance, high toughness, and low shrinkage during production compared to other polymers and its easy production. This study aimed to examine the effects of the negative air gap, selected infill pattern and tensile sample standard, annealing heat treatment temperature and time on tensile properties (Ultimate Tensile Strength (UTS) and Elastic Modulus (E)). For the first parameter set, 60 samples were produced. 20 of these samples were concentric and produced by ASTM D638 Type IV standard. The remaining 20 samples were also concentric ASTM D3039. To examine the infill pattern difference in the last 20 samples, they were produced in rectilinear infill in

accordance with the ASTM D3039 standard. All 5 samples were produced to have a 0%, 10%, 15%, and 20% negative air gap. As a result of the comparison of the infill patterns, it was seen that the concentric filling resulted in 29,65-50,54% higher results in E and 33,06%-47,88% higher results in UTS than the rectilinear infill. Another comparison was made between samples produced by ASTM D638 Type IV with concentric infill and 0%, 10%, 15% and 20% negative air gap, and samples produced according to ASTM D3039.

According to the comparison of the different infill patterns, the concentric infill samples produced according to ASTM D638 Type IV showed the highest properties of 16,33% in E and 20,69% - 48,16% in UTS compared to those produced according to ASTM D3039.

The effect of increased negative air gap was also investigated in both concentric (ASTM D638 Type IV and ASTM D3039) and rectilinear (ASTMD3039) samples. In all comparisons, the samples with a 0% negative air gap were compared with the samples produced with 10%, 15%, and 20% air gaps. As the negative air gap ratio increased, ASTM D638 Type IV concentric samples showed an increase of 11,38% - 31,54% in E and 37,18% - 63,89% in UTS. The effect of the air gap was found to be negative in the concentric filling produced according to the ASTM D3039 standard (as the gap increased, there was a decrease between 2,84% and 10,20% in E, while a decrease between 4,9% and 8,14% in UTS was observed. The effect of the air gap was found to be positive in the rectilinear filling produced according to the ASTM D3039 standard (when the negative air gap increased, there was a decrease between 2,51% and 32,44% in E, and an increase between 6,24% and 17,45% in UTS).

According to all these results, the parameter set that gave the best results was obtained in the sample with ASTM D638 Type IV, concentric infill, and 15% negative air gap (E: 1.87 Gpa and UTS: 41,84 Mpa). Another aim of this study is to examine the post-process effects. To examine the effects of annealing heat treatment, 20 samples of ASTM D638 Type IV, concentric and 15% negative air gap were produced. This study was planned for two annealing temperatures and two selected times.

The selection of the tensile test specimen is still a controversial issue, and the effect of the two standards was examined and discussed in this study.

In this study, the importance of the effect of heat treatment temperature and time on mechanical properties was emphasized. The effects of two temperatures, 80°C, and 55°C, were investigated. At these temperatures, each sample was held in the furnace for 1 hour and 4 hours. Samples that were heat treated at 80°C were first compared with those that were heat treated at 55 °C. The tensile test results of the samples annealed at 55°C for 1 hour are higher 17,94% in E and 13,73% in UTS than the samples kept at 80°C for 1 hour. In the same way, the tensile test results of samples that were heat treated at 55 °C kept for 4 hours, are higher 17,10% in E and 13,67% in UTS than compared to 80°C. In order to see the effect of the time, the temperature was kept constant and the samples were held for 1 hour and 4 hours. According to the results obtained, there was no high increase in E and UTS as the holding time increased. All results were compared with non-heat-treated concentric specimens

produced with 15% air gap and treated according to ASTM D638 Type IV. As a result of this comparison, while a 14,32% decrease was observed in E in the samples kept at 80°C 1 hour, this decrease was recorded as 2,16% in UTS. In the samples kept at 55°C 1 hour, it increased up to 4,42% in E and up to 13,41% in UTS. These results were also compared with the data in the literature, and the results were also compatible with the literature. In the samples processed at 80°C for 4 hours, a decrease of 13,77% was observed in E, while this decrease was recorded as 0,39% in UTS. In samples processed at 55°C for 4 hours, it increased by 4,01% in E and 15,38% in UTS. In the literature, 7% increase in E and 6% increase in UTS were obtained in the heat treatment of line infill samples produced with ASTM D638 Type I, 100% infill, and held at 55°C for 1 hour. The reason for the higher increase in literature compared to the samples produced with 100% infill is the effects of the negative air gap.

The mechanical properties of samples produced with FFF are always lower than those obtained by injection molding, due to molding defects (like voids) and anisotropy. It is known that due to the nature of the FFF method, there are many voids inside the structure in the parts printed with 100% infill ratio. All the results obtained in this thesis were also compared with the mechanical properties obtained by injection molding. As a result of this comparison, it was observed that the highest difference was in the rectilinear produced samples (57,76%-44,06% in E, 68,96%-61,21% in UTS). In concentric samples produced according to ASTM D3039, this difference was between 23,31% and 14,60% in E and 36,91%-42,05% in UTS. Samples produced according to ASTM D638 Type IV it was found to be lower in 10,78-32,18% in E; 14,14% and 47,6% in UTS compared to the samples produced by injection. It was determined that the results of the samples produced by injection were approached with the annealing heat treatment at 55°C at most. The difference was recorded as 6,84% in E; 5,09% in UTS for 1 hour and 7,21% in E; 3,44% in UTS for 4 hours. The novel approach of this study is that reach the injected molded part results with appropriate parameter optimization studies.

After the tensile tests, the fracture surfaces of the samples were also examined, and it was observed that 2 of the 60 samples were fractured in the GAT (G: Failure Type A: Failure Area T: Failure Location) rupture mode. It was observed that 20 samples produced according to ASTM D638 Type IV were broken from the inner narrow length, except for 2 of them.

In addition, PETG is an advantageous polymer; no delamination and shrinkage problems were encountered compared to other polymers. In this study, it has been seen that the effects of infill, tensile specimen standard selection and negative air GAP, heat treatment, time, and selected temperature have significant effects on mechanical properties.

PETG'NİN ERGİYİK YIĞMA MODELLEMESİ: MEKANİK ÖZELLİKLERİNİN PARAMETRE OPTİMİZASYONU İLE İNCELENMESİ

ÖZET

Katmanlı imalat yöntemleri günümüzde düşük maliyet, kompleks parçaların üretilebilmesi, hızlı prototipleme olanakları ve ulaşılabilir olmaları nedeni ile her geçen yıl artan bir talep görmekte ve diğer geleneksel yöntemler (döküm, dövme gibi) yerine tercih edilebilir hale gelmektedir.

Katmanlı imalat; havacılık, otomotiv, sağlık başta olmak üzere birçok alanda etkin bir şekilde kullanılmaktadır. Havacılıkta ise örneğin General Elektrik (GE) üretimi Advanced Turboprop motorunda motorun %35'i katmanlı imalat parçalarından üretilmiştir. Bu durum geleneksel yöntemlerle üretimde 825 parçadan oluşmuş bir parça servisinin 12 parça ile katmanlı imalattan elde edildiği bildirilmiştir. Ayrıca hızlı prototipleme özelliği ile hassas dökümde kullanılan mum modellerin de (wax-pattern) Ergiyik Yığma Modelleme (EYM/ FFF) yöntemi ile elde edildiği literatürde mevcuttur. Ancak burada da kullanılan polimer seçiminin çok önemli olduğu görülmektedir. Kullanılacak polimerin mukavemetinin yüksek olması, düşük termal genleşme katsayısına sahip olması, üretim esnasında çekme ve katlanmaya neden olmamaları istenen özellikleri arasındadır. Literatürde PLA, ABS ile üretilmiş mum modeller mevcuttur. Sadece prototiplemede değil, insansız hava araçlarınında da EYM ile üretilmiş parçaların kullanıldığı görülmektedir.

Katmanlı imalat yöntemleri malzeme türüne göre metal, seramik ve polimer bazlı olmak üzere kategorilere ayrılmaktadır. ISO/ASTM 52900:2015 standardına göre malzeme türleri de kendi alt başlıklarına metot bazlı bölünmektedir. Katmanlı imalatın temel çalışma prensibi ise besleyicinin (bu bir toz ya da polimer filamanı olabilir) bir ergitme kaynağı yardımı ile ergitilip bir tabla üzerinde istenen ölçülerde tekrar birleştirilmesi esasına dayanır. Öncelik olarak .STL(Standard Üçgen Dili) dosya formatında oluşturulan parçanın resmi bir dilimleyici (slicer) yardımı ile yazıcıda kullanılacak parametre bilgisi ile birleştirilir ve g-code oluşturulur. Bu oluşturulan g-code yazıcıya yüklenir ve serim işlemleri başlatılır. Parametre seçimleri parçaların mekanik özelliklerinin belirlenmesi önemli rol oynamaktadır. Polimer katmanlı yöntemlerinden olan EYM yönteminde kullanılan en önemli parametreler ise şu şekildedir; iç dolgu oranı (infill), katman kalınlığı (layer height), katman kalınlığı (layer thickness), katman genişliği (width of raster), dolgu deseni (infill pattern), hava boşluğu oranı (air gap ratio), katman serim yönü (raster orientations), yazıcı hızı, yazıcı serim sıcaklığı ve nozül çapı.

Polimer tipinin seçimi de diğer önemli bir parametredir. Polietilen tereftalat glikolle değişmiş (PETG), polipropilen (PP), polivinil klorür (PVA), akrilonitril bütadien stiren (ABS) ve Polyether ether ketone (PEEK) gibi birçok polimer katmanlı imalatında kullanılabilmektedir.

Bu çalışmada kimyasallara karşı direncinin yüksek olması, yorulma dayanımı göstermesi, üretim sırasında çekmelerin diğer polimerlere oranla düşük olması ve kolay üretilebilirliğinde dolayı PETG polmeri kullanılmıştır. Bu çalışma ile negatif hava boşluğunun, seçilen infill paterni ve çekme numunesi standardının, tavlama ısıl işlem sıcaklık ve süresinin çekme özelliklerine (UTS (en yüksek çekme mukavemeti) ve E (elastik modül)) etkilerinin incelenmesi hedeflenmiştir. İlk parametre seti için 60 adet numune üretilmiştir. Bu numunelerin 20 tanesi concentric ve ASTM D638 Tip IV standardına uygun olacak şekilde üretilmiştir. Kalan 20 adet numune de concentric olup ASTM D3039 a uygun üretilmiştir. Son 20 numune de infill pattern farkının incelenmesi amacı ile rectilinear infillde ASTM D3039 standardına uygun üretilmiştir. Her 5 numune ise %0, %10, %15 ve %20 negatif hava boşluğuna sahip olacak şekilde üretilmiştir. İç dolgu yapılarının mekanik özelliklerinin karşılaştırmasının sonucunda, concentric iç dolgunun rectilinear dolguya göre E'de %29,65- %50,54 ve UTS'de %33,06-%47,88 daha yüksek sonuçlar verdiği görülmüştür. Diğer bir karşılaştırma ise concentric iç dolguya ve %0, %10, %15 ve %20 negatif hava boşluğuna sahip olan ASTM D638 Tip IV'e uygun üretilmiş numuneler ile aynı şekilde ASTM D3039 a göre üretilen numuneler arasında yapılmıştır.

Tüm karşılaştırmalarda %0 negatif hava boşluğuna sahip olan numuneler ile %0 olanlar, örneğin %20 ile de %20 hava boşluğuna sahip numuneler karşılaştırılmıştır. Bu karşılaştırmaya göre ise ASTM D638 Tip IV'e göre üretilen concentric iç dolgulu numuneler ASTM D3039 a göre üretilenler göre E'de %16,33 ve UTS'te %20,69 ile %48,16 arasında daha yüksek özellik göstermişlerdir.

Artan negatif hava boşluğunun etkisi de hem concentric (ASTM D638 Tip IV ve ASTM D3039), hem rectilinear (ASTMD3039) numunelerde incelenmiştir. Tüm karşılaştırmalarda %0 negatif hava boşluğuna sahip olan numuneler ile %10, %15 ve %20 hava boşluğuna sahip üretilmiş numuneler ile karşılaştırılmıştır. Negatif hava boşluğu oranı arttıkça, ASTM D638 Tip IV concentric numunelerde E'de %11,38 ile %31,54; UTS'DE %37,18 ile %63,89 arasında artış sağlanmıştır. Hava boşluğunun etkisi ASTM D3039 standardına göre üretilen concentric iç dolguda negatif yönde bulunmuştur (boşluk arttıkça E'de %2,84 ile %10,20 arasında bir azalma görülürken, UTS'de de %4,09 ile %8,14 arasında azalma görülmüştür). Hava boşluğunun etkisi ASTM D3039 standardına göre üretilen rectilinear iç dolguda pozitif yönde bulunmuştur (boşluk arttıkça E'de %2,51 ile %32,44 arasında bir azalma görülürken, UTS'de de %6,24 ile %17,45 arasında artış görülmüştür).

Tüm bu sonuçlara göre en iyi sonucu veren parametre seti ASTM D638 Tip IV, concentric iç dolgu ve %15 negatif hava boşluğuna sahip numunede elde edilmiştir (E'si 1,87 Gpa ve UTS'i 41,84 Mpa). Bu çalışmanın diğer yenilikçi amacı da post-proses etkilerinin incelenmesidir. Tavlama ısıl işleminin etkilerini incelemek için ASTM D638 Tip IV, concentric ve %15 nagatif hava boşluğuna sahip 20 adet numune üretilmiştir. Bu çalışma iki tavlama sıcaklığı ve iki seçilen sürede planlanmıştır. İlk sıcaklık 55°C seçilmiş olup ikinci sıcaklık ise Tg 'nin (Camsı geçiş sıcaklığı) 5°C üzeri olan 80°C olmuştur. Her iki sıcaklıkta da 1 ve 4'er saat olmak üzere numuneler tutulmuştur.

Literatürde ABS ile çok çalışma olup PETG ile çalışmaların yeni yeni başlamış olması, PETG gibi diğer tüm polimerlerde bu parametre çalışmalarının yapılma ihtiyacı ile bu çalışma başlamıştır. Ayrıca polimerler ile ilgili net kullanılması önerilen bir standartta mevcut değildir.

Literatürde stres birikmesi oluşturduğu gerekçesi ile bazı standartların da karşılaştırıldığı ve kullanımının uygun olmadığının sonucuna varıldığı makaleler de mevcuttur. Hala bu konu tartışmalı bir konu olup, bu çalışma ile iki standardın etkisi incelenmiş ve sonuçları ortaya konulmuştur. Ayrıca literatür taramasının sonucunda ASTM D3039 ile üretilmiş PETG ye ait veri bulunamamıştır. Bu çalışmalar ile polimer katmanlı yönteminde seçilecek ve ileride kullanım kazanacak standardın da seçilmesinde bu çalışmaların önemli katkılarının olacağı görüşü de benimsenmiştir. Isıl işlemler ile birçok katmanlı üretilmiş polimerlerin iç yapıdaki kalıntı gerilimleri gidermek amaçlı uygulandığı, bazı örneklerde de mekanik özelliklere olumlu yönde etkilerinin olduğu kanıtlanmıştır. Bu çalışma ile de ısıl işlem sıcaklık ve sürenin mekanik özelliklere etkisinin önemi vurgulanmıştır.

Kırılma yüzeyleri çoğu çalışmalarda belirtilmemekte olup numune sonuçlarının geçerliliğinin de sorgulanmasının önemli olduğu da bu çalışmada vurgulanmak istenen değerler arasındadır. Bu çalışmada Tg nin altında sadece 55°C tavlama seçilmiş olup farklı sıcaklık değerleri de seçilerek buradaki etkiler de gözlemlenebilir.

Bu çalışmada ısıl işlemin mekanik özeliklere etkisi de incelenmiştir. Bu çalışmada 80°C ve 55°C olmak üzere iki sıcaklığın etkileri incelenmiştir. Bu sıcaklıklarda her numune 1 saat ve 4 saat olmak üzere etüv fırınında tutulmuştur. 80°C ısıl işlem görmüş numuneler önce 55°C de ısıl işlem görmüş numuneler ile karşılaştırılmıştır. 55 °C de 1saat tutulan numuneler 80°C de 1saat tutulan numunelere göre E de %17,94 kadar ve UTS de %13,73 kadar artış sağlamıştır. Aynı şekilde 4 saat tutulan 55 °C de ısıl işlem yapılan numuneler 80°C e göre E de %17,10 a kadar ve UTS de %13,67 kadar artış sağlamıştır. Sıcaklıklar sabit tutulup süre değişiminin etkisi incelendiğinde de 80°C de 4 saat tutma süresinin 1 saat tutmaya oranla E de %0,62, UTS'de 1,77 artışa neden olduğu görülmüştür. Aynı şekilde 50 °C de 4 saat tutmak 1 saate oranla E de %0,40 düşüşe neden olurken, UTS'de 1,71 artışa neden olmuştur.

Sürenin etkisini görmek için bu kez sıcaklık sabit tutulup numuneler 1 saat ve 4 saat tutulmuştur. Elde edilen sonuçlara göre süre arttıkça E ve UTS de yüksek bir artış görülmemiştir. Bu sonuca göre 1saat fırında tutmanın da aynı etkiyi verdiği görüşmüştür. Tüm sonuçlar ısıl işlem görmemiş concentric %15 hava boşluğu ile üretilmiş ASTM D638 Tip IV'e göre uygulanmış numuneler ile karşılaştırılmıştır. Bu karşılaştırmanın sonucunda 80°C de 1 saat tutulan numunelerde E de %14,32 düşüş görülürken, UTS de bu düşüş %2,16 olarak kaydedilmiştir. 55°C de 1 saat tutulan numunelerde ise E de %4,42 a kadar ve UTS de %13,41 kadar artış sağlamıştır. Bu sonuçlar literatürdeki veriler ile de karşılaştırılmıştır ve sonuçlar lit ile de uyumlu görüşmüştür. Literatürde ASTM D638 Tip I, %100 infill ile üretilmiş line numunelerin 55°C de 1 saat tutulan numunelerde ısıl işlemlerinde E de %7, UTS'de ise %6 artış elde edilmiştir. 80°C de 4 saat tutulan numunelerde E de %13,77 düşüş görülürken, UTS de bu düşüş %0,39 olarak kaydedilmiştir. 55°C de 4 saat tutulan numunelerde ise E de %4,01 kadar ve UTS de %15,38 kadar artış sağlamıştır. Bu sonuçlar literatürdeki veriler ile de karşılaştırılmıştır ve sonuçlar lit ile de uyumlu görüşmüştür. Literatürde ASTM D638 Tip I, %100 infill ile üretilmiş line numunelerin 55°C de 1 saat tutulan numunelerde ısıl işlemlerinde E de %7, UTS'de ise %6 artış elde edilmiştir. Lit de %100 iç dolgusu ile üretilen numunelere göre daha yüksek artış olmasının sebebi negatif hava boşluğudur.

EYM ile üretilmiş numunelerin mekanik özellikleri enjeksiyon kalıplama yöntemi ile elde edilenlere göre iç hatalar, anizotropi nedeni ile her zaman düşük gelmektedir. %100 doluluk oranı ile basılan parçalarda da EYM yönteminin doğası gereği boşluklu

yapının olduğu bilinmektedir. Bu tez kapsamında elde edilen tüm sonuçlar ayrıca enjeksiyon kalıplama ile elde edilen mekanik özelliklerle karşılaştırılmıştır. Bu karşılaştırmanın sonucunda ise en yüksek farkın rectilinear üretilmiş numunelerde olduğu görülmüştür (E'de %57,76-%44,06 arasında UTS'de %68,96-%61,21). ASTM D3039'a göre üretilmiş concentric numunelerde de bu farkın E'de %23,31-%14,60 arasında; UTS'de %36,91-%42,05 arasında olduğu görülmüştür. ASTM D638 Tip IV'e göre üretilmiş numuneler E'de %10,78-%32,18; UTS'de %14,14-%47,6 arasında enjeksiyon ile üretilmiş numunelere göre daha düşük bulunmuştur. En çok 55°C da yapılan tavlama ısıl işlemi ile enjeksiyon ile üretilmiş numune sonuçlarına yaklaşıldığı tespit edilmiştir, 1 saat tutulan sonuçlardaki fark E'de %6,84; UTS'de %5,09 iken 4 saat tutulan sonuçlarda E'de %7,21; UTS'de %3,44'tür. Bu çalışmanın özgün yanı ile de uygun parametre optimizasyon çalışmaları ile enjeksiyon kalıplama sonucun elde edilen numunelerin sonuçlarına yakın sonuçlar elde edileceği gösterilmiştir.

Ayrıca numunelerin iç yapılarını temsilen toplam 8 adet concentric ve rectilinear iç dolgu yapısına sahip dikdörtgen numuneler üretilmiştir. 4 adet sırası ile %0,10,15 ve 20 negatif hava boşluğuna sahip olacak şekilde üretilmiştir. Taramalı elektron mikroskobu (TEM) ile iç yapıları incelenen numunelerde açıkça negatif hava boşluğu artışı ile rasterlar arası mesafenin azaldığı tespit edilmiştir.

Çekme testleri sonrası numunelerin kırılma yüzeyleri de incelenmiş olup, 60 adet ASTM D3039 a göre üretilmiş numunelerden 2 si harici GAT (G: Kırılma tipi, A: Kırılma alanı, T: Kırılma bölgesi) kırılma modunda oldukları görülmüştür. 20 adet ASTM D638 Tip IV e göre üretilen numunelerde ise 2 si hariç iç dar uzunluğundan kırıldığı gözlemlenmiştir. Ayrıca ilk test denemelerinde ASTM D3039 a uygun üretilen numuneler gague bölgelerinden kırılmış olup tab kullanımına karar verilmiştir. Kalan ASTM D3039 a göre üretilen numuneler için tablar kullanılmış olup Pattex marka epoxy ile yapıştırılmıştır. Bu defa numuneler gauge tab arayüzeyden kopmuşlardır. Bu durumda testler geçerli duruma gelmiştir. Kırılma yüzeylerinde ise hiçbir numunede delaminasyon ayrılma, boşluk, yapışmamış PETG fiberler ile karşılaşılmamıştır. Isıl işlem görmüş tüm numunelerin görüntüleri literatür ile karşılaştırılmış olup benzer yapı görüntüsü elde edilmiştir.

İncelemelerin diğer bir sonucu ise kabuk yapısının parçayı koruduğu olmuştur. Kabuk yapısı direnç göstererek ayrılmaların iç yapıdan başlamasına neden olmuştur. Bu durum ile kabuktan başlayıp iç yapıya ilerleyen çatlakların da engellenerek etken kopmanın önüne de geçildiği görülmüştür.

Ayrıca PETG avantajlı bir polimer olup diğer polimerlere göre delaminasyon ve çekme problemleri ile karşılaşılmamıştır.

Bu çalışma ile iç dolgu, standart seçimi ve negatif hava boşluğunun etkileri ile ısıl işlem süre ve seçilen sıcaklığın mekanik özellikler üzerinde önemli etkilerinin olduğu görülmüştür.

1. INTRODUCTION

3D (three dimensional) printing technology which is also known as additive layer manufacturing, was first started for rapid prototyping and molding purposes [1]. It was firstly introduced at the University of Texas in 1986 [2]. It is revealed that the products produced by 3D printing methods have good accuracy, faster manufacturing, a wide range of materials, the easiest availability, and a cost of equipment compared to other additive methods [3]. As 3D printing has significant advantages, it is in increasing demand in the automotive, aerospace, biomedical, and food industries [4]

In the aerospace industry, the benefits of using additive manufacturing technology are always given in many areas. For example, while the production of a combustion chamber with traditional methods (welding, cutting, drilling, etc.) takes six months, it can be produced in a single piece in a shorter time with the additive production method [5]. Another example belongs to the advanced turboprop engine of General Electric (GE) company 35% of the engine parts consist of additive parts[5].

The WOHLER association is a recognized organization in the field combining new technology, market analysis, and examinations of 3D printing and AM (Additive Manufacturing), see Figure 1.1.

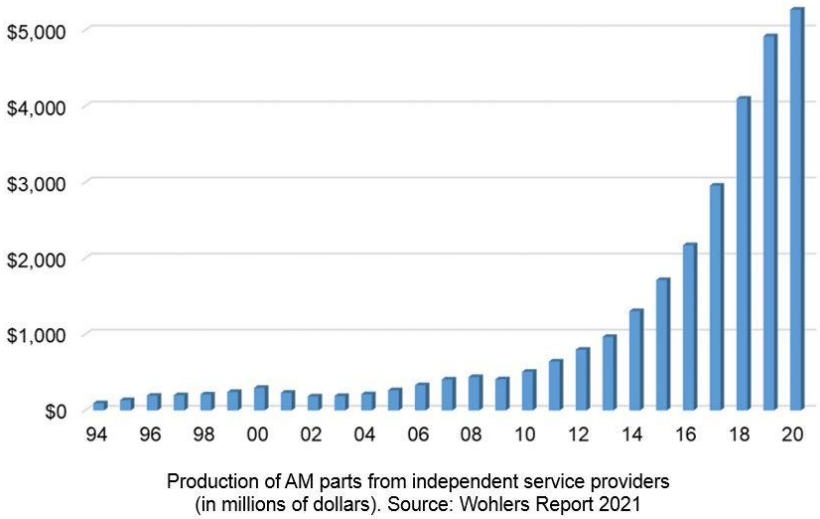

Figure 1.1 : Additive production amounts by years [6].

The latest worldwide annual report (Wohler's Report 2021) was published in 2021 thanks to supporting of 113 manufacturers and 88 contributors from 34 countries who are pioneers in this field. It is comprised that market analysis, technologies of 3D printing, and AM [6], see Figure 1.1. It is even though Covid-19 affects the 3d printing industry, it has grown by 7,5% and attained 12.8 billion in 2020. The annual growth of the last decade was 27% in the additive industry, see Figure 1.2 [7].

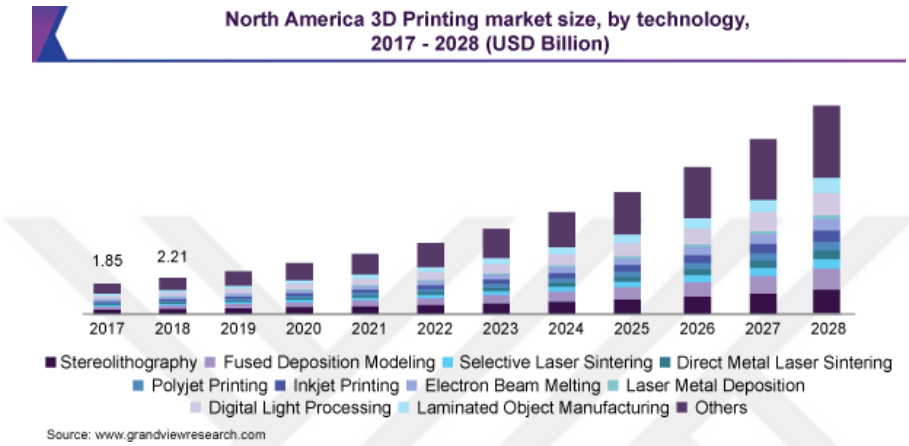

Figure 1.2 : The estimated market sizes for the years 2017-2028 [7].

Additive manufacturing is used based on the production of layers via melting powders, wires, or filaments using laser, electron beam, and heating energy. It is divided into three groups, according to material types, metals, polymer, and ceramic-based and each has three, seven, and one method in ISO/ASTM 52900:2015 respectively [8]. Additive manufacturing methods are detailly defined in ISO/ASTM 52910.

FFF (fused filament fabrication) is one of the material injection methods of polymer additive manufacturing methods. Its working principle is that a filament was melted with the aid of a heated nozzle, and printed onto a heated (if required) bed as the desired shape [9]. FFF method is an alternative, and cost-friendly method compared to injection molding which required tooling, machine operation costs, and a high volume of production. There was one drawback of the FFF method is that it is difficult to get the same mechanical properties with injected molded parts even if it is produced 100% infill. To get competitive mechanical properties with FFF-produced parts, the optimization of the various process parameters is required. Many research was conducted to investigation of the effects of the following process parameters; print orientation, layer height, infill density, layer thickness, air gap, print temperature, raster width, print speed, and infill pattern. The selection of the polymers and tensile

test specimens is another controversial topic for polymer additive manufacturing. In literature, the process parameters effects on mechanical properties were investigated [2]. Many research was focused on the development of the ABS and PLA polymers. According to recent research, PETG polymer has started to stand out among engineering polymers due to its superior properties compared to ABS and PLA [10]. The optimization studies were mostly completed with ABS and PLA and the effects of many process parameters were discussed. The PETG has high accuracy, easy for printing, has high mechanical properties, low thermal expansion coefficient, and no wrapping and shrinkage during printing. Having these properties has led PETG to be preferred both in wax-pattern production and in other applications [11].

The main issue of the FFF method is related to the standardization of the tensile test specimens. According to a review of research studies to date, it is noticed that the mechanical tests result from samples fabricated per ISO 527-2 and ASTM D638 were reported for PETG. In literature, there is only limited study subjected to the comparison of the tensile test specimen and none of them was not selected PETG as filament material. Many research is subjected to standard effects on the properties of ABS and PLA polymers and it is still a controversial topic due to stress concentration on samples and observing early cracks. There is still no consensus on which standard will be used to determine the polymer mechanical properties. For these issues, it is important to study the effects of different standards for each polymer.

Parameter optimization studies are also needed for PETG to have the same or close mechanical properties as injection molded parts. It was clearly shown that negative air gap and post-processing also improved mechanical properties based on the studies with ABS and PLA [4]. However, none of them is subject to effects on PETG of these parameters and no research was exist combination effects of these parameters on the sample which are produced as per ASTM D3039 and ASTM D638 Type IV.

This study aims to improve the mechanical properties of PETG with not only the combination of the negative air gap and annealing but also to reveal the effects separately. These studies were planned with the samples produced per ASTM D3039 and ASTM 638 Type IV to examine the effects of different standards on mechanical properties.

Additionally, a novel approach applied in this study is to examine the air gap and annealing effects using PETG and comparisons of the results obtained from ASTM D3039 and ASTM D638 Type IV samples. Along with this study, it also obtained the mechanical properties close to PETG parts produced by injection molding were obtained through the parameter optimizations.

1.1 Overview of the Intended Use of FFF Method in Aerospace for Prototyping, Wax-Pattern Tooling, Parts of Unmanned Aerial Vehicles

The investment casting method used in aviation, especially in the production of blades in gas turbine engines, is the process of pouring molten metal into a ceramic mold, see Figure 1.3 [12]. Before starting the casting, mold making, mold trial productions, and wax pattern formation processes are carried out, which take a long time and greatly affect the casting cost [12].

Mold cost varies from £1000 to £50,000 according to complex geometries, and mold production takes between 15 and 25 weeks. These processes are increased investment casting lead times. When patterns are produced with additive manufacturing [13], it has been observed that an improvement in 80% lead time and 60% cost is achieved [14].

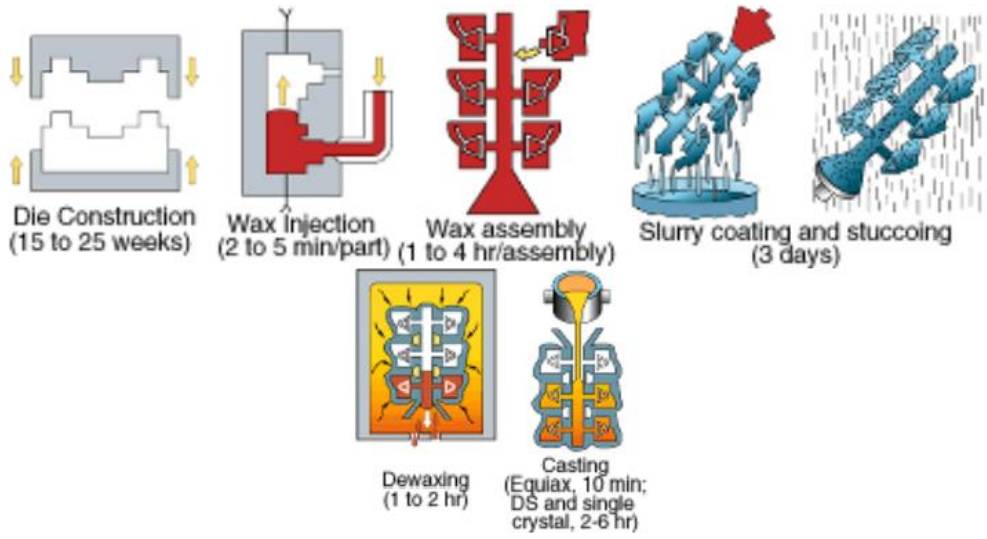

Figure 1.3 : Production steps of investment casting [12].

Thin-walled, thin thickness molds cannot be obtained with hard tooling because of using traditional methods such as drilling, and machining [15]. In addition to having no geometrical constraints, it quickly adapts to the changing geometries at the

preliminary design stage, and new wax pattern production can be made again quickly with additive manufacturing [11].

In the traditional method, while new design changes require a new mold design, the process returns to the beginning and the parts do not reach the motor lead times. In addition, another advantage of using the additive manufacturing method is that it has no geometrical restrictions, and since it is cheaper than other methods, it allows new production quickly with a new design change [16].

In investment casting, many additive methods for wax production have come to the fore, and these can be listed as follows; Selective laser sintering (SLS), Fused filament fabrication (FFF), and Stereolithography (SL). In some studies, it was seen that Quickcast and Voxelijet patterns were printed with SLA, ABS, and polyvinyl butyral (PVB) wax patterns were printed with FFF [16].

The main problems in SL fabricated wax patterns (epoxy) are their breakage during transportation and their poor strength. The main disadvantage here is that the ceramic is broken, and the reason is that the wax expands more than the ceramic before melting during the burn-out and cracks the ceramic [17]. In addition, it was stated that the surface quality of the parts produced with PC (polycarbonate) during burn-out was poor due to foaming. With new materials, for example, CastForm Polystrene powder is used to remove porosity by post-processing [16].

Due to these disadvantages in powder-based methods in additive manufacturing, the material jetting (MJ) method has become more preferred. When the FFF method is compared with other methods, it is seen that it has better accuracy than SLS and the same level of the surface is obtained with SLA and MJ methods.

As given in Figure 1.4, when the materials produced with these properties are compared, it is seen that the part produced with FFF can be produced at lower thicknesses, it has better surface roughness, as well as a more precise production in terms of dimensions, and the amount of residual ash after burn-out is less [11]. Thanks to these advantages, the use of FFF in wax-pattern production is becoming widespread.

RP technique	Process	Build materials	Layer thickness (mm)	Surface roughness (μm) Ra (as processed)	Part accuracy (mm)	Residual ash (%)
SL	Photocuring	Epoxy	0.1	12.5	±0.05	N.A.
SLS	Sintering of powders	Polystyrene Polycarbonate	0.075	13	±0.25	< 0.02 N.A.
FDM	Melt extrusion	ABS Wax	0.05	12.5	±0.127	0.05 ≈ 0
LOM	Paper lamination	Paper	0.05	25	±0.25	N.A.
SGC	Photocuring	Epoxy	0.06	25	0.1%	N.A.
3DP	Ink-jet printing	Starch	0.1	N.A.	±0.020	1-2%
MM II	Ink-jet printing	Wax	0.013	N.A.	0.03%	≈ 0
Thermojet	Ink-Jet printing	Organic polymer	0.04	5.090	N.A.	N.A.

Figure 1.4 : Rapid prototyping techniques and their properties [11].

The features expected from wax patterns produced by rapid-prototyping are high accuracy, good surface quality, low melting point, high strength, and toughness, no shrinkage, no infiltration, high infill as possible, and no warping [17].

In FFF production, surface roughness, warping, shrinkage, and infiltration of slurry are given as important design rules to be considered during design. In the production with FFF, the choice of polymer becomes important because of changing print behaviours of the polymers. There are trials produced with FFF ABS [18], PLA, and PVB in the literature. These materials were preferred because of their good strength, easy accessibility, low Tg, and easy removal from the shell. In addition, assuming that 3D parameter studies started with ABS and PLA in the literature, the use of these materials in wax pattern production is not surprising. However, these studies are very open to innovations. It is foreseen that experiments will be carried out with PETG, which has the potential to be used in thin-walled productions with higher strength and with better warpage properties than ABS and PLA [19].

For the production of TiAl blade [20], Inconel 718 blade with investment casting, ABS produced with FFF was used as a wax pattern and it was reported that it was poured successfully. However, it was added as a note that the surface should be improved. If surface quality will not be improved, the slurry starts to come into contact with the cavities on the surface of the wax and it causes a hollow, poor surface quality part after casting, see Figure 1.5.

Figure 1.5 : Surface after infiltration of the slurry [17].

Not only in the field of rapid prototyping, but it is also available in the literature where NASA's (National Aeronautics and Space Administration National Aeronautics and Space Administration) studies are carried out specifically for the gas turbine engine IGV (inlet guide vane) part produced with FFF, and deflection and strain measurement tests of the IGV part produced with ABS are performed. Again, it is clear that polymers with higher strength are needed in these studies.

In addition, Lockheed Martin's satellite design needs many configuration trials, so it performed tests on the fuel tank produced by Stratasys using FDM and PC in fuel tank simulations. In addition, unmanned space vehicles must first be tested in wind tunnels to determine their aerodynamic performance. In this case, both time and cost savings are obtained with models made of FDM.

It was reported that UAV (unmanned vehicle) produced with ABS was tested at The University of Sheffield, and some parts were produced from PLA in a study conducted at Istanbul Technical University [21], see Figure 1.6. In another project (collaboration of the Aurora Flight Sciences and Stratasys) [22], it was reported that the engine of a UAV was produced from PEI (polyetherimide), Figure 1.7 and ABS produced with FDM and passed flight tests.

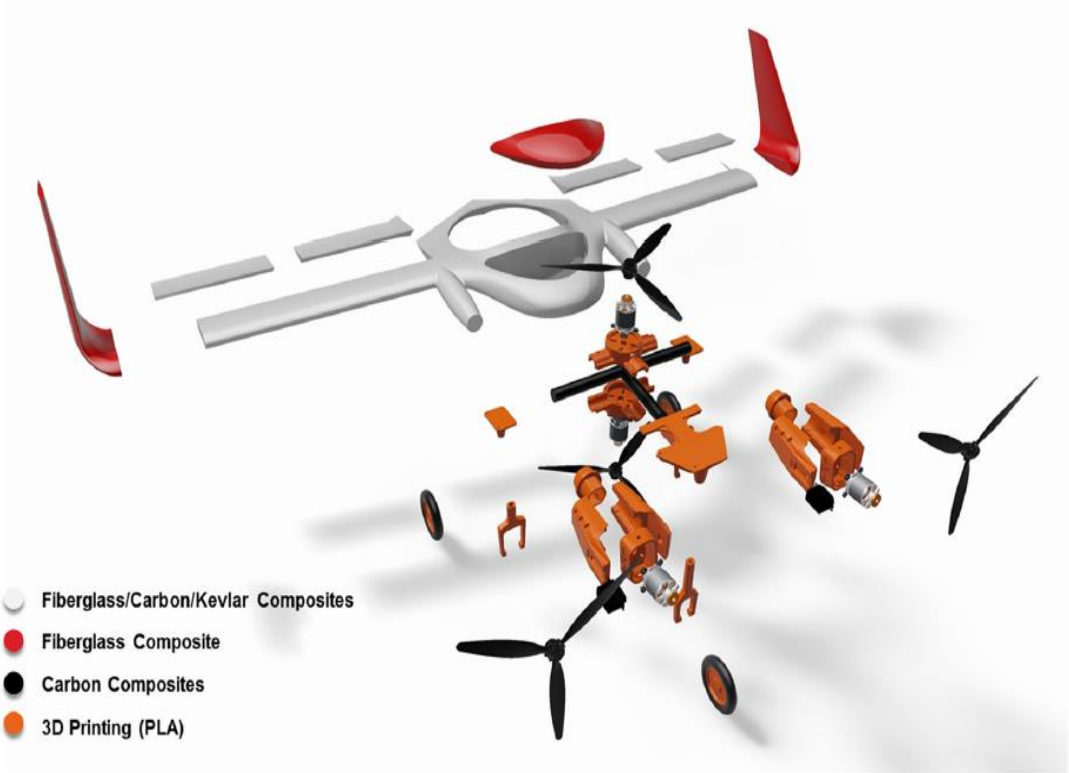

Figure 1.6 : The parts of unmanned aerial vehicles [21].

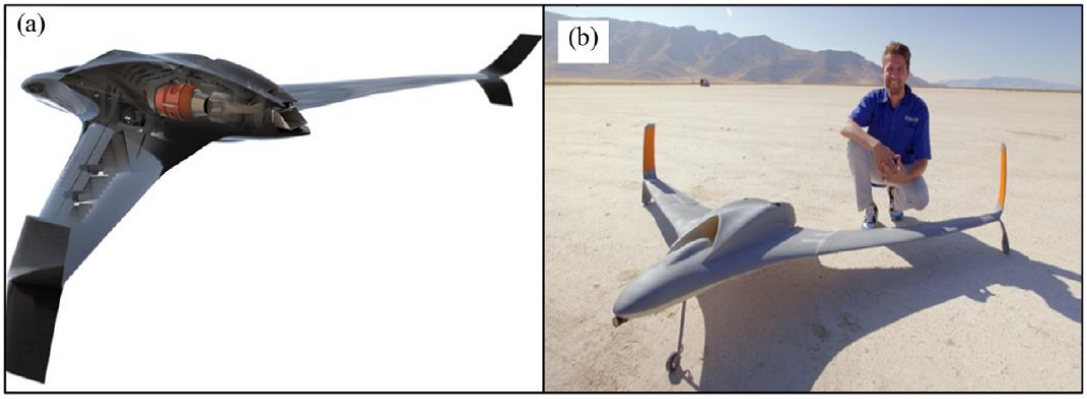

Figure 1.7 : UAV a) model of the jet engine produced with FDM b) flight test [22].

1.2 Motivation and Aim

In addition to obtaining wax patterns for rapid prototyping, and investment casting, the FFF method is also used in parts in the cold regions of gas turbine engines (e.g. Inlet Guide Vane (IGV)) [23], and in unmanned vehicles [21].

Many studies have been carried out based on ABS and PLA polymers. When the properties of the polymers used in the FFF method are compared, it is known that PLA has a fragile structure, low elongation, and low impact toughness, as well as being easily printable [24]. ABS is an amorphous polymer and has higher strength than PLA. At the same time, low ductility, and low thermal expansion coefficient provide the advantage of use in the FFF method. However, it causes disadvantages such as worse surface roughness than PLA, causing shrinkage, and warping due to its nature, causing cracks in the shell in wax-pattern production, and not being suitable for the part in terms of dimensions because it does not give suitable surface roughness.

Compared with other general-purpose polymers, PETG polymer has gained an important place in parameter studies in recent studies, which stands out due to its strength, not causing any warping or shrinkage during printing, and having low thermal expansions compared to ABS and PLA. However, in any study conducted with PETG, negative air gap, and post-processing effects were not studied on samples produced according to ASTM D638 Type IV and ASTM D3039. Postprocessing is an area open to development not only for PETG polymers, but also for other polymers. Since the Specimen standard is still a controversial issue and a common consensus cannot be reached, the existence of comparative studies in the literature should be needed.

This study, it is aimed to increase the strength of PETG produced by the FFF method, by a parameter optimization study, and to bring its tensile properties closer to the strength obtained by injection molding. Today, when the tensile test cannot be standardized, it is aimed to contribute to the literature by comparing the test results of the samples produced according to ASTM D638 Type IV and ASTM D3039.

1.3 Novelty and Insight

FFF parameter optimization of PETG, which is an engineering polymer class that does not cause any shrinkage problems during production, has high mechanical properties, has low thermal expansion, and is a good alternative with the surface quality compared to general purpose polymers (ABS and PLA) produced with FFF (for the first time). It is the new approach of this study by examining the negative air gap and post-processing effects together and, again for the first time, by comparing ASTM D638 Type IV and ASTM D3039 specifically for PETG, improving the mechanical properties and approximating them to PETG material data produced by injection molding. The following contributions were made with this study;

- A novel approach is an examination of the effects of both negative air gap and post processing on mechanical properties by using different tensile specimen standard types (ASTM D638 Type IV and ASTM D3039) and reaching the mechanical properties of parts produced via injection molding.
- In addition, test results obtained with ASTM D638 Type IV and ASTM D3039 tensile test specimens, which have not been made for PETG before, were also compared. With this study, it is also aimed to create an important input in the standardization of the tensile test specimen, as there is still no consensus on the tensile test specimen.

The road map of the thesis is given in Figure 1.8.

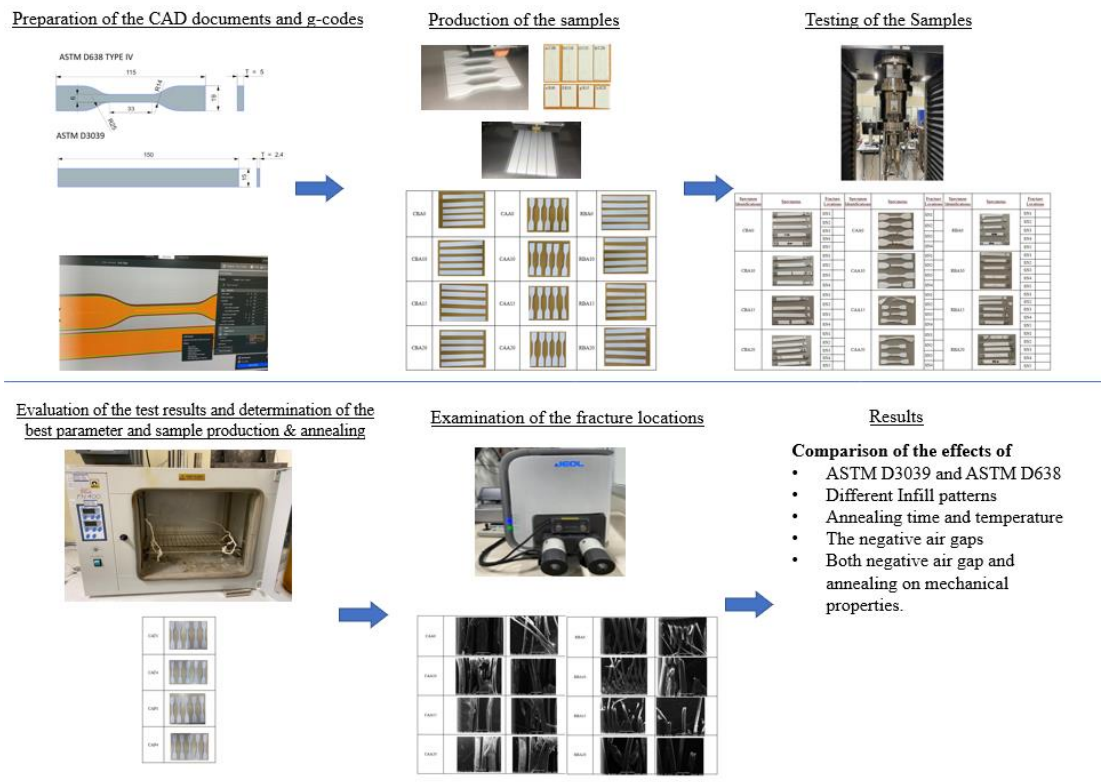

Figure 1.8 : Road maps of the thesis.

2. LITERATURE REVIEW

2.1 An Overview of Additive Manufacturing Methods for Both Metallic and Polymeric Materials

Additive Manufacturing Methods as for metallic materials (Directed Energy Deposition (DED), Powder bed fusion (PBF), Selective Laser Sintering (SLS), Selective Laser Melting (SLM), Electron Beam Melting (EBM), Sheet Lamination (SL)), and polymeric materials (Material extrusion (ME), Material jetting (MJ), Powder Bed Fusion (PBF), Binder Jetting (BJ), Vat Photopolymerization (VP), Sheet Lamination (SL) will be examined in this section.

Additive manufacturing methods for metallic materials are discussed in the following section.

DED is one the 7 categories of Additive Manufacturing Processes. During the DED process, electron beam, plasma arc and laser is used as an energy source, see Figure 2.1 and Figure 2.2. There are two options used as feedstock material wire and powder spraying. The first method is beginning with feeding the wire into the nozzle and melting the wire as the welding process. Another one is depending on feeding powder through the nozzle and melting them at the same time into part surface by laser or electron beam [25]. Although, this method is applicable for all material types, metal powders are mostly used with this technology [26].

Advantages of the DED method are faster production rate than PBF, enable to produce the large parts, use for repair technology, not need feed box required for PBF method, not distinguish material types and not need for supporting structure [25]. The drawbacks of the method are that it has high residual stresses, poor surface quality, need for post processing procedures such as stress relief heat treatment, machining, and vastly expensive due to the consuming high energy [26].

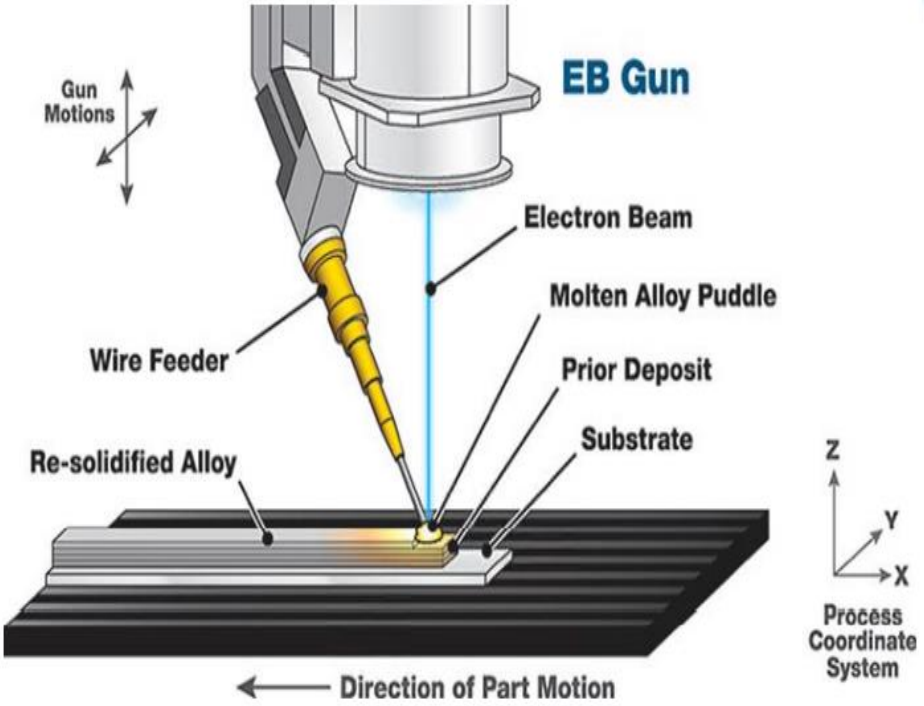

Figure 2.1 : Illustration of the DED method [11].

Figure 2.2 : Production of a large part by DED method [26].

Powder bed fusion is an additive manufacturing process aiming to melt thin powder layers one by one in an inert atmosphere. Layer is built onto a movable bed which is moving int the opposite direction with the powder feeding system, see Figure 2.3 [3], [27]. To spread a new layer the powder box has to move up and the fused layer moves down to build a new layer. PBF is divided into three groups as SLS (Selective Laser Sintering), SLM (Selective Laser Melting) and EBM (Electron Beam Melting). These

groups are separated using the types of energy source and melting. Produced parts via EBM and SLM fully melt and SLS is called a partial melting process.

SLS is one of the powder-based processes and the laser is used as a power source. Support structures are required during manufacturing, however SLS does not need to use them against SLM and EBM [27]. Layers fuse via laser in SLM systems and the laser is controlled by a mirror and focusing on the melted layer, see Figure 2.3-a, and Figure 2.3. The working principle of the EBM machine is similar to that of the SLM but it only uses electron beam in vacuum atmosphere. Using an electron beam is able to focus directly on particle melt without the need for an extra mirror system, see Figure 2.3-b [3], [27].

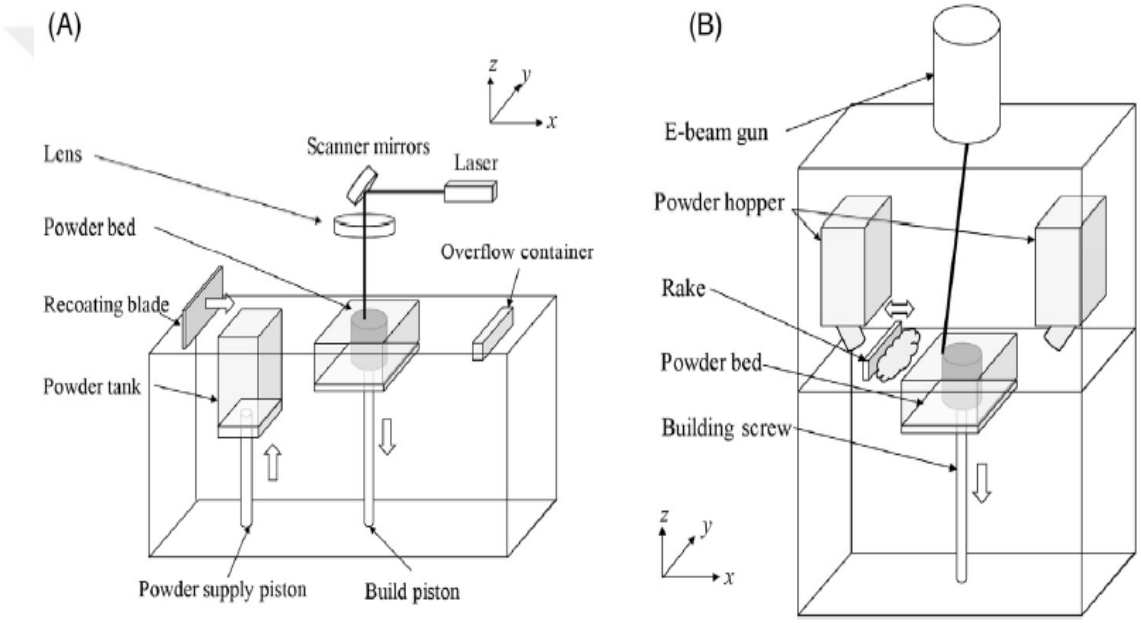

Figure 2.3 : Equipment of PBF a) for SLM(a), b) for EBM [3].

The sheet lamination method is based on joining of the sheet metals. The sheets are cut to requested shape and laminated together or laminate first then cut with final machining [27], [28]. The bonding between layers is gained with the application of ultrasonic waves, pressure or adhesions. Laser and ultrasonic waves are major used heat sources. The bonding between layers is produced by the aid of diffusional bonding against the melting which is produced by DED and PBF.

Sheet lamination is also frequently called LOM (laminated object manufacturing). The limitation of this process is wasting a high amount of material at the end of the process and not used for the production of complex parts [29], see Figure 2.4.

Techniques	Advantages	Disadvantages	Fiber alignment
Laminated object manufacturing	• Low cost. • Parts with high strength can be produced. • No requirement for post-processing. • No requirement of support structures.	• Higher wastage of material • It is relatively difficult to build parts with complex cavities.	• Random fiber orientation • Uniform direction of the fiber
Powder bed fusion	• Support structures can be removed easily. • Composites with higher reinforcement of loading can be achieved. • Fine resolution • Powders that remains unused can be used again	• Rough surface finish. • Slow printing • Not possible to fabricate composites with long fibers. • Expensive • High porosity in the final parts.	• Random fiber orientation
Vat photopolymerization	• Fibers can be aligned randomly. • Finer resolution	• Formation of bubbles takes place. • Limited materials can only be used. • Sedimentation of fiber in resin • Increased resin viscosity with the addition of fibers. • The issue with the penetration of UV rays.	• Random fiber orientation • Along the direction of electric-field. • Along the direction of magnetic-field. • Along the direction of laying. • In accordance with the fiber pattern of the mat.
Material extrusion	• Easy to fabricate. • Economical • Multi-material capability. • Print-heads can be easily modified.	• Degradation of the nozzle. • Obvious layer-by-layer effect. • At higher reinforcement loading, nozzle gets clogged.	• Along the direction of printing.

Figure 2.4 : Advantages and drawbacks of the AM [29].

The additive manufacturing methods for polymeric materials is discussed in the following section.

The additive manufacturing process is started with the creation of a model or part which is modelled in the Computer Aided Design/Computer Aided Manufacturing (CAD/CAM) system and the model is saved as an “STL” (Stereolithography) file format. .STL file is uploaded to a slicer as Ultimaker Cura, Ideamaker, Z-Suites and then g-code is created based on desired print parameters. This code is now ready for the uploading printer to start part productions, see Figure 2.5 for an illustration of the steps [28].

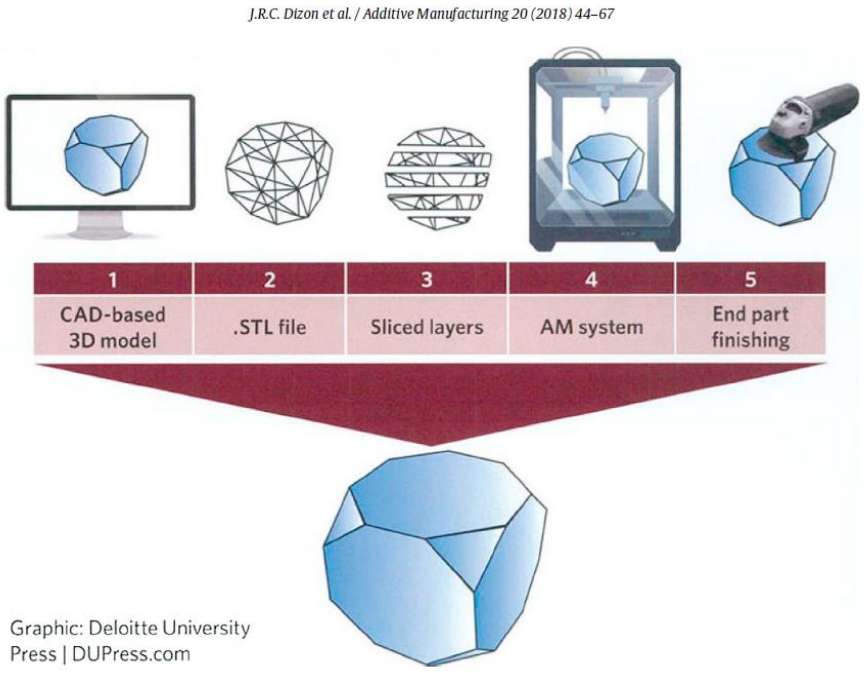

Figure 2.5 : Illustration of the additive manufacturing from code generation to part production [28].

Additive Manufacturing Methods for polymeric materials are divided into 6 groups, the details are given below. The advantages and disadvantages of each polymer additive method are given in this section.

Material extrusion (ME) technology is an additive manufacturing method in which material is selectively dispersed near a nozzle or orifice, see Figure 2.6. In the material extrusion system, raw material is melted in the extrusion head and selectively poured onto the print bed with the nozzle, or this movement can be achieved by moving the print area table in the XY plane. After a layer is complete, the build platform moves down or the extrusion head moves and prints the new layer over the previous layer [30].

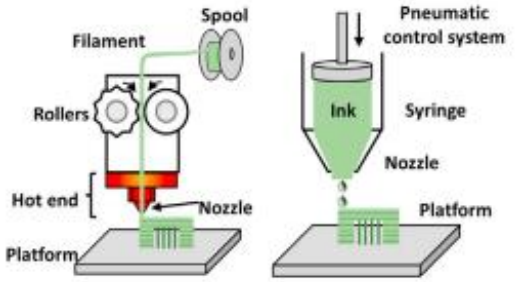

Figure 2.6 : Material extrusion method [30].

Material jetting (MJ) technology works by stacking the building material in drops, using a head like an inkjet print head, see Figure 2.7. The droplets move selectively over the build area with one or more print heads. Typically, a photopolymer material is used as raw material or a wax-based material is produced to be used in precision casting. The rheological properties, especially viscosity (<5 Pa·s), amount of particle and molecular weight the of polymer is the main limitation behind using of this process for limited types of material [30]

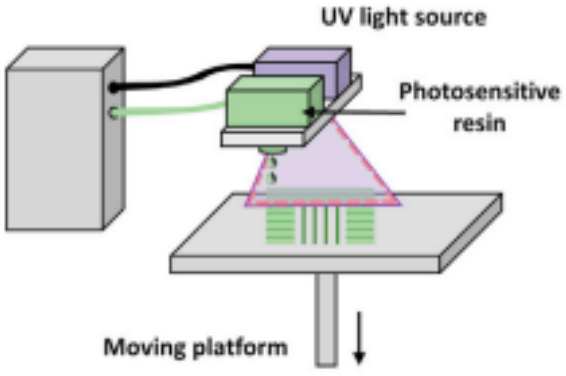

Figure 2.7 : Material jetting method [30].

The Powder Bed Fusion (PBF) process works by focusing laser or electron beam sources over selected areas on the powder bed, see Figure 2.8. The thermal energy melts the powdered material and then the formed part cools down. SLS type of additive manufacturing method is mainly used for polymer production [27]. The significant disadvantage of this process producing porosities inside part due to using powder stock [27].

Both polymer and metal materials are used as raw materials in this technology. During the production of the polymer material, there is no need to assign extra support because the powder granules surrounding the part are supported while it is being formed. For this reason, the unsintered powder raw material can only be used in a few cycles. Therefore, the user must constantly refresh the unsintered powder raw material in the tank by replacing it with a new one [29].

In the production of metal parts, there is a need for binders that can keep the part connected to the production table and act as a support during the production of the part. This is because metal powders need high temperatures to melt [29].

Due to the high degree of thermal change in the production volume, the part may cause thermal stress and it causes distortions. In addition to porosity problems, distortion and thermal stresses caused by heat are potential problems that may occur for all materials [27].

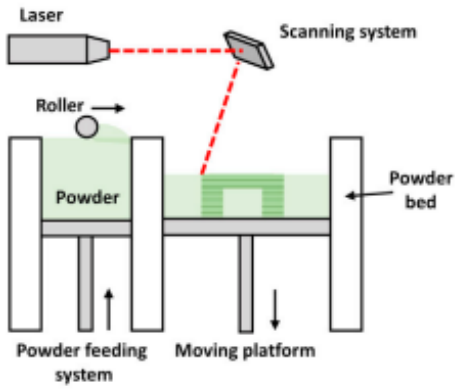

Figure 2.8 : PBF method [30].

Binder jetting (BJ) system works by the method of bringing together the liquid binder material by selectively dripping on the powdered material from the nozzles in an inkjet head, see Figure 2.9. Binder jetting technology is very similar to material jetting technology in that it disperses the material with the inkjet head. The difference between

it and material jetting is that the material distributed from the printing head from the binding jetting technology is not the building material, but the liquid adhesive material used to bring the powdered raw material together [30].

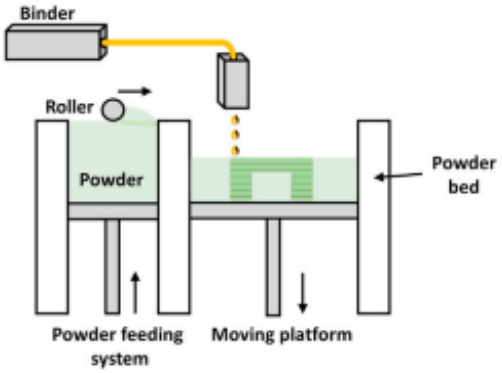

Figure 2.9 : Binder jetting method [30].

Vat Photopolymerization (VP) is a layered production method in which a liquid photopolymer material in a tank is selectively cured by a light source and polymerized, see Figure 2.10. This method, also called as Stereolithography (SLA) is one of the first additive manufacturing methods has been commercialized and patented. In this system, an ultraviolet laser selectively cures the surface of the photopolymer material in the liquid state in the tank. The movement of the laser is provided by computer-controlled galvanometers [31] [27].

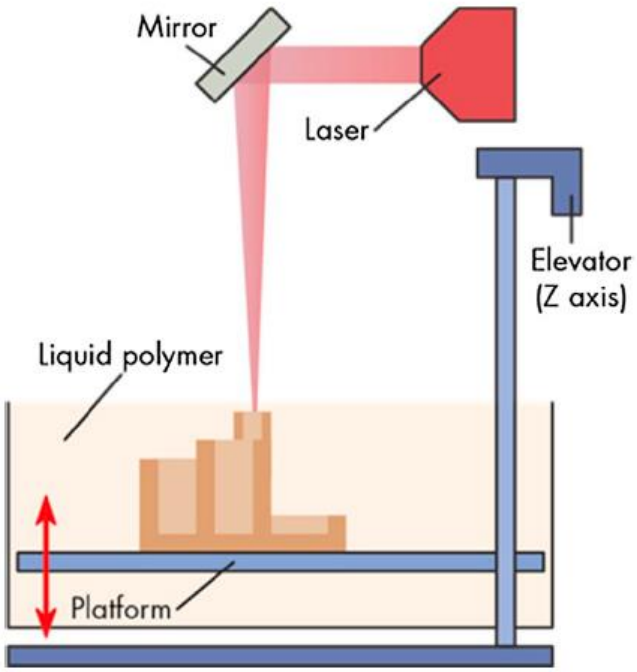

Figure 2.10 : Vat- polymerization method [28].

Sheet lamination (SL) technology is a polymer additive method. Binding between polymers is accomplished by application of the adhesive instead of welding. Like metals, sheet formed laminates are used as a feedstock and bring them together to produce desired shapes, see Figure 2.11. Heat and pressure are also helping to get proper bond strength. Heat treatment or surface treatment processes can be used to improve adhesive strength.

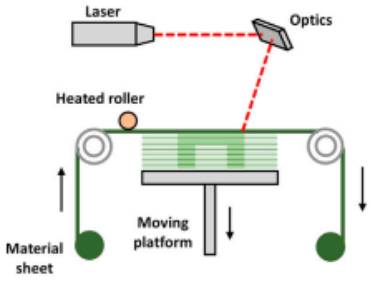

Figure 2.11 : Sheet lamination method [30].

2.2 An Overview of Fused Filament Fabrication (FFF), Process Parameters and Annealing

Fused filament fabrication is a most common polymer material extrusion method, see Figure 2.12. Before starting the FFF process, the STL. File has to be generated by CAD (computer aided design) then the software is sliced into layers and prepared g-code [30], [32]–[34]. After files are ready, it is uploaded to the FFF machine then production starts.

The FFF method allows the selection of many process parameters to obtain the desired properties (e.g., superior mechanical properties, good surface quality) in the final product. These parameters are explained in detail below.

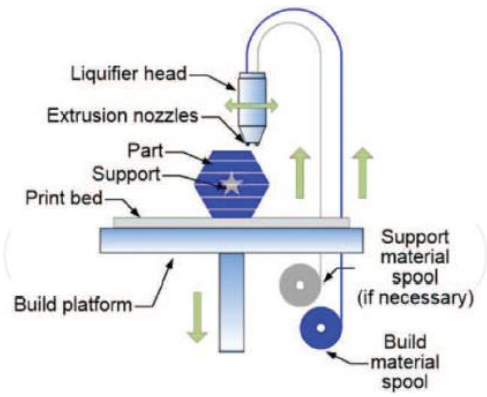

Figure 2.12 : FFF equipment [33].

Infill pattern is one of the parameters that have to be decided before printing parts. The infill pattern represents the internal geometry of the part.

Since parts are not produced in fully solid form due to the cost and time concerns, specific patterns are created by printer producers. The various types of patterns can be selected from the printer program. Eight examples of infill patterns are shown in Figure 2.13. The other parameter is that the infill density usually varies between 60% to 100% to obtain the appropriate mechanical properties. It should be considered that even if 100% infill density is chosen to print the part, it does not mean that the part will be completely solid. Figure 2.13 shows what different infill percentages look like depending on the infill patterns selected and high infill density also means the highest tensile properties [4], [35]. For instance, among the infill patterns being rectilinear, concentric, and Hilbert curves, the rectilinear pattern has the highest ultimate tensile strength (UTS) compared to the others, see Figure 2.14, and Figure 2.15 [27].

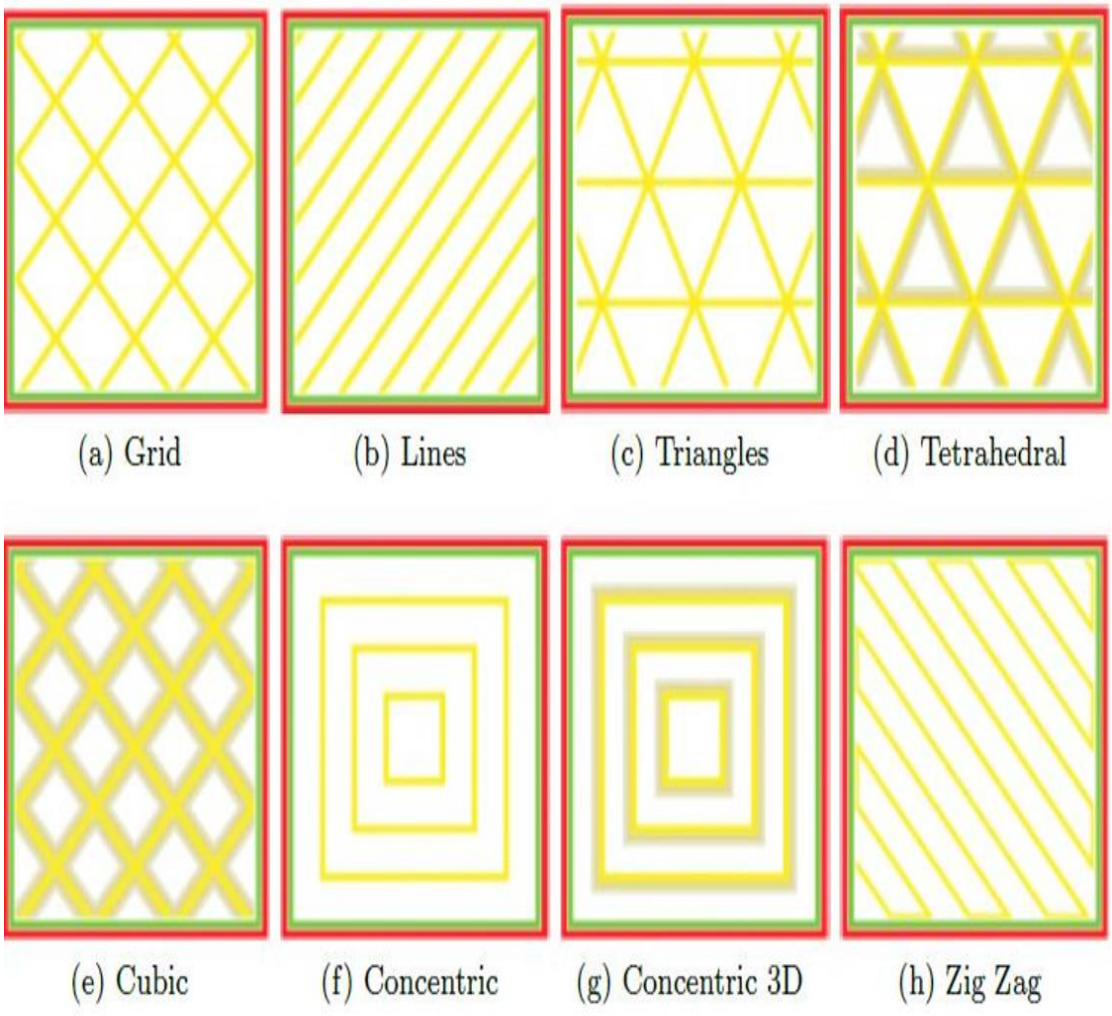

Figure 2.13 : Examples of infill patterns [4].

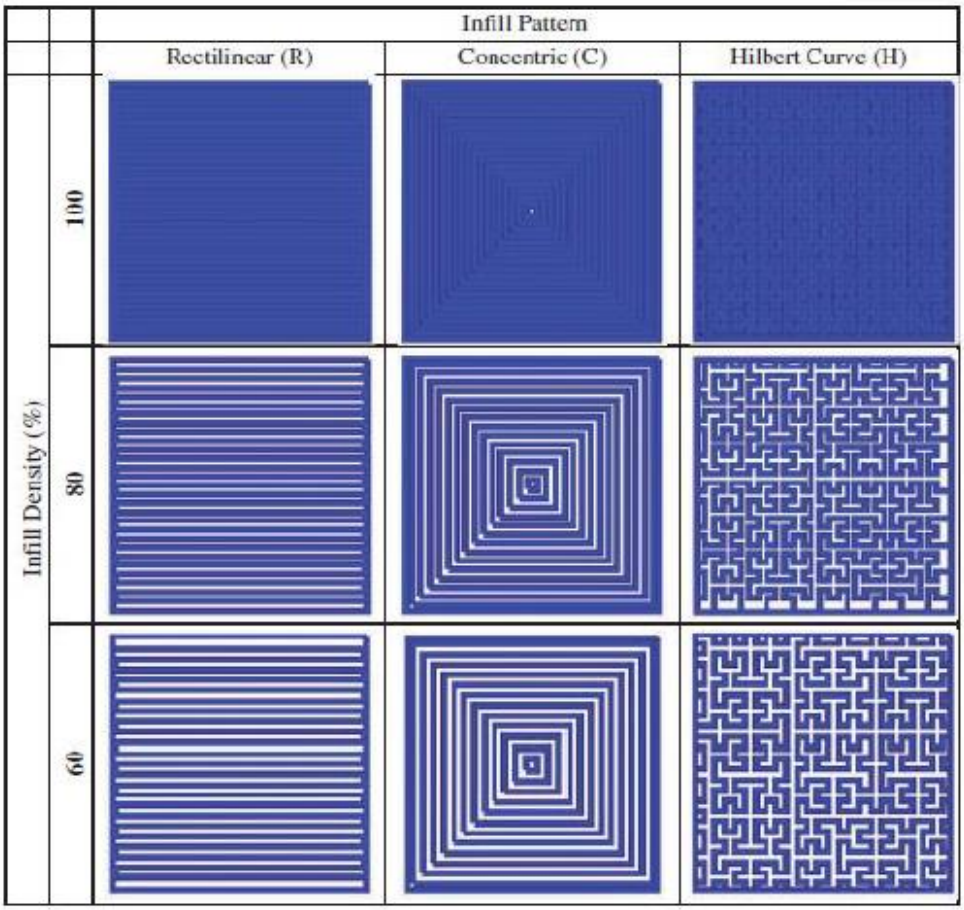

Figure 2.14 : Example of infill patterns according to infill density [36].

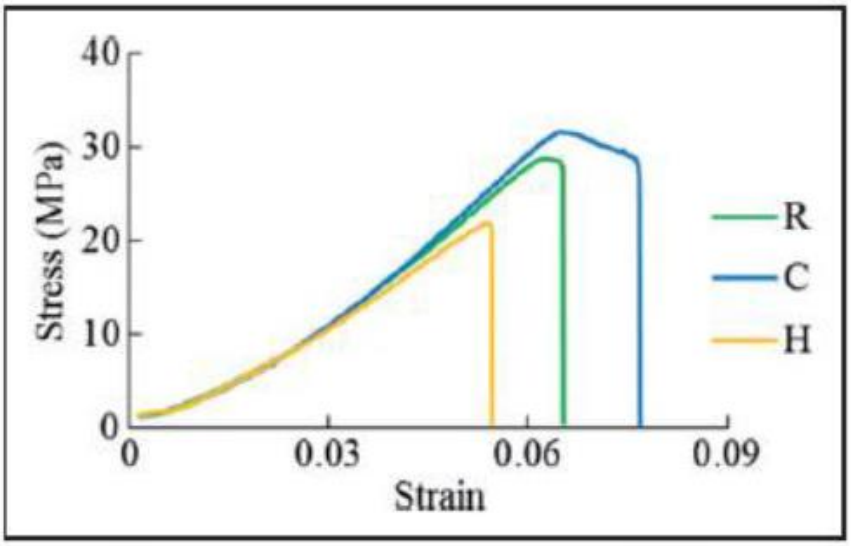

Figure 2.15 : Stress-strain curves (R rectilinear, C concentric, H Hilbert curve) [36].

As seen in Figure 2.16, and Figure 2.17, the angle measured between the raster and x-direction is called the raster angle. According to desired properties, parts can be printed with 0°, +45°, -45°, and 90 °, and their combinations.

The research illustrated that if the tensile load is parallel to the raster orientation, this structure shows the highest strength due to the trans-raster failure mechanism [4].

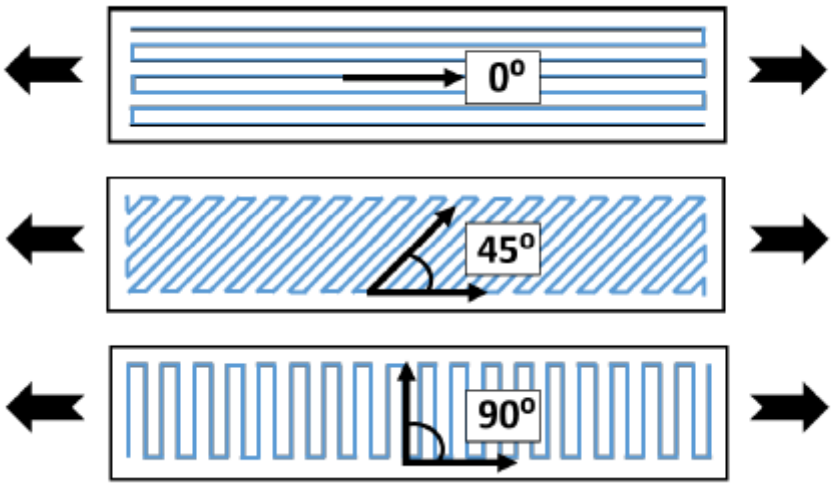

Figure 2.16 : Raster build directions [4].

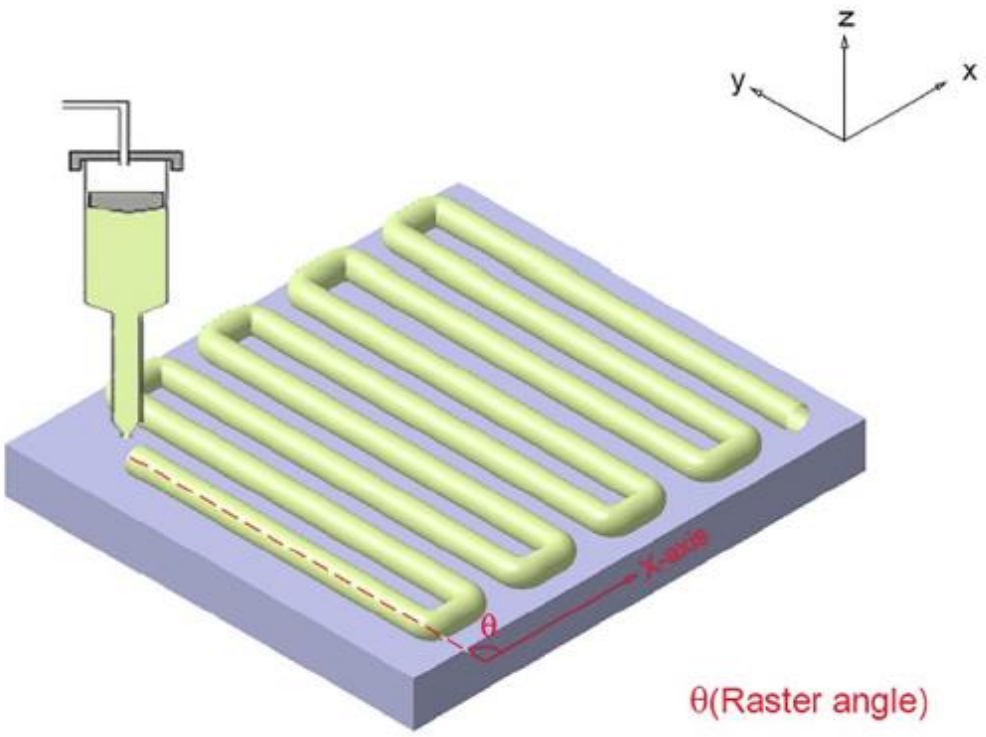

Figure 2.17 : Illustration of the raster angle [36].

Print direction and locations of the parts (specimens) are determined based on the printer's coordinate system, see Figure 2.18. Three different orientations are valid for 3d printing systems as XY (flat), YZ (on-edge/on-long edge) and XZ (up-right/on short edge) [9]. As seen in Figure 2.19, the highest mechanical properties of samples

produced from PLA are obtained by selecting flat specimens. Since the wide portion of the sample is exposed to its heated bed, it helps improve the bond strength between the raster and reduces porosities that occur inherently in the FFF process [4] [37]

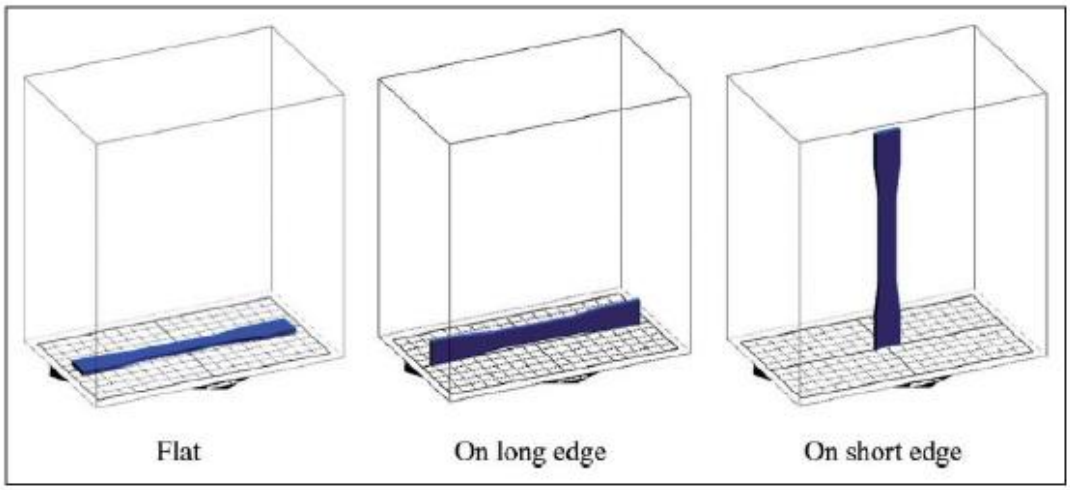

Figure 2.18 : Illustration of part orientation [36].

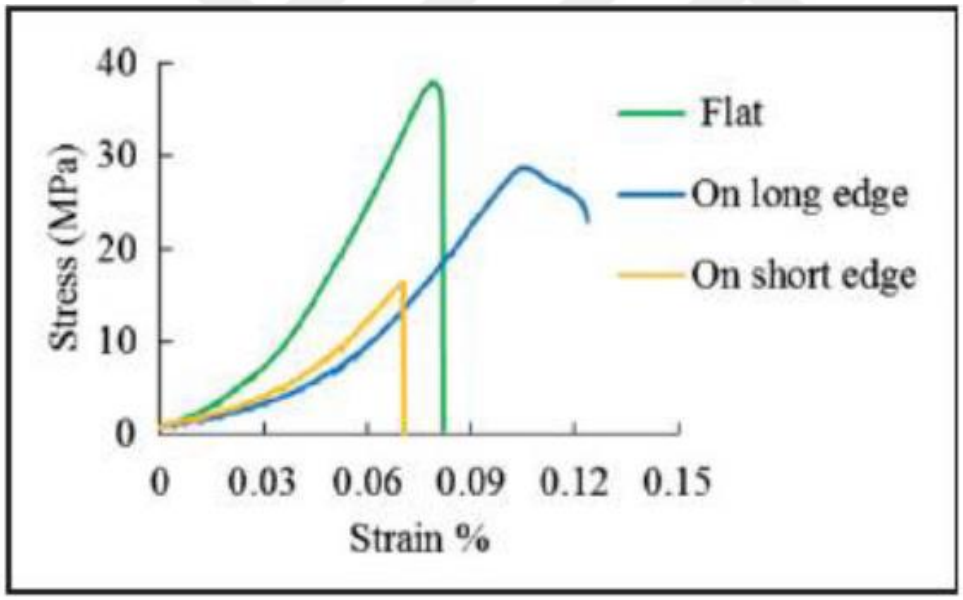

Figure 2.19 : Stress-strain curves given in build orientations [36].

As seen in Figure 2.20, layer height, also called layer thickness, is the height of a raster bead. The lower thickness helps to create a strong bonding strength between the layers due to the easy diffusion of the heat. A lower height is always obtained than the nozzle diameter used [35].

To have better surface roughness and high surface quality, lower layer thickness has to be selected to reduce the stair-case effect. Not only layer thickness, but also together

with the optimization of the other printer parameters are vital to have lower surface roughness. For instance, the combination of printer parameters such as printer speed and print orientations affect the surface roughness. Since high surface roughness is obtained in constructions in the Z direction, it is recommended to print the shortest height of the part in the z-direction[37].

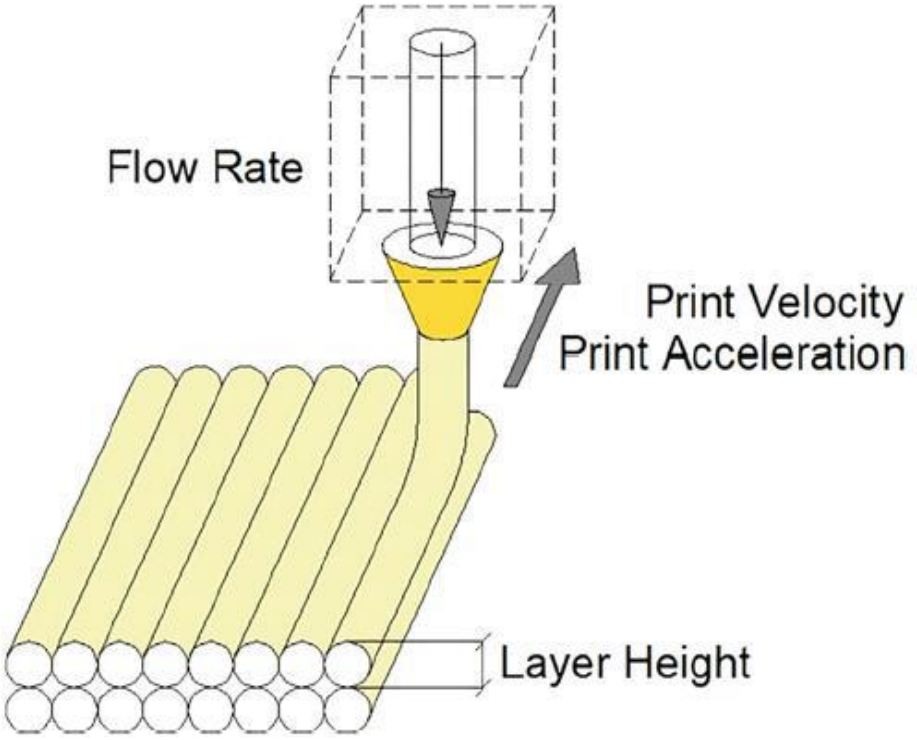

Figure 2.20 : Illustration of layer height [37].

If the highest value of the raster width is selected, layers will have come into contact with a large area, see Figure 2.21. The highest tensile properties will be obtained according to the high-level heat transfer between the layers.

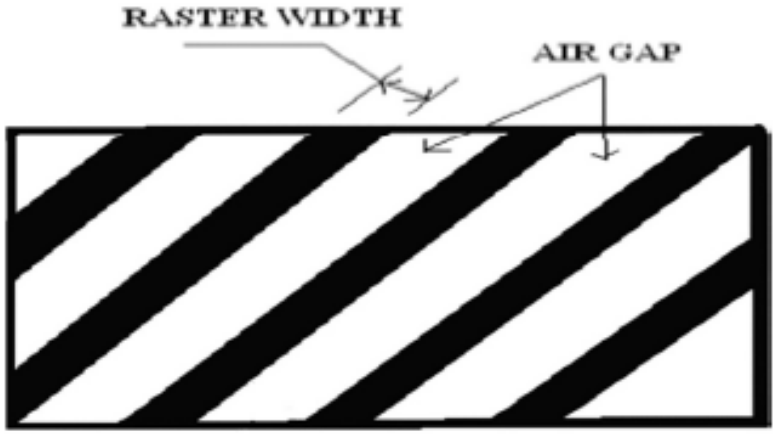

Figure 2.21 : Illustration of raster width [37].

The air gap is the distance between the raster and it is selected as a positive and negative direction as seen in Figure 2.22. The negative air gap represents the overlapping of the layers, while the positive air gap is the distance measured between layers.

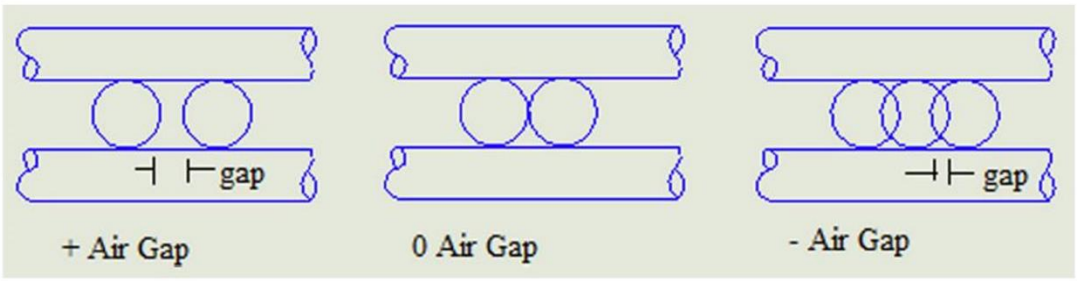

Figure 2.22 : Illustration of air gap [4].

Although there is limited research on air gap, air gap has recently become an important parameter in parameter optimization in 3d printers. As seen in Figure 2.23, contrary to the positive air gap, the negative air gap has the highest tensile strength as well as the maximum UTS at 0° when compared to 45° and 90°.

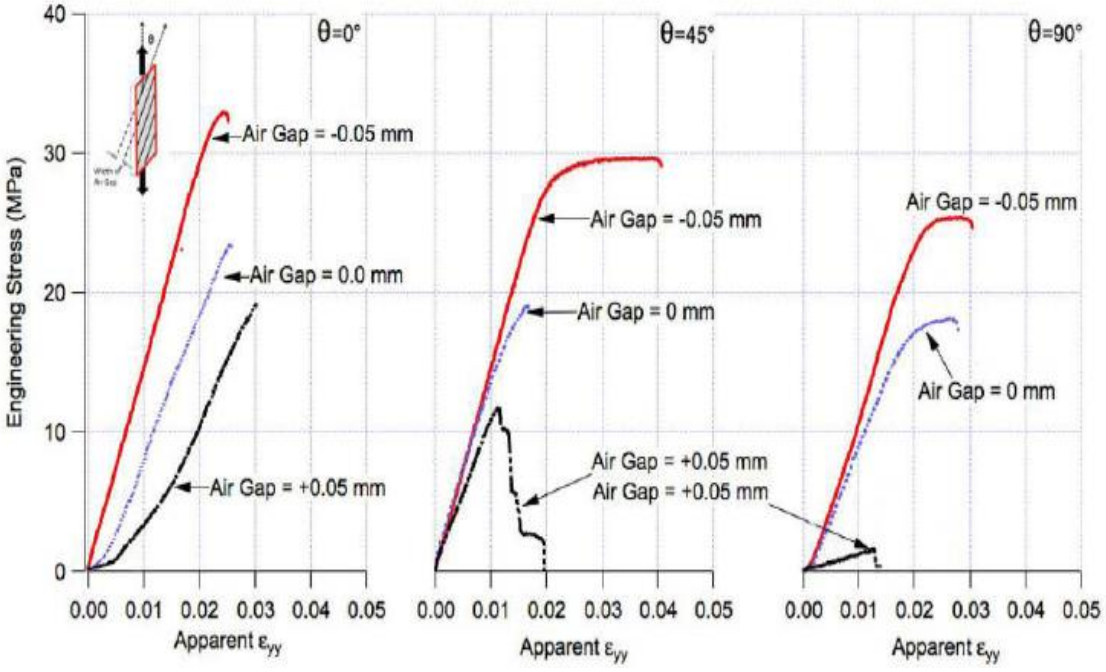

Figure 2.23 : Negative air gap effects on tensile properties of ABS.

The outer shell created first in the parts produced with a 3d printer is called the counter, see Figure 2.24. Generally, the first and last layers are produced to be fully solid, while a shell is used in one or two rows as the internal support structure. Shell in a 3d printer

system is illustrated in Figure 2.24 [35]. High strength obtains by using a high number of shells [37].

It is stated that if a part has a high number of shells, its impact on mechanical properties is higher than build orientation. Research shows that flat and short edge with the same shell number demonstrates the equivalent tensile strength [9].

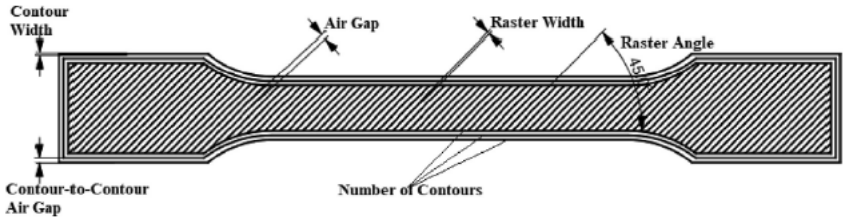

Figure 2.24 : Illustration of contour [35].

Print speed is the deposition rate of the melted feedstock in the XY plane [2]. Print speed is a parameter that directly affects the print time. The printing speed is given for certain polymers and it is generally chosen between 30% and 80%. Since it is low, it slows down the flow of the melted material, so sufficient adhesion may not be achieved. However, since residual stresses will remain on the part due to rapid cooling and heating at high speeds, the printing speed should not be selected at high speeds either. Since this effect will be low in thin-structured parts, high print speeds may be preferred.

3d printers have different nozzle heads according to their diameters. Nozzle diameters vary between 0.1 and 0.4mm, and 0.2mm diameter nozzles are generally chosen in research. With the increase of the diameter, thicker layer thicknesses can be obtained, the general rule of thumb is that the layer thickness should not exceed 0.75 times the nozzle diameter [38]. Figure 2.25 is illustrates different nozzle diameters produced by Markforged.

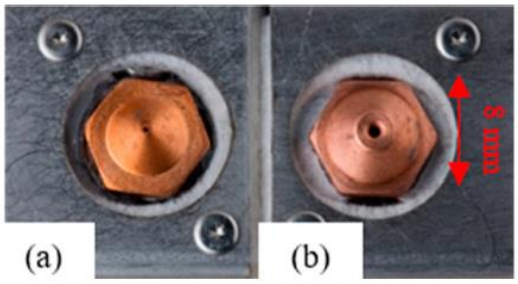

Figure 2.25 : Markforged manufactured nozzle diameters a) 0,35 mm b) 0,9 mm [39].

In 3D printing systems, some types of polymers require pre-bed heating to ensure adhesion, reduce internal residual stresses and thus prevent shrinkage.

The print temperature is the temperature the melted polymer reaches before printing. As the temperature increase reduces the viscosity, it makes printing easier and also increases the strength [35].

Annealing is the favoured post processing method recently used in 3D printing, and has become an important parameter currently being studied. According to research, annealing assists to recover the structure and help to get molecular diffusion between rasters, see Figure 2.26 [40]. Depending on whether the polymer is amorphous or crystalline, it is recommended to select the annealing temperature over Tg for both and not to exceed cold- crystalline temperature for crystalline structures [35].

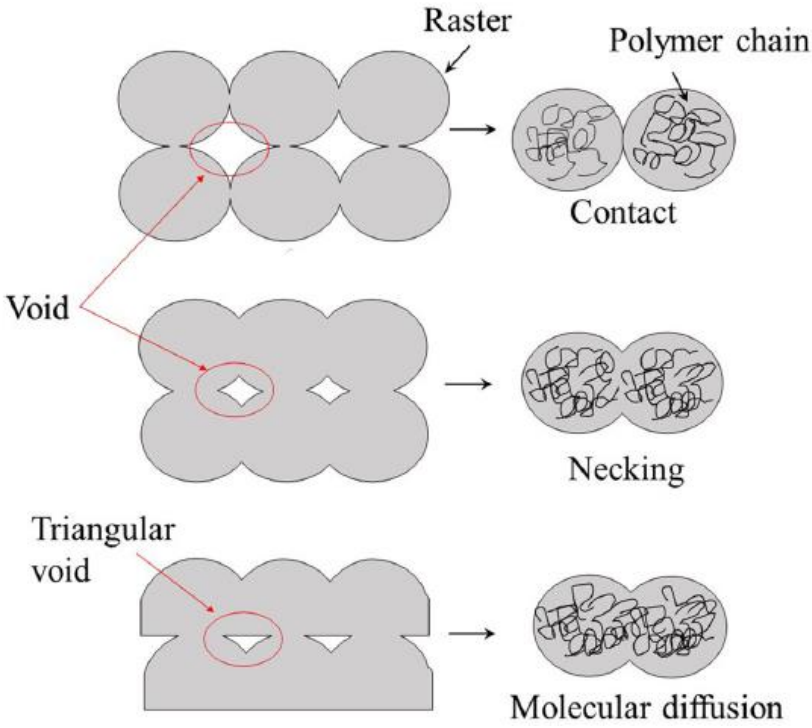

Figure 2.26 : Molecular diffusion after annealing of FFF parts [40].

Fast heating and slow cooling during heat treatment are important as it is recorded that the reason for warpage in ABS and PLA printed in concentric pattern [35].

Finally, as seen in Figure 2.27, whichever feature is desired to be developed, the parameters affecting the feature that is desired to be developed should be optimized for the selected feedstock.

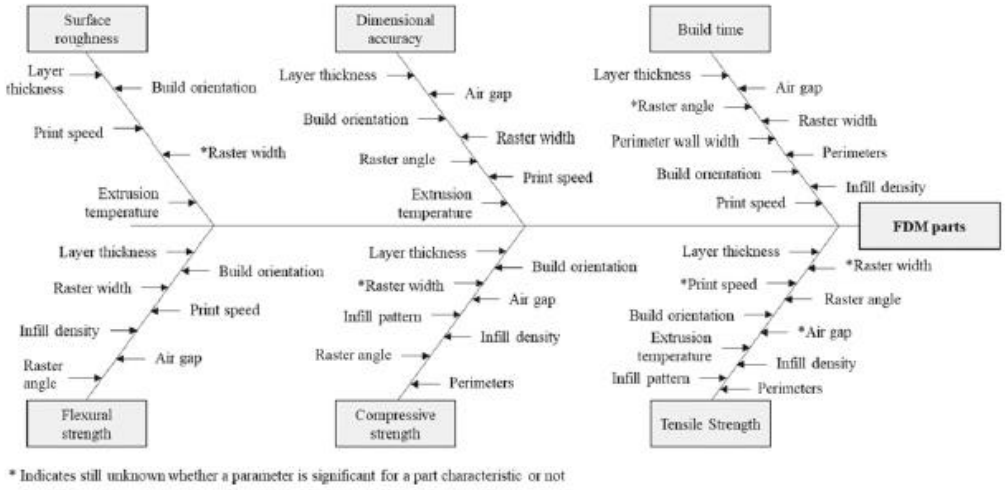

Figure 2.27 : Fishbone diagram for FFF parameters [35].

2.3 Commodity and Engineering Thermoplastic Materials Commonly Used in Polymer Additive Manufacturing Technology

Selection of the proper feedstock for polymer additive manufacturing is essential. According to their molecular structure (amorphous and semicrystalline), there are 3 main polymer groups as thermosets, thermoplastics, and hydrogels. A schematic view of this structure is given in Figure 2.28.

Production of the thermosets, except UV-curable types, are needed much more time during the curing stages. For example, a long period of time and high temperatures are required during curing time. Additionally, thermoset materials cannot be used after processing, and a reaction is irreversible [9].

This prevents the use of thermoset materials as feedstock. Due to these reasons, UV-curable thermosets and thermoplastics are commonly preferred polymers.

Thermoplastics are divided into two groups. The first one is an amorphous crystalline structure that has disorder crosslinks between molecules [32]. This characteristic is that not the melting temperature does not drop suddenly, making it easily processable after enough time to heat exposure. Another molecule type is a semi-crystalline structure. The highly ordered crystalline type rather than amorphous structure, tends to decrease behaviour on melting temperature after sufficient heat exposure time. The second group has high mechanical properties thanks to intermolecular bond strength [9]. One of the main features of thermoplastics is that being reusable due to the melting

mechanism, which is no longer linked after melting and solidification contributes to the formation of new links [2]. These properties make them useful for material extrusion additive methods (FFF). Examples of the some thermoplastic materials are acrylonitrile butadiene styrene (ABS), polylactic acid (PLA), Nylon/polyamide, polypropylene (PP), polyethylene (PE), polyether ether ketone (PEEK), polyetherimide (PEI), polycarbonate (PC), polyethylene tetraphthalate (PET), polyethylene tetraphthalate glycol-modified (PETG), polyamideimide (PAI), see Figure 2.29 [41], [33].

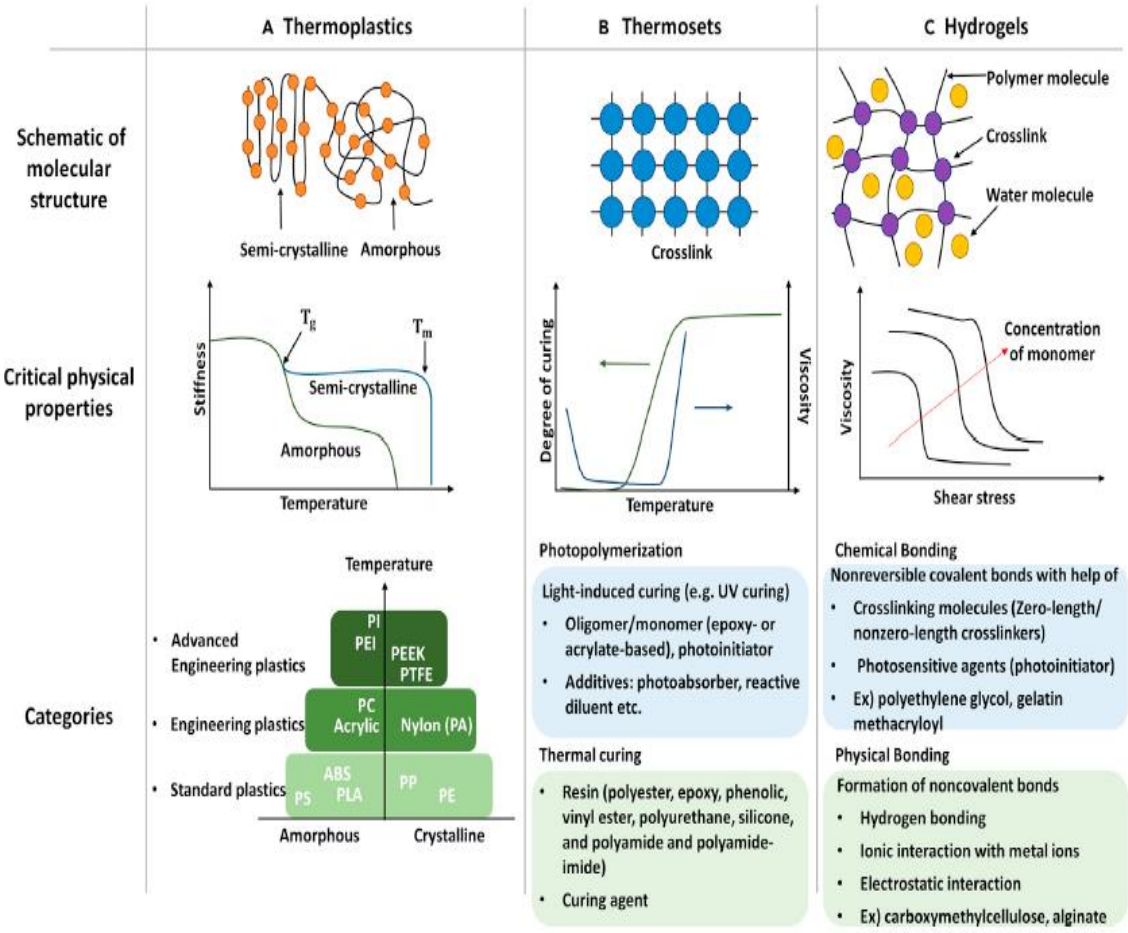

Figure 2.28 : Schematic view of polymer structures [16].

As seen in Figure 2.29, there are three groups of thermoplastics based on performance and cost such as commodity, engineering, and high-performance thermoplastics. The properties of the acrylonitrile butadiene styrene (ABS), polylactic acid (PLA), nylon, polyethylene (PE), and polypropylene (PP) from commodity thermoplastics, and glycol-modified polyethylene terephthalate (PETG) from engineering thermoplastics are given in below.

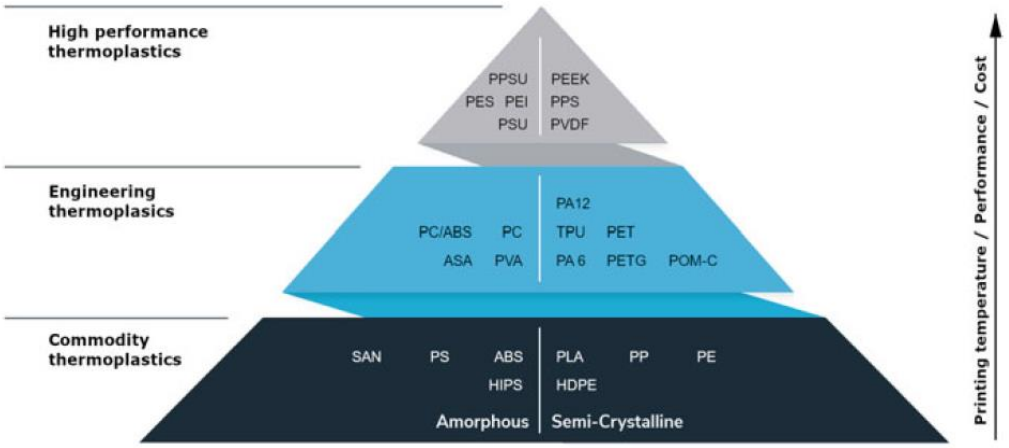

Figure 2.29 : Illustration of filament materials pyramid [9].

ABS is the first preferred polymer having an amorphous structure. It is used for 3D printing due to its cost, wear and impact resistance, and durability against harmful chemicals [16]. Tg of ABS is 215- 250°C. The major drawback has a high melting point (215- 250°C). Due to high temperatures, the print bed needs to be heated more to prevent it from wrapping. According to the researchers, since ABS tends to have high porosity inherently, it is recommended that the print thickness be low and applied to the pressure. Micro voids cause weak bond strength between layers. One of the ways to eliminate voids is to use a large nozzle diameter. Figure 2.30 contains comparisons of different polymer types from particular perspectives [28], [30], [34].

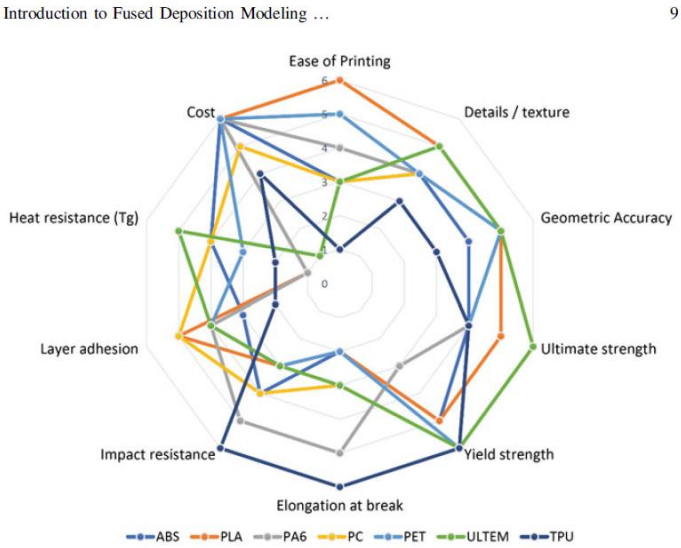

Figure 2.30 : Six-point ranking diagram for filament materials [9].

PLA is the most preferred polymer type for 3D printing. The fact that it is not expensive, has high tensile strength, is reusable and does not contain harmful gradients makes PLA preferable in a wide area of usage. PLA has glass transition temperature and extrusion temperature between 60-65°C and 160-230°C respectively. Hot bed is not required during printing [1], [28], [30], [34].

One of the favourite types of polymers is Nylon because of its competitive with the tensile properties of other types. Since durability against humidity is low, printing problems can be observed. PA12 (polyamide 12), and PA6 (polyamide 6) are the known materials in the group of nylon polymers. Nylon 6 (PA6) has glass transition temperature and extrusion temperature between 47-57°C and 220-270°C respectively [1], [28], [30], [34].

One of the semi-crystalline polymer types is polypropylene. As seen in Figure 2.31, the main problem of polypropylene due to its high expansion rate is heat degradation. To solve the shrinkage problem, the nozzle temperature must be 165 °C and the printing speed must be slower when printing the first layers [28], [42].

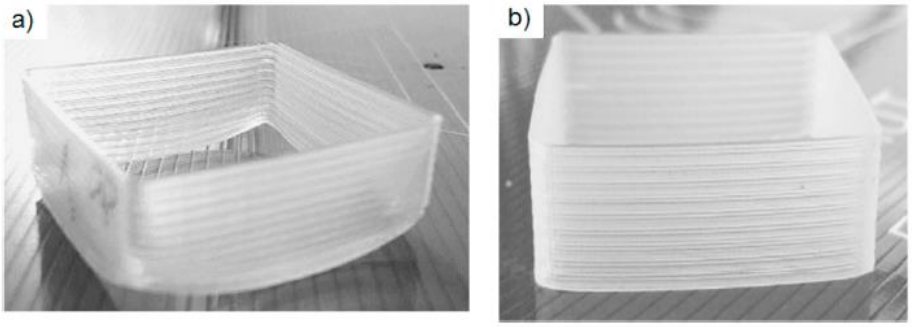

Figure 2.31 : PP production by FDM a) distortion b) after solving distortion problem [42].

Polyethylene which is the most favoured polymer because of its high recovery rates, indicates weak adhesion to the printer bed similar to PP. An alternative solution is to use adhesives to solve delamination problems between the part and the bed system The glass transition temperature of PC is between 140°C - 151°C and it is required a high bed temperature (80-120°C). Additionally, the melting temperature of PC is also high (260- 310°C) [39] [43]. As for nylon, PC filaments need to be protected from the air due to moisture entrapment. It tends to warp and shrink like PP [39] [43]. Similar to PP, its bed temperature has to be carefully determined and special precautions have to

be taken during the production of the first layer to improve good adhesive strength [41].

PET has a molecular structure similar to PETG with the difference in glycol. This difference makes PETG an amorphous polymer unlike PET, which has a semi-crystalline structure. PETG is a more elastic material and easy to print compared to PET. Its flexible structure allows being able to print high volume parts without shrinkage [44]. The fact that PETG not only has high impact resistance but also chemical resistance makes it a new polymer used in 3d printing. The usage areas of PETG are mostly dental, food, and chemical industries.

The main drawback of the PETG is its tendency to pick up the moisture but not more than polyamide. The moisture removal is the recommended process of PETG before use [45]. The PETG exhibits higher strength unlike their counterparts such as ABS.

In the past decade; even though PETG has remarkable characteristics, there are only a few studies examining the properties of 3D-printed PETG. It is estimated that the studies will increasingly gain the attention it deserves.

2.4 Literature Studies for The Effects of FFF Parameters on The Mechanical Properties of Commodity and Engineering Polymers

One of the specified metal extrusion methods is the FFF. The working principle of the FFF method is melting the feedstock and extruding it into the bed with the aid of a nozzle. The main advantage of this method is making it possible to produce high volume parts in a short time with lower cost than extrusion. It is known that interlayer strength of FFF produced parts is lower than extrusion and injection molding parts. The researches show that FFF is subject of the many researches to improve mechanical properties with parameter optimizations.

As seen in Figure 2.29, thermoplastic polymers are examined under three main headings as a commodity (ABS, PLA, PP), engineering (PC, PETG, PET, PA) and high performance thermoplastics.

In these studies; the effects of FFF process parameters on a variety of polymer feedstocks, from commodity thermoplastics (ABS, PLA, and PP) to engineering plastic (PETG) have been examined [4]. The effects of the following parameters on mechanical properties have been widely discussed in many researches for ABS and

PLA polymers, print orientation, layer height, infill density, layer thickness, air gap, print temperature, raster width, print speed, and infill pattern [35].

ABS and PLA are the most dominant polymer materials used for FFF technology. The properties of ABS and PLA were compared with samples produced by injection molding. It was stated that PLA was shown similar properties, however ABS has always lower properties than injected molded parts and PLA samples. Another comparison was completed between ABS and PC and ultimate tensile strength at the break of PC samples was the highest value. Raster orientation effects on ABS samples were evaluated in the research and the samples were produced as per ASTM D3039 and ISO527-2. A study showed that samples having 0° raster angle were found so close to injected molded ABS samples (94% of injected molded parts). Not only the above samples but also the samples produced as per ASTM D638 Type IV were also discussed and resulted in highest values via 0° raster angle. For PLA polymers, the raster orientation effects on UTS were also discussed and results were compared with injected molded parts. It was surprisingly found to have higher properties than molded parts [4].

In a research, it was focused on the comparisons of the PLA, PETG, PEEK, and ABS FFF printing polymers via raster angle, infill percentage and layer thickness [2]. The aim of this study is to examine the effects of selected process parameters on mechanical properties. It is also referred to as having superior properties of PETG while comparing PLA and ABS polymers [2].

In recent researches are focused to developing tensile strength of PETG polymers. A PETG is a modified polymer from PET [41]. With the addition of glycol monomer, it enables use in FFF technology due to its durability. The prominent properties of PETG are ease of printing, low ash amount, high chemical resistance, no tendency on shrinkage and response to heat treatment. The common usage areas of PETG are the food, chemical and dental industries. Additionally, PETG will become widespread for prototyping, wax-pattern production for aerospace applications.

The selection of the printing parameters is playing a vital role to enhance mechanical properties. Most studied printing parameters are specified as raster angle, layer height (layer thickness), raster width, infill pattern, air gap ratio, number of outer shells and

heat treatment [35]. Printer bed, nozzle temperature, print speed are other printer parameters varying depending on polymer properties [35], [37].

In a research, it was investigated that grid pattern is having highest tensile strength (54,1 Mpa) among the patterns as grid, rectilinear, cubic, and honeycomb by keeping the other parameters as constant (infill density, raster angle, layer thickness, print speed, platform temperature, and print temperature) [46]. The same research is studying the effects of annealing on different infill patterns and it is observed that annealing improves 22% (average) tensile strength of PETG [46].

The effects of raster orientation, build direction and infill ratio have been considered in research. Finally, it is found that the results taken from the Z direction showed 60% and 65% lower tensile strength than X and Y directions respectively. Y direction with 45/-45 raster angle shows the 15% higher strength than X direction. The 0° raster angle shows the superior tensile results among different raster angles by holding the following parameters as constant 0,2mm layer thickness, straight infill pattern, X build direction, and 100% infill density. It is inevitably recorded that decreasing the infill density as 50% is decreasing the results in all build directions [47].

Another study demonstrated the effects of annealing exposure time at 120°C with the 0,36-layer thickness. It is seen that there are no remarkable differences on tensile properties [48].

A study discusses the overlap ratio and layer thickness effects of PETG polymer. Based on the results, 20% negative air gap improves 15% tensile properties and 10% elastic modulus without considering the layer thickness effect. Based on the best tensile properties, the optimum layer thickness is recorded as 0,2 mm by fixing the raster width as 0,4mm [49].

The raster angle, layer thickness, print speed, and infill patterns effects are subjected to find out which parameter is predominant on mechanical properties. The optimum configuration is achieved by selection of the 0 degree raster angle, and 0.15mm layer thickness [2].

In another study evaluate the effects of layer thickness, infill density, and infill patterns on ultimate tensile strength. It is found that 80% infill ratio, 0.1 mm layer thickness with grid pattern have highest value while comparing other combinations. It is obvious that lower layer thickness with the highest infill ratio is the best option [50].

To investigate effects on tensile strength, printer speed and layer thickness are selected as variable parameters in this research [51]. It is seen that lower layer thickness and print speed with high percent infill ratio give the best results.

The research compared as-print and annealing samples with 100% infill density in the X build direction. An improvement (8%) was recorded thanks to the annealing being above 5°C of Tg at 60 minutes [52].

The effect of two different samples designed per ISO 527-2- 5A and ISO 527-2-1A with 5mm and 1mm thickness were investigated. Even though the validity of the test specimens was not considered in this study, samples prepared as at 1mm is 8% higher than other. Among the samples prepared according to these two standards, those produced with ISO 527-2- 5A were found to have 5% higher mechanical properties [44].

The different raster angels were used during fabrication of the samples as per ASTM D638 Type I by fixing layer thickness as 0,2mm. Additionally, the highest tensile value seen in the samples produced was concentric and at 0°C, the tensile strength increased by 6% with annealing [35]. Similar to other papers, it is stated that the annealing temperature was selected at 5°C above glass transition temperature [33]. The annealing time and temperature are the significant parameters to modify inter raster strength. It is seen that 55°C and 10 hours is enough to reach the highest yield strength [35].

It is seen that the samples were prepared by various standards listed below. These concomitant variations bring validity problems. However, all tensile tests were performed without taking into account the broken location of the specimens.

- ISO 527-2-1A, 1B, 1BA, 1BB, 5A,5B [53]
- ASTM D638 Type I, II, III, IV, V [54]
- ASTM D 3039 [7]

There is limited research discussing the effects of sample preparation standards and their validity.

Only one research has revealed the differences between ASTM D638 type I & IV and ASTM D3039. The following parameters are constant flat sample, solid and sparse high density, -45/+45 and 0/90 degree raster angle and 0,30 mm layer thickness (average). The elastic modulus of ASTM D3039 in all conditions is overwhelmingly

higher than other specimens prepared with the different combinations. The results of UTS (ultimate tensile strength) are very close to each other but ASTM D3039 shows the lowest values [55].

The aim of the first part of this study is to reveal which infill pattern between concentric and rectilinear shows the highest mechanical properties produced with different sample standards and air gaps.

The aim of the first part of this study is to reveal the effect of air gap and infill patterns by producing two different sample standards on mechanical properties. With the completion of the first part of this study, it is observed which parameter set significantly shows the highest properties.

The second part of this study presents effects of the annealing time and temperature with the best parameter set to be decided.

In summary, this research aims to reveal the importance of air gap selection, sample standard types, infill patterns, temperature & time selection after post heat treatment and different printer machines on mechanical properties through comparative studies.

2.5 An Overview of Literature Studies for Selection of Tensile Testing Specimen Standards of 3D Printed Parts

The determination of the tensile test specimen standard is subject of development for 3D printing technology. It is still seen that tests are carried out using different types of specimens. Since the test method has not been standardized yet, following types of standards are used in research.

- ISO 527-2-1A, 1B, 1BA, 1BB, 5A,5B [53]
- ASTM D638 Type I, II, III, IV, V [54]
- ASTM D 3039 [7]

For dimensions of the specimens, see Appendix A.

A study was done to compare ASTM D638 and ASTM 3039 and studied with ABS. Different process parameters are selected to observe the effects of specimen standards and flat samples were used. As a general rule for ASTM D638, if the sample is broken outside of the narrow length, the test is failed and a retest is required [54].

As a general rule for ASTM D3039, if the sample is not broken inside of the gauge length, a test is failed and a retest is required [54].

Generally, ASTM D638 IV have a narrow-gauge length and a small radius. Some of the samples failed outside of the narrow length. According to the comparison of UTS results, samples show higher value than ASTM D3039 but lower value for elastic modulus (E). The advantages of the ASTM D638 are that highest production speeds than the ASTM D 3039. While it took 6 hours to produce 22 and 13 samples, respectively, from ASTM D638 I & IV, almost one sample was produced in 1 hour according to ASTM D3039. However, since ASTM D3039 does not have stress concentration regions such as ASTM D638, it is not necessary to produce a large number of samples against invalid status [55].

In another study completed using ISO 527-2 1A specimens, it was reported that peak stresses were observed at the radius of the specimens at which fracture would occur exactly, see Figure 2.32. Additionally, as it is referred to that ISO 527 (Type 1A and 1B) samples having smaller radius than ASTM D638 (Type I, II, and III), ASTM D638 is preferred mostly [4].

The main concern of the studies is the reliability of the results due to not being considered the fracture locations. Moreover, these results are published without considering invalidity, and commonly pictures of the tested samples are not involved. There is limited study in literature discussing the fracture locations of specimens.

In summary, recent studies demonstrate that selection of standards is the most significant and controversial topic to reveal that the actual properties of 3D-printed polymers.

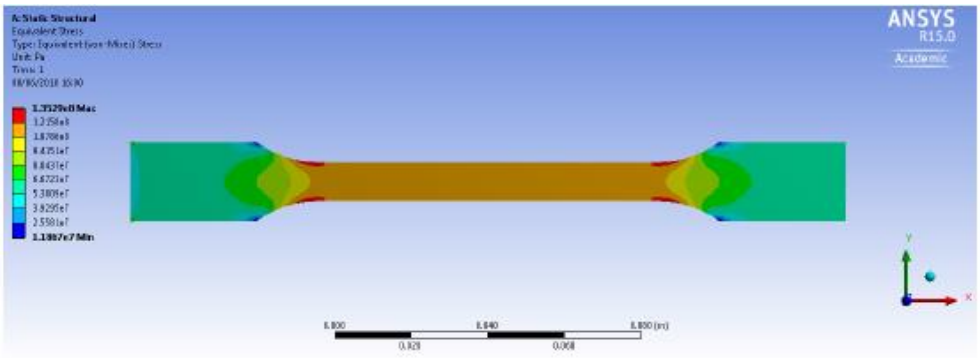

Figure 2.32 : Stress locations of samples prepared as per ISO 527 [4].

3. EXPERIMENTAL STUDIES

3.1 Material and Method

This chapter explains the fabrication of the PETG specimens, test methods, and examination techniques. Firstly, PETG specimens are produced with selected parameter sets. The first set is fabricated to find out the effects of specimen standard and overlap percentage. Afterward, production is followed with different infill patterns with the same specimen standard given the highest values to find the strongest infill pattern and overlap ratio. The second experimental set includes post processing effects by continuing with a parameter that is given high mechanical properties. Details are given in this chapter.

3.2 Production of Tensile Test Specimen of FFF Printed PETG

Firstly, specimens were made from PETG (glycol modified polyethylene terephthalate) polymer due to its outstanding properties. The brand of PETG used is Smart Materials 3D, the properties of Smart Materials are given in Table 3.1. Specimens were created as per ASTM D638 Type IV and ASTM 3039 using the CAD software NX (Unigraphics), Figure 3.1, and saved as STL formats. After model creation, G codes were prepared with Ultimaker Cura 4.13.1, see Figure 3.2.

Table 3.1 : Properties of smart materials 3D branded PETG.

General Printer Properties	Raise3D Pro2 Plus
Density	1,27 g/cm^3
Tensile Strength	50 Mpa
Flexural Strength	69 Mpa
Flexural Modulus	2100 Mpa
Print temperature	225-245 °C

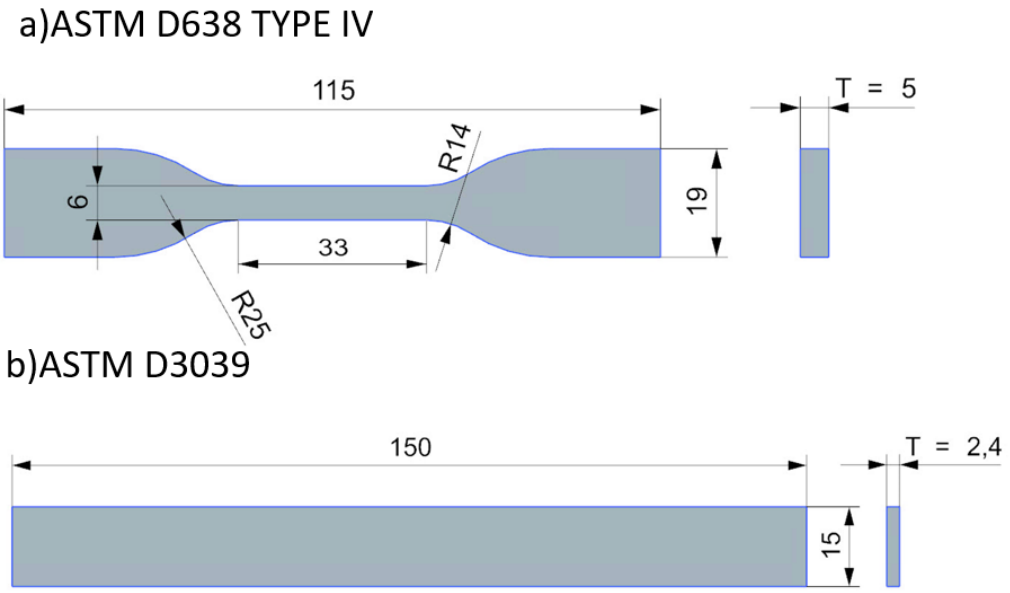

Figure 3.1 : CAD pictures a) for ASTM D638 Type IV b) ASTM D3039.

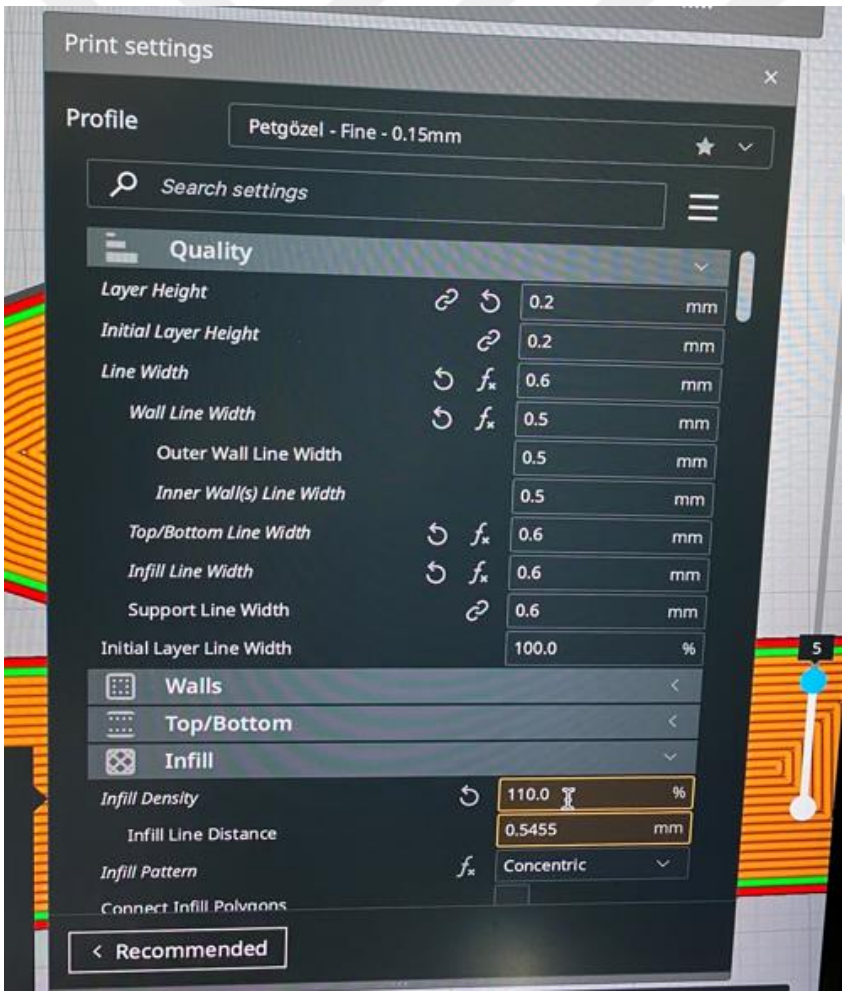

Figure 3.2 : Illustration from the slicer user interface**.**

RAISED 3D PRO 2 Plus FFF machine was used to fabricate samples and their properties are given in Table 3.2, see Figure 3.3.

Table 3.2 : General printer properties of RAISED 3D PRO 2 Plus.

General Printer Properties	Raise3D Pro2 Plus
Machine Size	620×590×1105 mm
Nozzle Diameter	0.4 mm / 0.3 mm /0.6 mm
Material Diameter	1.75 mm
Print Head Travel Speed	30- 150 mm/s
Max build temperature	110 °C
Max nozzle temperature	300 °C
Supported Materials	PLA, ABS, PC, PETG, PP etc.
Resolution	90-290 micron

Figure 3.3 : RAISED 3D PRO 2 PLUS printer.

Five tensile specimens were fabricated for each parameter set, three of five specimens were planned to be tested and two off five specimens were produced as spare parts intended to be used in case of test rejection or any unexpected situation in the test. Finally, a total 80 samples were produced per the given parameters in Table 3.3, Table 3.4, and Table 3.5. Additionally, production charts are given as seen in Figure 3.4, Figure 3.5, and Figure 3.6. All images of the samples are given in Appendix B.

Table 3.3 : Constant process parameters of 3D-Printed PETG samples.

Parameters	Properties
Infill Density	100%
Nozzle Dia	0,4mm
Layer thickness= Layer Height= Resolution	0,2mm
Orientation	0 degree (flat)
Tbed (°C)	70

Table 3.3 (continued) : Constant process parameters of 3D-Printed PETG samples.

Parameters	Properties
Raster Width	0, 6mm
First Layer speed	30%-50% of Vnominal
Top and Bottom Surface Skin	Open (selected as 4 top and 4 bottom lines)
Speed	40-50 mm/s
Te (°C)	230-240

Table 3.4 : Variable process parameters of 3D-Printer PETG samples for 1st set.

Sample Identification	Sample Number	Air Gap (%)	Infill Pattern	Variable Parameters	Additional Variable Parameters
CBA0	5	0	Concentric	ASTM D3039--150*15*2,4mm	No Post Processing
CBA10	5	10	Concentric	ASTM D3039--150*15*2,4mm	No Post Processing
CBA15	5	15	Concentric	ASTM D3039--150*15*2,4mm	No Post Processing
CBA20	5	20	Concentric	ASTM D3039--150*15*2,4mm	No Post Processing
CAA0	5	0	Concentric	ASTM D638 TYPE IV 115*19*5mm	No Post Processing
CAA10	5	10	Concentric	ASTM D638 TYPE IV 115*19*5mm	No Post Processing
CAA15	5	15	Concentric	ASTM D638 TYPE IV 115*19*5mm	No Post Processing
CAA20	5	20	Concentric	ASTM D638 TYPE IV 115*19*5mm	No Post Processing
RBA0	5	0	Rectilinear	ASTM D3039--150*15*2,4mm	No Post Processing
RBA10	5	10	Rectilinear	ASTM D3039--150*15*2,4mm	No Post Processing
RBA15	5	15	Rectilinear	ASTM D3039--150*15*2,4mm	No Post Processing
RBA20	5	20	Rectilinear	ASTM D3039--150*15*2,4mm	No Post Processing

Table 3.5 : Variable process parameters of 3D-Printer PETG samples for 2nd set**.**

Sample Identification	Sample Number	Air Gap (%)	Infill Pattern	Variable Parameters	Additional Variable Parameters
CAT1	5	15	Concentric	ASTM D638 TYPE IV 115*19*5mm	Set 1 : 5°C above Tg- 1 hour
CAT4	5	15	Concentric	ASTM D638 TYPE IV 115*19*5mm	Set 2: 5°C above Tg- 4 hours
CAP1	5	15	Concentric	ASTM D638 TYPE IV 115*19*5mm	Set 3: 55 °C – 1 hour
CAP4	5	15	Concentric	ASTM D638 TYPE IV 115*19*5mm	Set 4: 55 °C – 4 hours

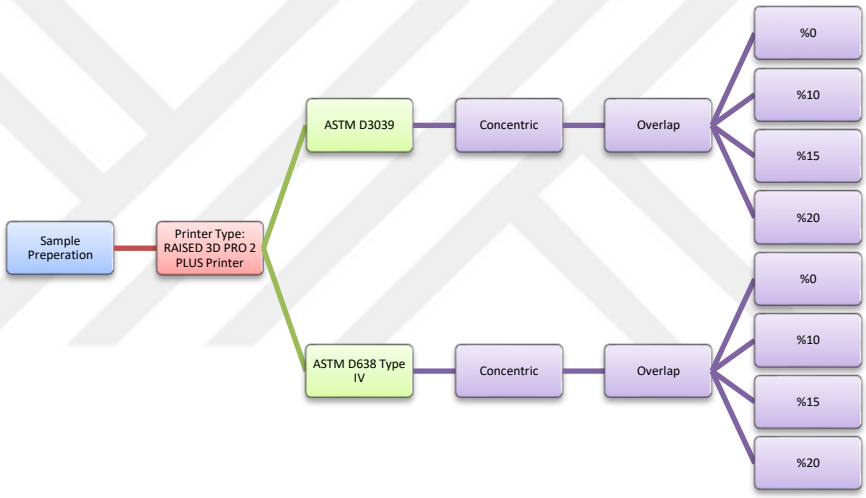

Figure 3.4 : First set of sample preparation for concentric infill**.**

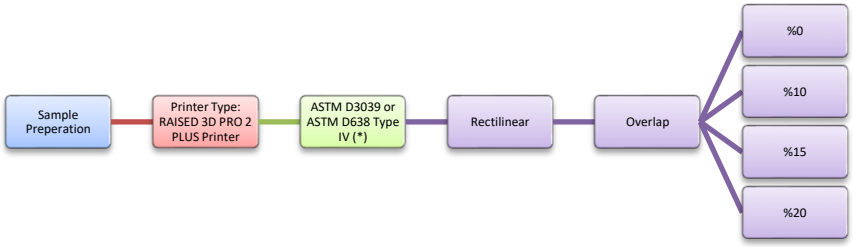

Figure 3.5 : First set of sample preparation for rectilinear infill.

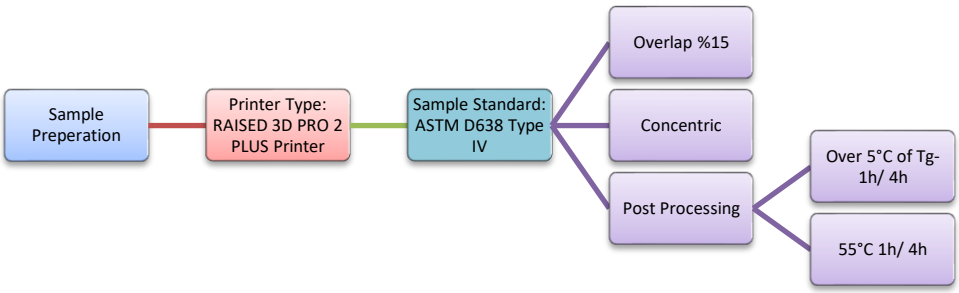

Figure 3.6 : Second set of sample preparation.

Before starting the production of the samples, eight small rectangular shaped parts were built to verify the inner structure by SEM, see Figure 3.7. 4 off 8 small samples were produced as 0%, 10%, 15%, and 20% negative air gaps with concentric patterns. The remaining small samples (4 quantities) were produced as 0%, 10%, 15%, and 20% negative air gaps with rectilinear patterns.

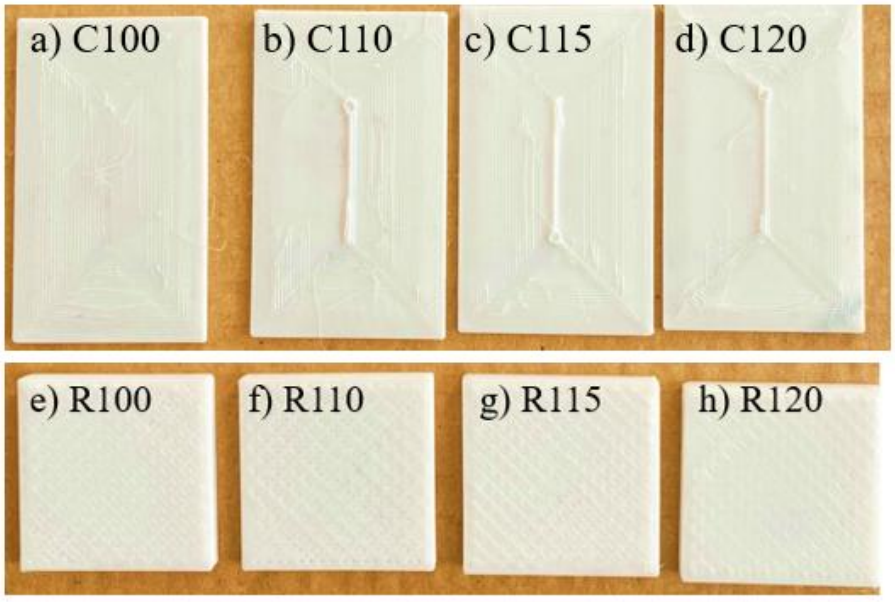

Figure 3.7 : Small rectangular shaped parts produced as concentric (from a to d) and rectilinear infill pattern (from e to h); C: Concentric, R: Rectilinear, 100 0% negative air gap- 110 10% negative air gap - 115 15% negative air gap - 120 20% negative air gap.

The image of the test specimens during the manufacturing process are shown in Figure 3.8, and Figure 3.9.

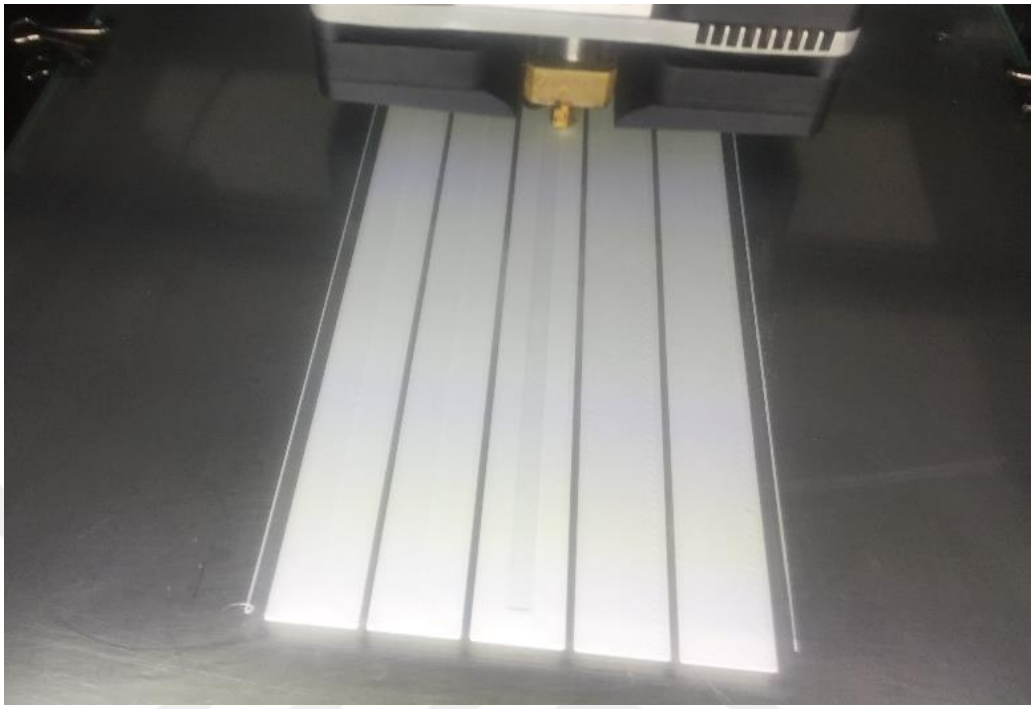

Figure 3.8 : Production of the ASTM D3039 samples.

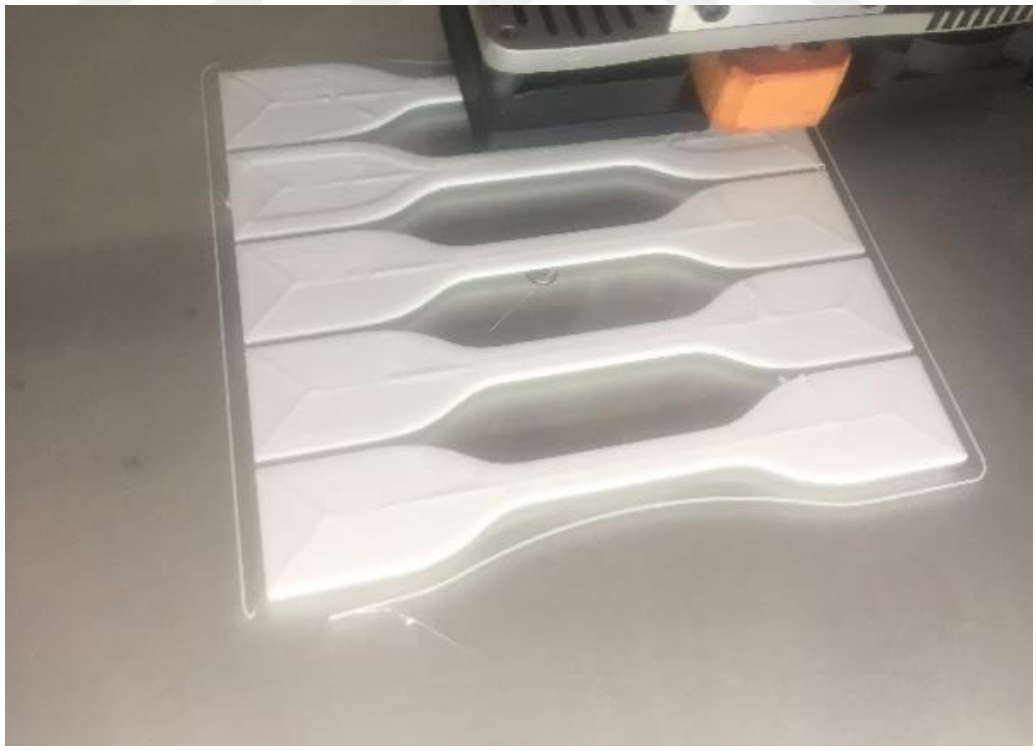

Figure 3.9 : Production of the ASTM D638 samples.

Usage of the tab is not a requirement referred to in ASTM D3039 section 8.2.1.2 [2]. It is recommended to be used if early failures were observed. After the production of

ASTM D3039 samples, some failures were recorded during trial tests, and the remaining coupons were prepared with tabs. To get good adhesion epoxy adhesive was used, see Figure 3.10. This epoxy has two components, part A is liquid metal (epoxy resin) and part B is given as hardener. The properties of this epoxy are as follows;

- It can be used for metal to metal, metal to polymer surfaces
- It has 130 kg/cm2 (12,74 Mpa) bond strength
- It can be used between -30 and +150 °C
- Chemical and water-resistant

Recommended tab geometries and tab materials are given in ASTM D3039 section 8.2.2.3. and 8.2.2.6. respectively [xx]. It refers that E-glass fibers, steel, or the same materials can be used for tabs. In this study, steel tabs were used, see Figure 3.11. The bonded tab length has to be calculated as per equation 3.1. [7]. It was calculated as min 15,96 mm. Tabs were prepared based on this dimension, see Equation 2.1.

$$L_{min} = F^{tu}h/2F^{su} \tag{3.1}$$

According to ASTM D3039 section 8.2.2.6.(2014), "Lmin = minimum required bonded tab length, mm [in.], Ftu = ultimate tensile strength of coupon material, MPa [psi]h = coupon thickness, mm [in.]; and Fsu = ultimate shear strength of adhesive, coupon material, or tab material (whichever is lowest), MPa [psi]" (p.6).

Figure 3.10 : Epoxy adhesive**.**

Figure 3.11 : Used tabs.

3.3 Annealing

To obtain the effects of the annealing process on mechanical properties, 20 samples produced with the parameters seen in Figure 3.6 and Figure 3.12.

Annealing was performed at two different temperatures and times as follows,

- 55 °C 1h/ 4h
- Over 5 °C of Tg 1h/ 4h

Annealing is performed NUVE FN400 brand oven, as seen in Figure 3.12. The properties of the oven are given in Table 3.6.

Figure 3.12 : Lab scale oven (Nuve FN400 brand).

Table 3.6 : Properties of the oven.

Properties	
Temperature Range	+70-150°C
Temperature Stability	0,2°C
Temperature Tolerance	±2
Power	800W
Dimensions (inner)	420 X 320 x 360 mm

3.4 Scanning Electron Microscopy (SEM)

The print structure and fracture locations of the samples were investigated using scanning electron microscopy (SEM) (Jeol Branded) as seen in Figure 3.13. The effects of air gaps on microstructure were examined via SEM from small samples as seen in Figure 3.13.

Figure 3.13 : Scanning electron microscopy (SEM)**.**

3.5 Tensile Testing

Specimens are tested to find out the tensile properties of samples that produce by different parameters. A total of 80 samples were tested with a 2 mm/min deformation rate by using Zwick/Roell Z100 at room temperature as seen in Figure 3.14. At least 3 repeat tests were performed for a one constant parameter set.

Figure 3.14 : Tensile test machine.

4. RESULTS AND DISCUSSIONS

This chapter includes the tensile test results of the PETG specimens and comparisons between the literature and the results. The effects of infill patterns, test standards, negative air gap, and annealing were detailly discussed.

4.1 Mechanical Properties of 3D-printed PETG Polymer

Tensile properties such as ultimate tensile strength (UTS) and elastic modulus (E) of both as-printed and annealed PETG were performed with three repeat tests at least. Five specimens for each sample fabricated per ASTM D3039 were tested due to test results and failure locations. Tested specimens were given in Appendix C. When the tensile specimens reached the UTS, the test was stopped due to no need to measure the elongation of the specimens.

4.1.1 Effects of specimen standard types on mechanical properties

40 samples that are produced as only concentric infill patterns with two different tensile test standards (ASTMD3039 and ASTM D638) were tested and results were given in Figure 4.1, and Figure 4.2.

Note: 20 samples off 40 were printed as 0%, 10%, 15%, and %20 negative air gaps as per ASTM D3039.

Note: 20 samples off 40 were printed as 0%, 10%, 15%, and %20 negative air gaps as per ASTM D638.

It was observed that there is no linear relation between the two different standards, as seen in Figure 4.1, and Figure 4.2. According to the comparison of the elastic modulus, three off four samples of ASTM D3039 were higher than ASTM D638. Instead of elastic modulus, three off four samples of ultimate tensile strength of ASTM D638 were higher than ASTM D3039. The highest results were marked as * in Table 4.1 and the calculations of the % differences were given in Table 4.2. As a result of these reasons, it was decided to continue with ASTM D638 for the second set.

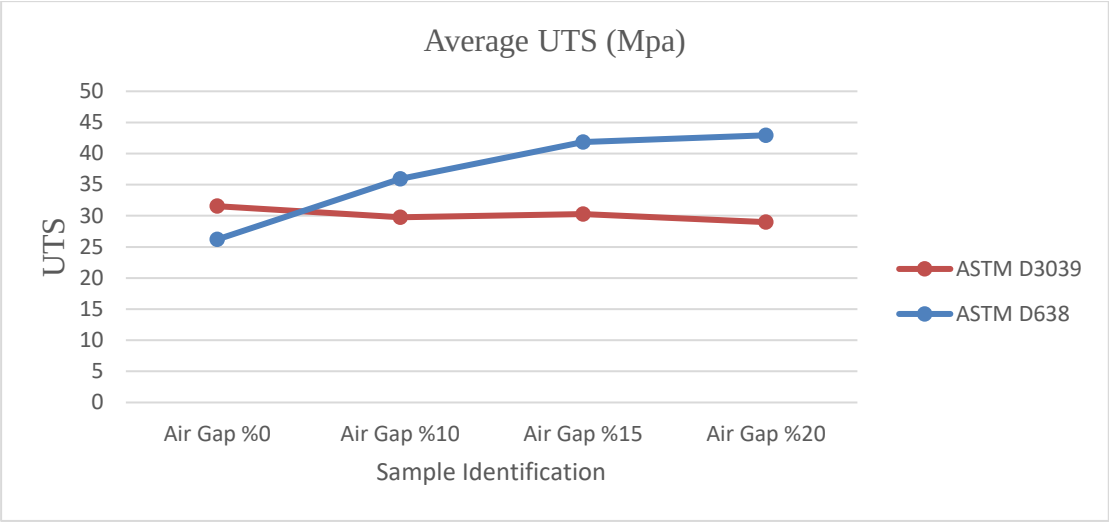

Figure 4.1 : UTS Results of the samples fabricated as two different standards with the concentric patterns.

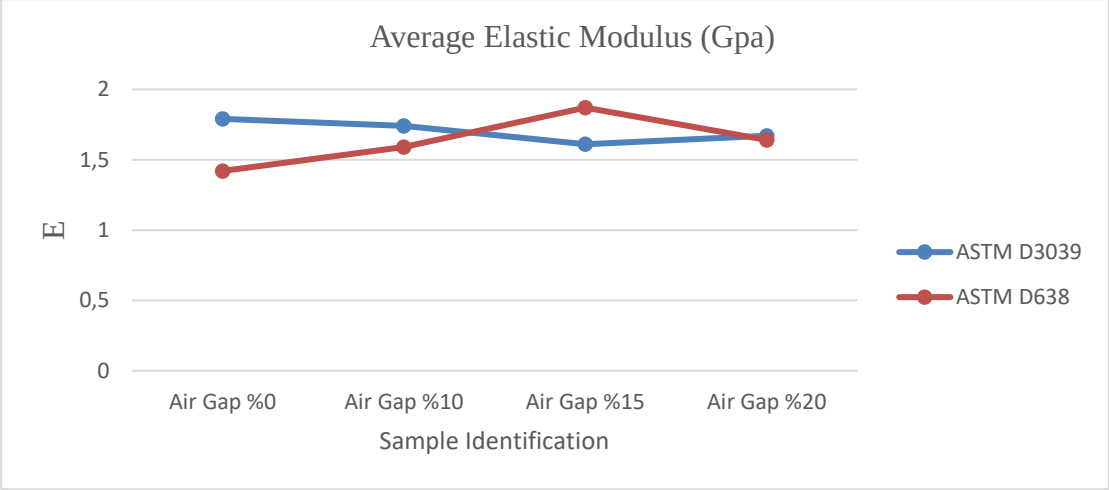

Figure 4.2 : E (Mpa) Results of the samples fabricated as two different standards with the concentric patterns.

Table 4.1 : Average test results of the samples fabricated as two different standards with the concentric pattern.

Sample Identification	E (Gpa) Average	U.T.S. (Mpa Average)
CBA0-ASTM D 3039	1,79	31,54
CBA10-ASTM D 3039	1,74	29,77
CBA15-ASTM D 3039	1,61	30,25
CBA20-ASTM D 3039	1,67	28,98
CAA0-ASTM D638 TYPE IV	1,42	26,2
CAA10-ASTM D638 TYPE IV	1,59	35,94
CAA15-ASTM D638 TYPE IV	1,87*	41,84*
CAA20-ASTM D638 TYPE IV	1,64	42,93*

Table 4.2 : Comparison of the test results of the samples fabricated as concentric with two different standards**.**

Comparison Details	% Comparison Between Sample Identification	% Differences in E	% Differences in UTS
Comparison of the Different Specimen Standards (ASTM 3039 vs ASTM D638 TYPE IV at concentric)	CBA0 vs CAA0	20,58	16,96
Comparison of the Different Specimen Standards (ASTM 3039 vs ASTM D638 TYPE IV at concentric)	CBA10 vs CAA10	8,96	-20,69
Comparison of the Different Specimen Standards (ASTM 3039 vs ASTM D638 TYPE IV at concentric)	CBA15 vs CAA15	-16,33	-38,31
Comparison of the Different Specimen Standards (ASTM 3039 vs ASTM D638 TYPE IV at concentric)	CBA20 vs CAA20	1,80	-48,16

(*) Negative values indicated a % increase in properties. Positive values were shown that there was no improvement in mechanical properties.

4.1.2 Effects of infill pattern on mechanical properties

40 samples that were produced with two different infill patterns (concentric and rectilinear) as per ASTM D3039 were tested. It was seen that the specimens producing concentric patterns showed the highest E and UTS properties compared to the rectilinear ones, see Table 4.3, and Table 4.4. In the literature review, it was also seen that rectilinear samples give the lowest properties than concentric samples [35]. According to the comparison of the results with literature studies [36], the results are found to be compatible with literature values, as seen in Figure 4.3 and Figure 4.4.

Table 4.3 : Test results of the samples fabricated as two different infill patterns with the same specimen standard.

Sample Identification	E (Gpa) Average	U.T.S. (Mpa Average)
CBA0-ASTM D 3039	1,79	31,54
CBA10-ASTM D 3039	1,74	29,77
CBA15-ASTM D 3039	1,61	30,25
CBA20-ASTM D 3039	1,67	28,98
R100-ASTM D 3039	0,89	16,52
R110-ASTM D 3039	0,91	15,52
R115-ASTM D 3039	1,04	17,55
R120-ASTM D 3039	1,17	19,40

Table 4.4 : Comparison of the test results of the samples fabricated as two different infills with ASTM D3039 standard.

Comparison Details	% Comparison Between Sample Identification	% Differences in E	% Differences in UTS
Comparison of the Different Infills (Rectilinear vs concentric)	CBA0 vs RBA0	50,54	47,64
Comparison of the Different Infills (Rectilinear vs concentric)	CBA10 vs RBA10	47,82	47,88
Comparison of the Different Infills (Rectilinear vs concentric)	CBA15 vs RBA15	35,39	42,01
Comparison of the Different Infills (Rectilinear vs concentric)	CBA20 vs RBA20	29,65	33,06

(*) Positive values indicated % decreasing properties. Positive values were shown that there was no improvement in mechanical properties.

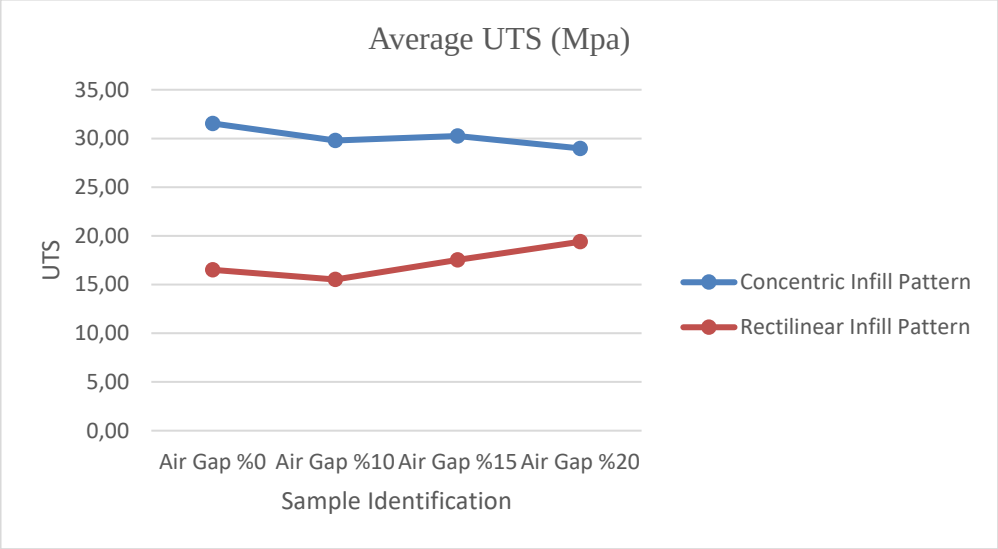

Figure 4.3 : UTS Results of the samples fabricated as two different patterns as per ASTM D638 Type IV.

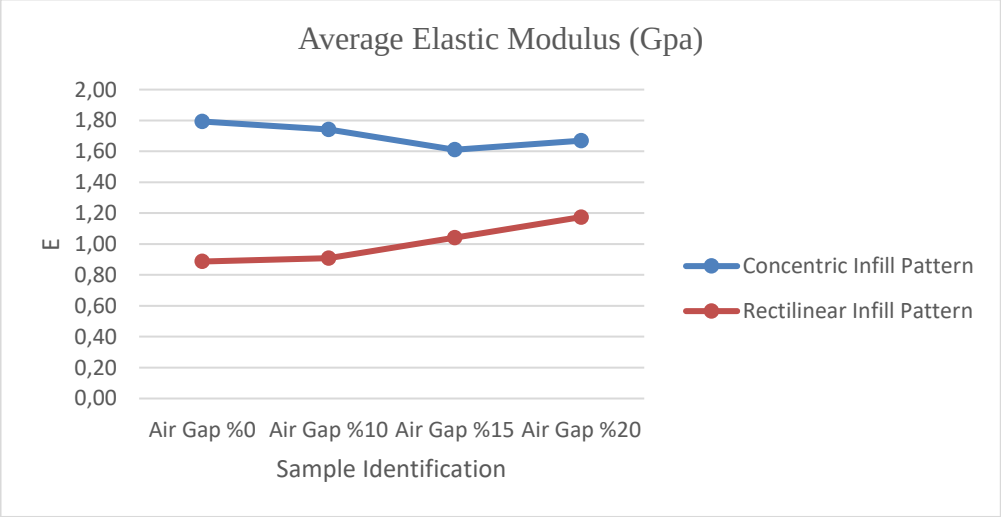

Figure 4.4 : E (Mpa) Results of the samples fabricated as two different patterns as per ASTM D638 Type IV.

4.1.3 Effects of negative air gap on mechanical properties

Effects of the negative air gap on tensile properties were investigated from samples produced in concentric and rectilinear infills. The air gap effect on samples produced not only with different patterns but also with different sample standards was examined.

Although the negative air gap is increased, there is no relation between samples built as concentric ASTM D3039 as seen in Table 4.3. Instead of samples produced as concentric infill, rectilinear samples (ASTM D3039) show that a 20% air gap resulted

in the highest elastic modulus and UTS, as seen in Figure 4.3 and Figure 4.4 . However, rectilinear samples (ASTM D3039) have the lowest E and UTS properties than other samples.

The highest increase on UTS properties (63,89% between C100 and C120) was reported with concentric samples manufactured as per ASTM D638 Type IV, seen in Table 4.5. Based on the comparison of elastic modulus values, the samples produced with 15% negative air gap exhibit the highest positive influence of decreased air gap.

There is a linear relationship while increasing the negative air gap from 0% to 20% for all samples except concentric ones produced as per ASTM D3039. Due to this reason, it was considered to continue with concentric samples (produced as per ASTM D638 Type IV) instead of rectilinear samples (produced as per ASTM D3039) for a second set to be examined annealing effects on samples. For the second set, it was decided to continue with a 15% negative air gap due to high differences not only on elastic modulus but also on UTS properties. Although, a 20% negative air gap resulted in a 63,89% increase on UTS, it continued with a 15% negative air gap for the second set due to both having a 59,74% increase in UTS and showing the highest increase in elastic modulus was found to be more reasonable.

Table 4.5 : Comparison of the negative air gaps for two different specimen standards.

Sample Identification	% Differences of E (Gpa) Average based on increasing air gap	% Differences of UTS (Mpa) Average based on increasing air gap
CAA0-ASTM D638 TYPE IV vs CAA10-ASTM D638 TYPE IV	11,38	37,18
CAA0-ASTM D638 TYPE IV vs CAA15-ASTM D638 TYPE IV	**31,54**	59,74
CAA0-ASTM D638 TYPE IV vs CBA20-ASTM D638 TYPE IV	15,12	**63,89**
R100-ASTM D3039 vs R110-ASTM D3039	2,51	-6,03
R100-ASTM D3039 vs R115-ASTM D3039	17,31	6,24
R100-ASTM D3039 vs R120-ASTM D3039	**32,44**	**17,45**

(*) Positive values indicated % increasing on properties.

A study discussed the effects of overlap ratio from samples produced per ISO 527-2. Based on the results, it was recorded that a 20% negative air gap improves 15% UTS and 10% E [49]. Based on our results, 15,12% improvement on UTS and 63,89% improvement on E were observed. It was concluded that our results were in line with the results as discussed in the paper above [49].

4.1.4 Effects of annealing temperature and time on mechanical properties

Effects of annealing were investigated in two stages time and temperature variables. The temperature was selected as 55°C and 80°C (5°C above Tg) and the holding times were decided as 1 hour and 4 hours. All test samples were produced as per concentric infill and 15% negative infill per ASTM D368 Type IV. The average results and comparisons were given in Table 4.6.

- At 1 hour, 55°C was 17,94% (for E) and 13,73% (for UTS) higher than 80°C.
- At 4 hours, 55°C was 17,10% (for E) and 13,67% (for UTS) higher than 80°C.
- At 80°C, 4 hours hold time was 0,62% (for E) and 1,7 % (for UTS) higher than 1 hour.
- At 55°C, 4 hours hold time was 0,40% (for E) lower and 1,71% (for UTS) higher than 1 hour.

The last comparison was done between annealed and non-annealed samples, see Table 4.7, Table 4.8, Figure 4.5, and Figure 4.6. For this study, the given properties of CAA15 were taken in Table 4.1.

Comparison of the Set1 vs non-annealed part results

Non-annealed parts were 14,32% (for E) and 2,16% higher than results of Set 1.

Comparison of the Set2 vs non-annealed part results

Non-annealed parts were 13,77% (for E) and 0,39% higher than results of Set 2.

Comparison of the Set3 vs non-annealed part results

Non-annealed parts were 4,42% (for E) and 13,41% lower than the results of Set 3.

Comparison of the Set4 vs non-annealed part results

Non-annealed parts were 4,01% (for E) and 15,38% lower than the results of Set 4.

Table 4.6 : The test results of the annealed samples.

Sample Identification	Sample Number	Air Gap (%)	Infill Pattern	Variable Parameters	Results (Average) - Elastic Modulus (Gpa)	Results (Average)- UTS (Mpa)	Additional Variable Parameters
CAT1	5	15	Concentric	ASTM D638 TYPE IV	1,61	40,94	Set 1: 80°C- 1 hour
CAT4	5	15	Concentric	ASTM D638 TYPE IV	1,62	41,68	Set 2: 80°C- 4 hours)
CAP1	5	15	Concentric	ASTM D638 TYPE IV	1,96	47,45	Set 3: 55 °C – 1 hour
CAP4	5	15	Concentric	ASTM D638 TYPE IV	1,95	48,28	Set 4: 55 °C – 4 hours

Table 4.7 : The comparisons of the annealed samples vs non-annealed samples.

Comparison Details	% Comparison Between Sample Identification	% Differences on E	% Differences on UTS
Set 1: 80°C - 1 hour	CAA15 vs CAT1	14,32	2,16
Set 2: 80°4 hours	CAA15 vs CAT4	13,77	0,39
Set 3: 55 °C – 1 hour	CAA15 vs CAP1	-4,42	-13,41
Set 4: 55 °C – 4 hours	CAA15 vs CAP4	-4,01	-15,38

(*) Negative values indicated % increasing properties. Positive values were shown that there was no improvement in mechanical properties.

Table 4.8 : The % comparison of the annealed samples based on time and temperature effects.

Comparison Details	% Comparison Between Sample Identification	% Differences on E	% Differences on UTS
Comparison of the Different Annealing Temperatures (5°C above Tg) keeping ASTM D638 TYPE IV and time (1h) as a constant	CAP1 vs CAT1	17,94	13,73
Comparison of the Different Annealing Temperatures (5°C above Tg) keeping ASTM D638 TYPE IV and time (4h) as a constant	CAP4 vs CAT1	17,10	13,67
Comparison of the Different Annealing times (1h) keeping ASTM D638 TYPE IV and temperature (5°C above Tg) as a constant	CAT4 vs CAT1	0,62	1,77
Comparison of the Different Annealing times (4h) keeping ASTM D638 TYPE IV and temperature (5°C above Tg) as a constant	CAP4 vs CAP1	-0,40	1,71

(*) Negative values were indicated % increasing properties.

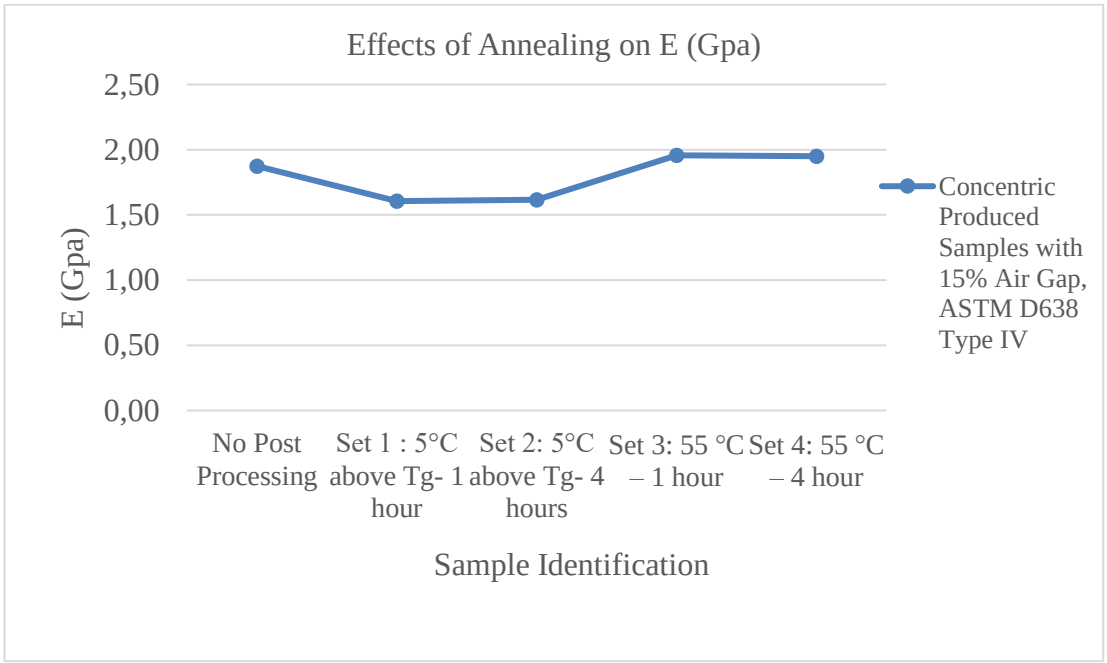

Figure 4.5 : E (Gpa) Results of the samples.

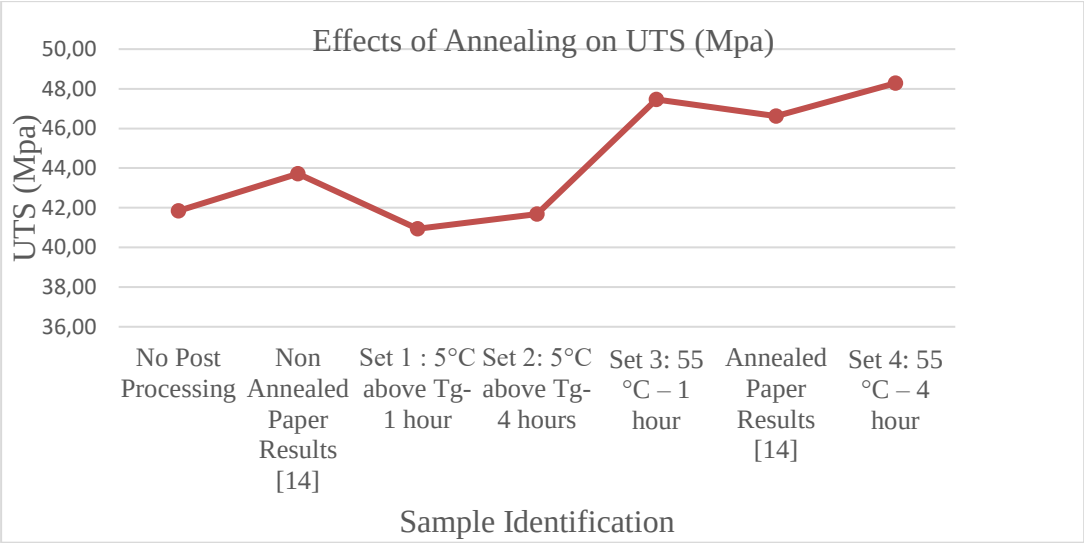

Figure 4.6 : UTS (Mpa) Results of the samples.

(*) Negative values indicated % increasing properties. Positive values were shown that there was no improvement on mechanical properties.

It has also been explained in the literature that the heat treatment performed above Tg (120 °C) does not cause any improvement in the UTS properties of PETG [48].

These results were compared with literature results were examined annealing effects from PETG samples produced with the following properties; line pattern, ASTM D638 Type I (see Figure 4.7), annealed at 80°C (5°C above Tg), 0° (flat samples) 0,2mm raster thickness, 100% infill, two shells, two top/bottom layers and three specimens [35]. The increase was recorded as a maximum 7,84% increase, see Table 4.9 [38]. In our studies, a 13,41% increase was recorded. There was a difference between using the samples in the literature was as the negative air gap. Based on this comparison, it concluded that both air gap and annealing show the highest mechanical properties.

UTS result of PETG in this literature study was added in Figure 4.5, and Figure 4.6 to show improvement clearly [38].

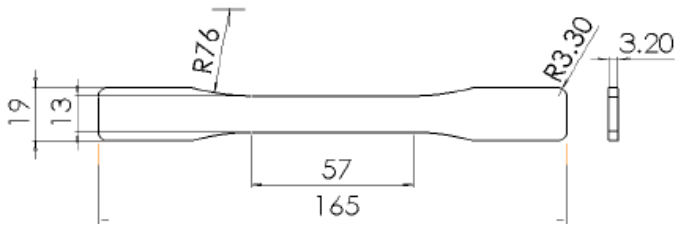

Figure 4.7 : Dimensions of the used specimen standard per ASTM D638 Type I **[38]**.

Table 4.9 : Calculated % increase from annealed PETG samples produced as per ASTM D638 [38].

Specimen	Non-Annealed (psi)	Annealed (psi)	% Increase
PETG-Line-0°-90°	4,92	5,53	12,40
PETG-Line ± 45	4,26	4,44	4,27
PETG-Concentric-0°	6,34	6,76	6,70
Average PETG	5,17	5,58	7,84

4.2 Comparison of the All Test Results with Injection Molded Results

In addition, the annealing effect was studied with the parameters of the CAA15 sample, which gave the best results. The results of annealed and injected molded samples (IM) were compared, see Table 4.10, Figure 4.8 and Figure 4.9. According to these results, it was seen that the results at 55°C were better than those with annealing at 80°C. With this study, it has been reported that the samples kept at 55°C for 1 hour are only 7,21% for E and 3,44% for UTS lower than the molded samples. At the same time, the results of samples held at 55°C for 4 hours were only 6,84% lower in E and 5,09% in UTS, and the results closest to the results of molded samples were obtained.

Table 4.10 : Comparison of the tensile test results injection-molded sample results.

Sample Identifications	Results (Average) - Elastic Modulus (Gpa)	Results (Average)-UTS (Mpa)	% Comparison Between Sample Identification	% Differences on E	% Differences on UTS
CBA0	1,79	31,54	CBA0 vs IM	14,60	36,91
CBA10	1,74	29,77	CBA10 vs IM	17,02	40,45
CBA15	1,61	30,25	CBA15 vs IM	23,31	39,49
CBA20	1,67	28,98	CBA20 vs IM	20,49	42,05
CAA0	1,42	26,20	CAA0 vs IM	32,18	47,61
CAA10	1,59	35,94	CAA10 vs IM	24,46	28,13

Table 4.10 (continued) : Comparison of the tensile test results with the injection molded sample results.

Sample Identifications	Results (Average) - Elastic Modulus (Gpa)	Results (Average)- UTS (Mpa)	% Comparison Between Sample Identification	% Differences on E	% Differences on UTS
CAA15	1,87	41,84	CAA15 vs IM	10,78	16,31
CAA20	1,64	42,93	CAA20 vs IM	21,92	14,14
RBA0	0,89	16,52	RBA0 vs IM	57,76	66,97
RBA10	0,91	15,52	RBA10 vs IM	56,7	68,96
RBA15	1,04	17,55	RBA15 vs IM	50,45	64,91
RBA20	1,17	19,4	RBA20 vs IM	44,06	61,21
CAT1	1,61	40,94	CAT1 vs IM	23,55	18,12
CAT4	1,62	41,68	CAT4 vs IM	23,07	16,64
CAP1	1,96	47,45	CAP1 vs IM	6,84	5,09
CAP4	1,95	48,28	CAP4 vs IM	7,21	3,44
SMART MATERIAL 3D (IM)	2,1	50			

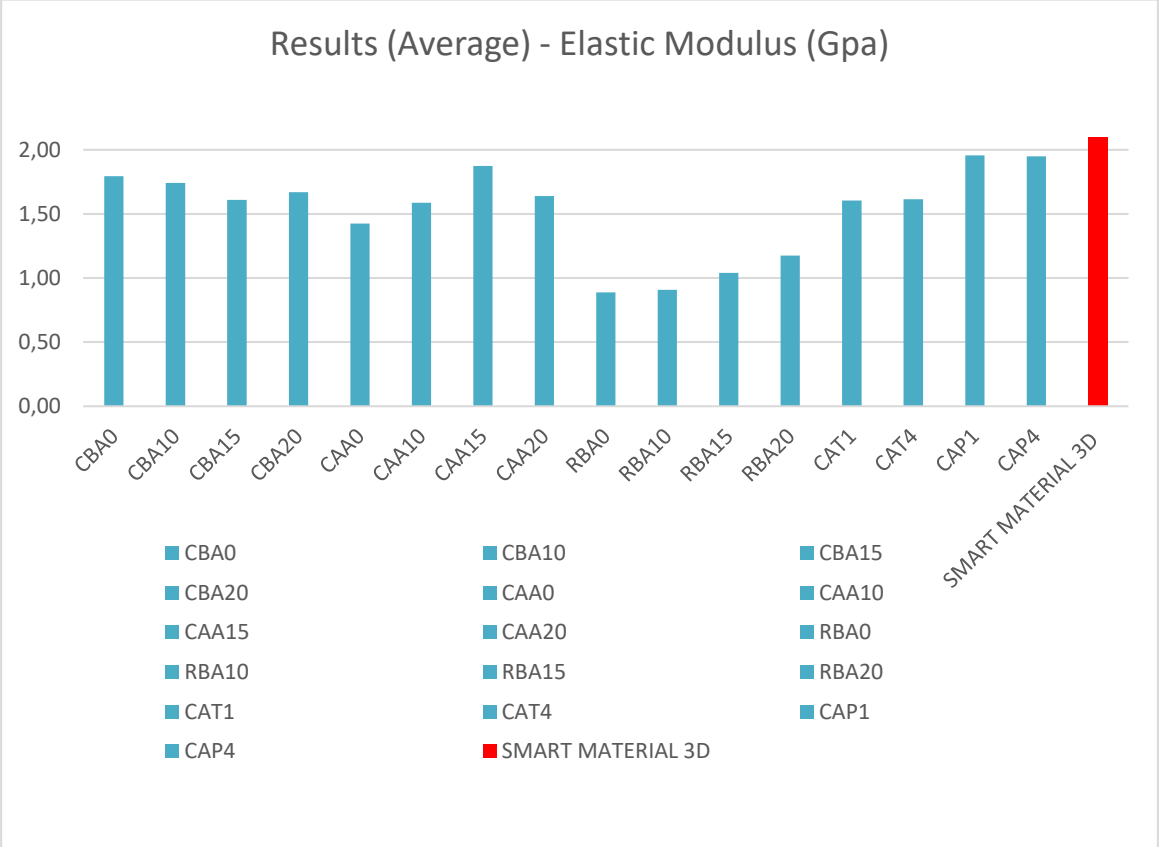

Figure 4.8 : Comparison of the FFF test results with injection molded results for E.

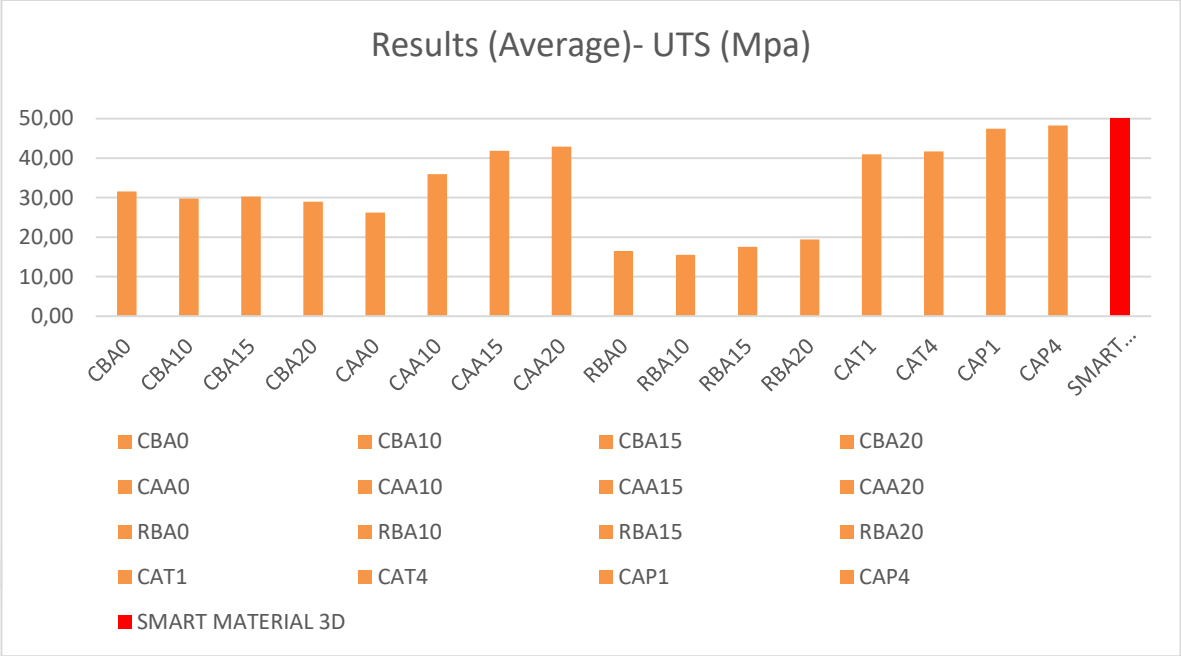

Figure 4.9 : Comparison of the FFF test results with injection molded results for UTS.

4.3 Examinations of the Airgaps in the SEM

Firstly, the small rectangular shaped parts (8 quantities) were produced to check the producibility based on desired parameters. After visual inspection of these small samples, delamination was observed, as seen in Figure 3.7. To get a better surface finish, top/a bottom surface skin setting was found and applied in Ultimaker Cura Slicer program. All tensile samples were produced by using a top/bottom surface skin setting of the ULTIMAKER CURA 4.13.1. to get a high-quality surface. Thanks to the top/bottom surface skin delamination problem of the layers was solved and a high surface finish was obtained.

All these small samples were examined in SEM to check inner structures and air gaps, as seen in Figure 4.10, Figure 4.11, Figure 4.12, Figure 4.13, Figure 4.14, Figure 4.15, Figure 4.16, and Figure 4.17. Based on the SEM images, it was seen that increasing the negative air gap decreased layer width as expected and closed the gap between layers which was measured as 28.2 microns from the sample produced as a 0% air gap, see Figure 4.10. As observed in section 4.1.3, increasing air gap resulted as high in the tensile properties. It can be noted that it was difficult to distinguish layers by SEM while increasing the negative air gap.

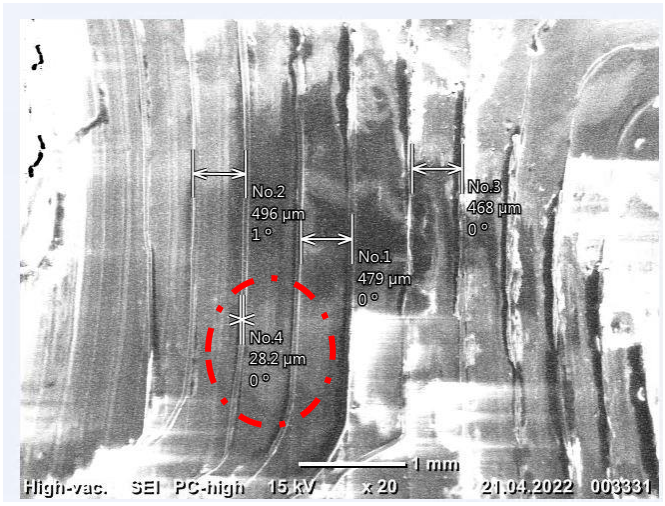

Figure 4.10 : SEM Image of samples produced with concentric and 0% negative air gap.

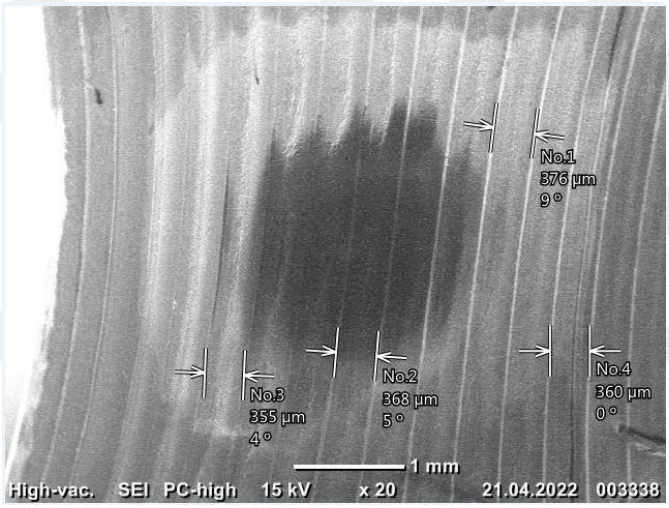

Figure 4.11 : SEM Image of samples produced with concentric and 10% negative air gap.

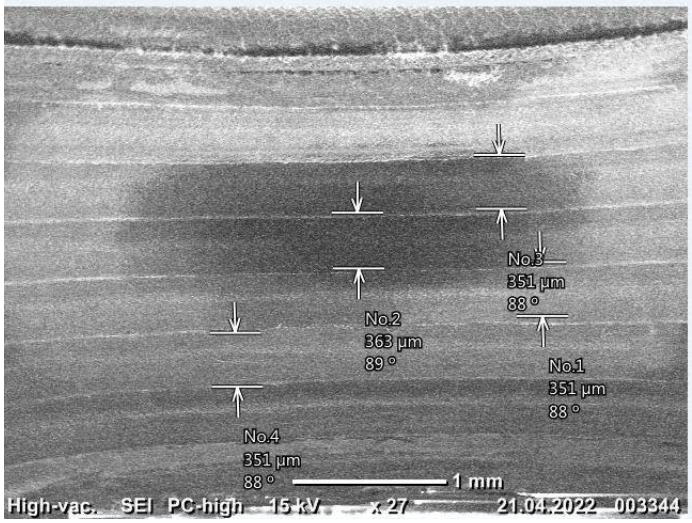

Figure 4.12 : SEM Image of samples produced with concentric and 15% negative air gap.

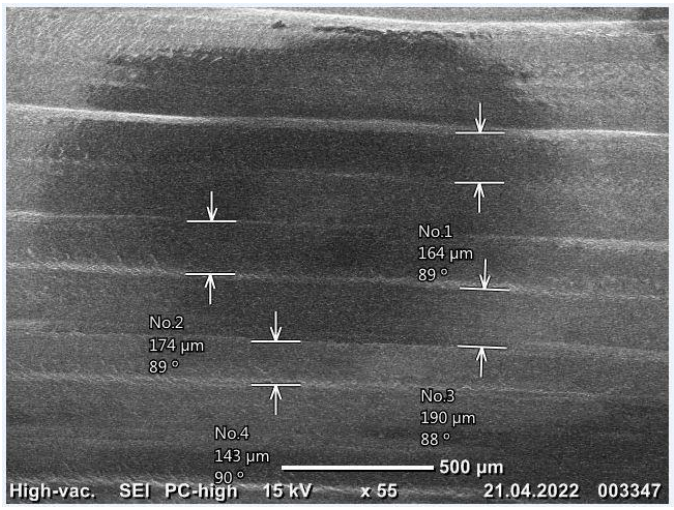

Figure 4.13 : SEM Image of samples produced with concentric and 20% negative air gap.

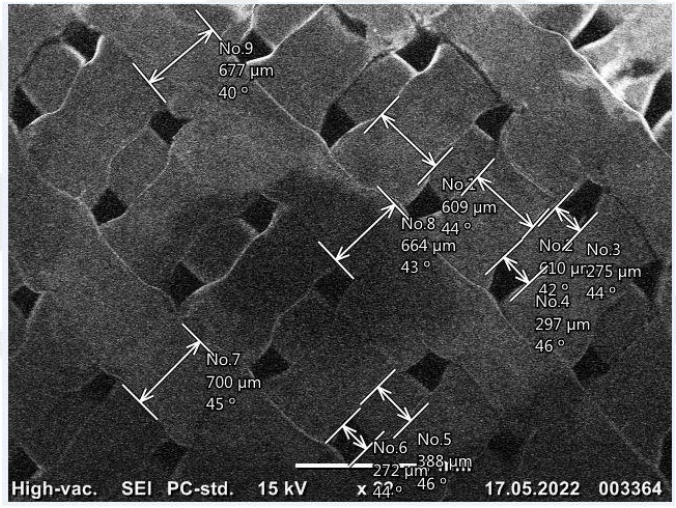

Figure 4.14 : SEM Image of samples produced with rectilinear and 0% negative air gap.

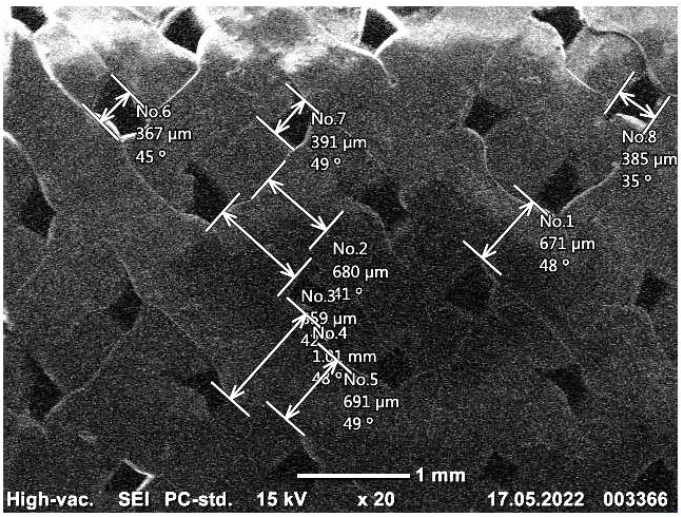

Figure 4.15 : SEM Image of samples produced with rectilinear and 10% negative air gap.

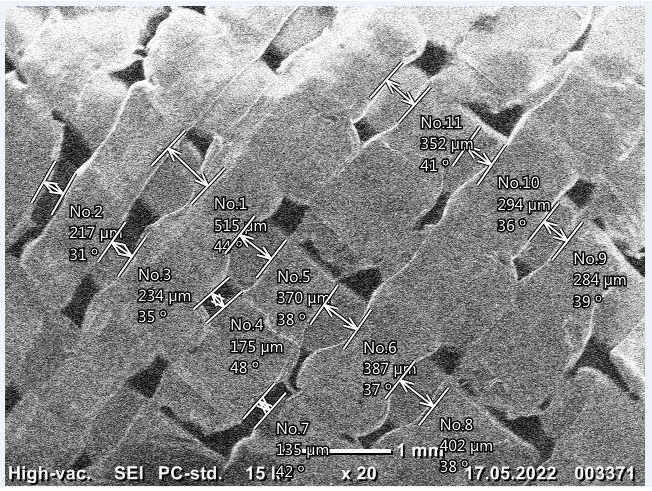

Figure 4.16 : SEM Image of samples produced with rectilinear and 15% negative air gap.

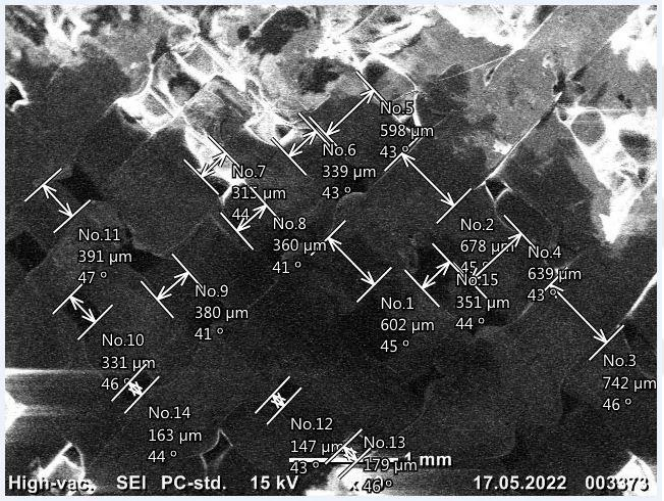

Figure 4.17 : SEM Image of samples produced with rectilinear and 20% negative air gap.

4.4 Examinations of the Failure Locations of the 3D-printed PETG Polymer

In this study, failure locations of the all tested tensile specimens were visually examined to check the validity of the results, as seen in Appendix C. Failure mode and locations were given as per ASTM D 3039 section 11.9 [7]. Tensile specimens prepared per ASTM D638 Type IV were evaluated according to whether the fracture surfaces remained in the inner narrow length or not. All details were given in Appendix C.

Non-Annealed concentric samples (ASTM D3039)

0% Air Gap: All specimens were fractured from the GAT (G: Grip/tab A: At grip/tab T: Top) zone.

10% Air Gap: One off four specimens were fractured from the LGM (L: Lateral G: Gage M: Middle) zone. The others were broken from the GAT zone.

15% Air Gap: One off four specimens were fractured from the LGM zone. The others were broken from the GAT zone.

20% Air Gap: All specimens were fractured from the GAT zone.

Non-Annealed concentric samples (ASTM D638 TYPE IV)

0% Air Gap: All specimens were fractured from the inner narrow length.

10% Air Gap: Two off four specimens were fractured from the outside narrow length zone. The others were broken from inner narrow length.

15% Air Gap: Two off four specimens were fractured from the outside narrow length zone. The others were broken from inner narrow length.

20% Air Gap: All specimens were fractured from the inner narrow length.

Non-Annealed rectilinear samples (ASTM D3039)

0% Air Gap: All specimens were fractured from the GAT zone.

10% Air Gap: All specimens were fractured from the GAT zone.

15% Air Gap: All specimens were fractured from the GAT zone.

20% Air Gap: One off four specimens were fractured from the AGM (A: Angled G: Gage M: Middle) zone. Remainers were broken from the GAT zone.

Annealed samples

All annealed samples were broken from inside of the narrow length and all specimens were found valid, see Appendix C.

Due to the sample orientation selecting flat, trans raster failure was observed as expected. There is no brittle fracture observed which is also seen on specimens. It is also in line with the literature results [36], [38]. Examinations of the fracture locations in SEM are given in Appendix D.

Annealed sample fracture surfaces were found similar to other annealed tensile samples of PEEK and ABS, see Figure 4.18, Figure 4.19, and Figure 4.20.

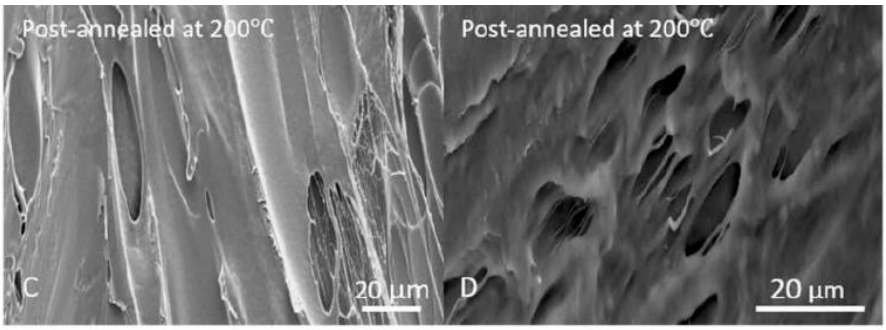

Figure 4.18 : Examination of PEEK samples after annealing at 200 °C at (50 °C above Tg of PEEK) [56].

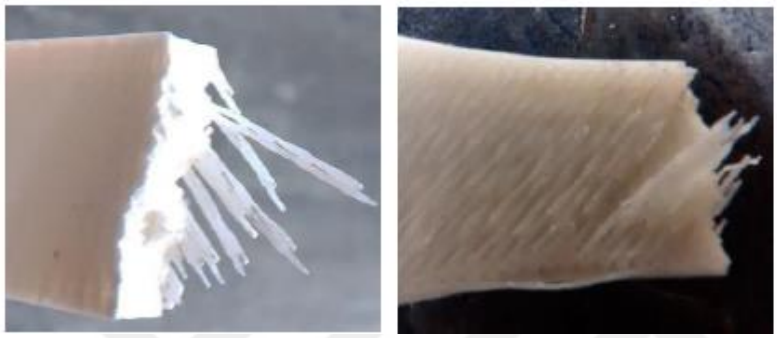

Figure 4.19 : Fracture surface of ABS samples after annealing 110 °C (at 5 °C above Tg of ABS) [35].

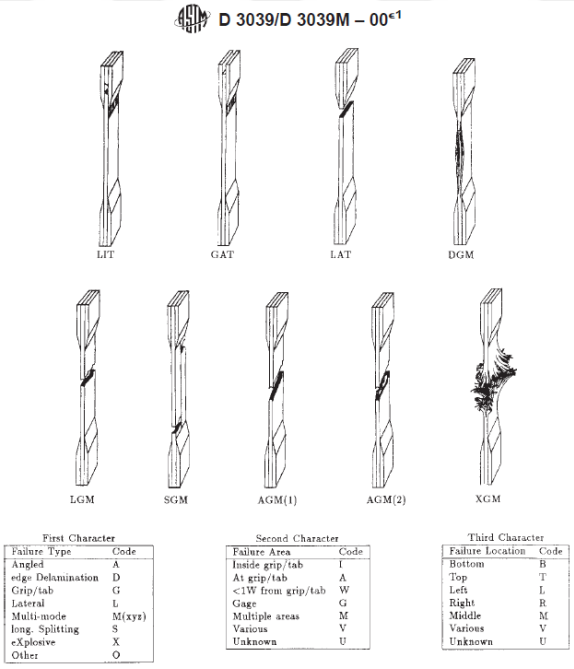

Figure 4.20 : Fracture location definitions as per ASTM D3039 [7].

Based on the literature review, it was also noticed that stress concentration is another main factor to explain failure locations for specimen standards [3]. This issue is still a controversial topic.

5. CONCLUSION

This research involving comprehensive parametric studies investigated the effects of the negative air gap (0%, 10%, 15%, and 20%), sample standard types (ASTM D638 Type IV and ASTM D3039), infill patterns (concentric and rectilinear), temperature & time selection (Over 5°C of Tg- 1h/ 4h and 55°C- 1h/ 4h) for the post heat treatment on mechanical properties of PETG samples produced by FFF method.

The main contributions of this study are summarized as follows:

- The concentric pattern has higher properties than rectilinear samples (29,65-50,54% improvement for E and 33,06-47,88% improvement for UTS).
- The samples prepared accordingly ASTM D638 TYPE IV concentric infill have highest tensile properties than ASTM D3039 concentric infill (16,33% improvement for E and 20,69-48,16% improvement for UTS).
- The negative air gap effects were investigated on samples fabricated as concentric and rectilinear patterns. The improvement was not recorded in ASTM D3039 the concentric samples. However, rectilinear samples showed an increase trend, (2,51-32,44% for E and 6,24-17,45 for UTS).
- The negative air gap effects were investigated on samples fabricated as per ASTM D638 TYPE IV and ASTM D3039 with the concentric pattern. Increasing negative air gap on ASTM D638 TYPE IV samples (close to porosities inside of the structure) resulted in high tensile properties. Improvement was recorded for E as 11,38-31,54% and improvements were recorded for 37,18 and 63,89%.
- Increasing negative air gap on ASTM D3039 samples (close to porosities inside of the structure) did not result in high tensile properties, there was no increasing trend.

- Based on the first results, it was recorded that samples produced as per ASTM D638 TYPE IV with the concentric pattern and 15% negative air gap had highest tensile properties (E: 1,89 Gpa, UTS: 41,84 Mpa) than other specimen results. It was decided to continue with this best parameter set to investigate the annealing time and temperature.
- 4 parameters set was selected based on literature reviews.
- According to the comparison of the tensile test results at 80°C, the specimens were held for 4 hours in a furnace as 0,62% for E and 1,77% UTS higher than 1 hour.
- According to the comparison of the tensile test results at 55°C, the specimens held for 4 hours were 0,40 % lower for E and 1,71% higher for UTS higher than 1 hour.
- Tensile properties at 55°C for 1 hour were higher 17,94% for E and 13,73% for UTS than at 80° 1 hour.
- Tensile properties at 55° for 4 hours were higher 17,10% for E and 13,67% for UTS than at 80°C for 4 hours.
- The results of annealing at 80°C for 1 hour were lower than non-annealed parts (14,32% for E and 2,16% for UTS). If annealing time was increased from 1 hour to 4 hours at 80°C, the difference was decreased but it was still lower than non-annealed parts (13,77% for E and 0,39% for UTS).
- The results of annealing at 55°C for 1 hour were lower than non-annealed parts (4,42% for E and 13,41% for UTS). When annealing time was increased from 1 hour to 4 hours at 55°C, E and UTS were increased respectively, by 4,01% and 15,38%.
- When the results of the 4 annealing parameter sets were compared, it was concluded that the highest improvement between the sets was in Set 4. The effects on tensile properties of increasing time at 55°C were found to be remarkable. It can be concluded that increasing time at high temperature (Above 5°C Tg) affects the mechanical properties negatively. On the contrary to this result, it has been observed that increasing time has benefits on mechanical properties, especially on UTS.

- All results are compared with injected molded sample results. As a result of all comparisons, it was seen that the concentric ASTM D3039 and rectilinear ASTM D3039 samples were far below the molded samples. According to ASTM D638 TYPE IV concentric results, it has been determined that as the air gap closes, the molded samples are approached, 32.18%-10.78% for E and 47.61%-14.14% for UTS.
- Within the scope of this thesis, the annealing effect was also studied and these comparisons were completed with annealing samples. According to the results, it was observed that the samples annealed at 55 °C for 1 and 4 hours converged the most to the molded results. Although it is seen that the difference in samples still is 6,84% for E and 5,09% for UTS (held for 1 hour in the furnace) and 7,21% for E and 3.44% for UTS (held for 4 hours in the furnace), it has been proven that injection molded results can be approached by optimization studies of the right sample and parameter pairs.
- Based on visual inspection: Except for two specimens (LGM), all remaining specimens were fractured from the GAT zone (Non-Annealed Concentric Samples- ASTM D3039).
- Except for one specimen (AGM), all remainder specimens were fractured from the GAT zone (Non-Annealed Rectilinear Samples- ASTM D638 TYPE IV):
- All annealed samples were broken from inside of the narrow length.
- Based on the investigation of the fracture surfaces via SEM, it was observed that trans-raster fracture was as expected. All rasters did not show a brittle fracture, it has ductile fracture surfaces. It was not observed not-melted or semi-melted, unexpected porosity structure inside. All SEM images showed that shell structure supported the samples and prevented early deformation of the samples. If the shell was firstly damaged, that can affect the integrity of the sample and given the early cracks, and reduce the strength. It was concluded that 3 shells worked well and enough to support the structure. All samples show that shell structure that existed even inside was fractured. There was no delamination problem in the structure.
- Finally, it can be concluded that a negative air gap helps to decrease the gap between rasters and give the highest strength. Increasing the negative air gap

by reaching overlap limits of the structure was 20% in this study. Since the decrease in E (Gpa) and high standard deviations were recorded, the second parameter study for the investigation of the annealing was continued with a 15% negative air gap at the concentric structure.

- According to tensile test results, it was seen that the strength of PETG produced with the FFF method can reach 92,8– 96,56% of the injection-molded PETG's strength.
- The studies on negative air gap cannot always be decreased porosities due to the raster print way. It is recommended that before starting air gap studies, small rectangular shaped samples have to be fabricated to measure the levels of closure on porosities.
- Finally, with parameter optimization, the strength of PETG produced with FFF has been maximized, and it is concluded that the FFF method is a competitive alternative to conventional methods.

REFERENCES

[1] A. Cano-Vicent *vd.*, "Fused deposition modelling: Current status, methodology, applications and future prospects", *Addit. Manuf.*, c. 47, s. 102378, Kas. 2021, doi: 10.1016/j.addma.2021.102378.

[2] M. Algarni ve S. Ghazali, "Comparative Study of the Sensitivity of PLA, ABS, PEEK, and PETG's Mechanical Properties to FDM Printing Process Parameters", *Crystals*, c. 11, sy 8, s. 995, Ağu. 2021, doi: 10.3390/cryst11080995.

[3] Y. Zhang, "2 - Additive manufacturing processes and equipment", *Addit. Manuf.*, s. 13.

[4] T. J. Gordelier, P. R. Thies, L. Turner, ve L. Johanning, "Optimising the FDM additive manufacturing process to achieve maximum tensile strength: a state-of-the-art review", *Rapid Prototyp. J.*, c. 25, sy 6, ss. 953-971, Tem. 2019, doi: 10.1108/RPJ-07-2018-0183.

[5] C. Scott, D. Design, D. Printing, ve D. Printing, "Up Close and Personal with GE's 3D Printed Advanced Turboprop Engine", Print., s. 5.

[6] *New Wohlers Report 2021 Finds 7.5% Growth in Additive Manufacturing Industry Despite Pandemic.* Wohlers Associates Press Release. (n.d.). Retrieved June 1, 2022, from https://www.wohlersassociates.com/press83.html

[7] ASTM International, *Standard Test Method for Tensile Properties of Polymer Matrix Composite Materials,* ASTM D3039, (2017).

[8] ASTM. I.: ASTM52900–15 standard, Terminology for Additive Manufacturing-General Principles-Terminology (2015)

[9] H. K. Dave ve J. P. Davim, Ed., *Fused Deposition Modeling Based 3D Printing*. Cham: Springer International Publishing, 2021. doi: 10.1007/978-3-030-68024-4.

[10] M.-H. Hsueh *vd.*, "Effect of Printing Parameters on the Thermal and Mechanical Properties of 3D-Printed PLA and PETG, Using Fused Deposition Modeling", *Polymers*, c. 13, sy 11, s. 1758, May. 2021, doi: 10.3390/polym13111758.

[11] C. M. Cheah, C. K. Chua, C. W. Lee, C. Feng, ve K. Totong, "Rapid prototyping and tooling techniques: a review of applications for rapid investment casting", *Int. J. Adv. Manuf. Technol.*, c. 25, sy 3-4, ss. 308-320, Şub. 2005, doi: 10.1007/s00170-003-1840-6.

[12] N. Cannell ve A. S. Sabau, "Predicting Pattern Tooling and Casting Dimensions for Investment Casting, Phase II", s. 72.

[13] M. Shah, D. R.Patel, ve S. Pande, "Additive manufacturing integrated Casting-A review", *Mater. Today Proc.*, s. S2214785322017552, Nis. 2022, doi: 10.1016/j.matpr.2022.03.413.

[14] P. Kumar, I. P. S. Ahuja, ve R. Singh, "Application of fusion deposition modelling for rapid investment casting - a review", *Int. J. Mater. Eng. Innov.*, c. 3, sy 3/4, s. 204, 2012, doi: 10.1504/IJMATEI.2012.049254.

[15] S. Körber, R. Völkl, ve U. Glatzel, “3D printed polymer positive models for the investment casting of extremely thin-walled single crystals”, *J. Mater. Process. Technol.*, c. 293, s. 117095, Tem. 2021, doi: 10.1016/j.jmatprotec.2021.117095.
[16] T. Mueller, “Investment casting and 3D printing – Perfect combination for quality castings”, s. 7.
[17] J. Wang, S. R. Sama, P. C. Lynch, ve G. Manogharan, “Design and Topology Optimization of 3D-Printed Wax Patterns for Rapid Investment Casting”, *Procedia Manuf.*, c. 34, ss. 683-694, 2019, doi: 10.1016/j.promfg.2019.06.224.
[18] P. Blake, E. Fodran, M. Koch, U. Menon, B. Priedeman, ve S. Sharp, “FDM of ABS Patterns for Investment Casting”, s. 8.
[19] K. Ukey, S. Hiremath, ve H. Majumder, “Investigation of Investment Casting Pattern Using Fused Deposition Modeling”, *Eng. Sci. Technol.*, ss. 201-207, Tem. 2021, doi: 10.37256/est.222021904.
[20] A. Brotzu, F. Felli, A. Mondal, ve D. Pilone, “Production issues in the manufacturing of TiAl turbine blades by investment casting”, *Procedia Struct. Integr.*, c. 25, ss. 79-87, 2020, doi: 10.1016/j.prostr.2020.04.012.
[21] Y. O. Aktas *vd.*, “Rapid Prototyping of a Fixed-Wing VTOL UAV for Design Testing”, *J. Intell. Robot. Syst.*, c. 84, sy 1-4, ss. 639-664, Ara. 2016, doi: 10.1007/s10846-015-0328-6.
[22] H. Klippstein ve L. Seneviratne, “Fused Deposition Modeling for Unmanned Aerial Vehicles (UAVs): A Review”, *Adv Eng Mater*, s. 17, 2017.
[23] J. E. Grady *vd.*, “A Fully Nonmetallic Gas Turbine Engine Enabled by Additive Manufacturing”, *Rapid Prototyp.*, s. 24, 2015.
[24] N. M. Lacerda, L. P. L. Oliveira, ve C. B. S. Vimieiro, “COMPARATIVE STUDY BETWEEN 3D PRINTING MATERIALS FOR APPLICATION IN A CESR PROSTHESIS”, s. 11, 2021.
[25] R. Gradl, P. (2021). *Principles of Directed Energy Deposition for Aerospace Applications*. https://doi.org/10.13140/RG.2.2.10504.75527
[26] NASA. (n.d.). *Qualification & Certification of additively manufactured parts for NASA applications - NASA technical reports server (NTRS).* NASA. Retrieved June 1, 2022, from https://ntrs.nasa.gov/citations/20190000354
[27] D. Zindani ve K. Kumar, “An insight into additive manufacturing of fiber reinforced polymer composite”, *Int. J. Lightweight Mater. Manuf.*, c. 2, sy 4, ss. 267-278, Ara. 2019, doi: 10.1016/j.ijlmm.2019.08.004.
[28] J. R. C. Dizon, A. H. Espera, Q. Chen, ve R. C. Advincula, “Mechanical characterization of 3D-printed polymers”, *Addit. Manuf.*, c. 20, ss. 44-67, Mar. 2018, doi: 10.1016/j.addma.2017.12.002.
[29] S. C. Daminabo, S. Goel, S. A. Grammatikos, H. Y. Nezhad, ve V. K. Thakur, “Fused deposition modeling-based additive manufacturing (3D printing): techniques for polymer material systems”, *Mater. Today Chem.*, c. 16, s. 100248, Haz. 2020, doi: 10.1016/j.mtchem.2020.100248.
[30] S. Park, W. Shou, L. Makatura, W. Matusik, ve K. (Kelvin) Fu, “3D printing of polymer composites: Materials, processes, and applications”, *Matter*, c. 5, sy 1, ss. 43-76, Oca. 2022, doi: 10.1016/j.matt.2021.10.018.
[31] T. Balint, J. Živčák, R. Hudák, T. Tóth, M. Kohan, ve S. Lancoš, “Destructive and non-destructive testing of samples from PLA and PETG materials”, *IOP Conf. Ser. Mater. Sci. Eng.*, c. 1199, sy 1, s. 012045, Kas. 2021, doi: 10.1088/1757-899X/1199/1/012045.
[32] Q. Shi, R. Xiao, H. Yang, ve D. Lei, “Effects of physical aging on thermomechanical behaviors of poly(ethylene terephthalate)-glycol (PETG)”,

Polym.-Plast. Technol. Mater., c. 59, sy 8, ss. 835-846, May. 2020, doi: 10.1080/25740881.2019.1695273.
[33] E. Yasa ve K. Ersoy, "Additive Manufacturing of Polymer Matrix Composites", içinde *Aircraft Technology*, M. C. Kuşhan, Ed. InTech, 2018. doi: 10.5772/intechopen.75628.
[34] S. Wickramasinghe, T. Do, ve P. Tran, "FDM-Based 3D Printing of Polymer and Associated Composite: A Review on Mechanical Properties, Defects and Treatments", *Polymers*, c. 12, sy 7, s. 1529, Tem. 2020, doi: 10.3390/polym12071529.
[35] A. Jaisingh Sheoran ve H. Kumar, "Fused Deposition modeling process parameters optimization and effect on mechanical properties and part quality: Review and reflection on present research", *Mater. Today Proc.*, c. 21, ss. 1659-1672, 2020, doi: 10.1016/j.matpr.2019.11.296.
[36] H. K. Dave, N. H. Patadiya, A. R. Prajapati, ve S. R. Rajpurohit, "Effect of infill pattern and infill density at varying part orientation on tensile properties of fused deposition modeling-printed poly-lactic acid part", *Proc. Inst. Mech. Eng. Part C J. Mech. Eng. Sci.*, c. 235, sy 10, ss. 1811-1827, May. 2021, doi: 10.1177/0954406219856383.
[37] I. J. Solomon, P. Sevvel, ve J. Gunasekaran, "A review on the various processing parameters in FDM", *Mater. Today Proc.*, c. 37, ss. 509-514, 2021, doi: 10.1016/j.matpr.2020.05.484.
[38] S. Rangisetty ve L. D. Peel, "The Effect of Infill Patterns and Annealing on Mechanical Properties of Additively Manufactured Thermoplastic Composites", içinde *Volume 1: Development and Characterization of Multifunctional Materials; Mechanics and Behavior of Active Materials; Bioinspired Smart Materials and Systems; Energy Harvesting; Emerging Technologies*, Snowbird, Utah, USA, Eyl. 2017, s. V001T08A017. doi: 10.1115/SMASIS2017-4011.
[39] N. Krajangsawasdi, L. G. Blok, I. Hamerton, M. L. Longana, B. K. S. Woods, ve D. S. Ivanov, "Fused Deposition Modelling of Fibre Reinforced Polymer Composites: A Parametric Review", *J. Compos. Sci.*, c. 5, sy 1, s. 29, Oca. 2021, doi: 10.3390/jcs5010029.
[40] M. T. Sepahi, H. Abusalma, V. Jovanovic, ve H. Eisazadeh, "Mechanical Properties of 3D-Printed Parts Made of Polyethylene Terephthalate Glycol", *J. Mater. Eng. Perform.*, c. 30, sy 9, ss. 6851-6861, Eyl. 2021, doi: 10.1007/s11665-021-06032-4.
[41] S. Park ve K. (Kelvin) Fu, "Polymer-based filament feedstock for additive manufacturing", *Compos. Sci. Technol.*, c. 213, s. 108876, Eyl. 2021, doi: 10.1016/j.compscitech.2021.108876.
[42] P. K. Penumakala, J. Santo, ve A. Thomas, "A critical review on the fused deposition modeling of thermoplastic polymer composites", *Compos. Part B Eng.*, c. 201, s. 108336, Kas. 2020, doi: 10.1016/j.compositesb.2020.108336.
[43] N. Singh ve G. Singh, "Advances in polymers for bio-additive manufacturing: A state of art review", *J. Manuf. Process.*, c. 72, ss. 439-457, Ara. 2021, doi: 10.1016/j.jmapro.2021.10.045.
[44] K. Szykiedans, W. Credo, ve D. Osiński, "Selected Mechanical Properties of PETG 3-D Prints", *Procedia Eng.*, c. 177, ss. 455-461, 2017, doi: 10.1016/j.proeng.2017.02.245.
[45] I. Molnár, R. Hrušecký, L. Morovič, ve A. Görög, "Observation of Shape and Dimensional Accuracy Changing of Parts in Time Intervals Manufactured by

Additive Method Fused Deposition Modeling", *Mater. Sci. Forum*, c. 919, ss. 182-189, Nis. 2018, doi: 10.4028/www.scientific.net/MSF.919.182.
[46] M. S. Srinidhi, R. Soundararajan, K. S. Satishkumar, ve S. Suresh, "Enhancing the FDM infill pattern outcomes of mechanical behavior for as-built and annealed PETG and CFPETG composites parts", *Mater. Today Proc.*, c. 45, ss. 7208-7212, 2021, doi: 10.1016/j.matpr.2021.02.417.
[47] M. M. Hanon, R. Marczis, ve L. Zsidai, "Anisotropy Evaluation of Different Raster Directions, Spatial Orientations, and Fill Percentage of 3D Printed PETG Tensile Test Specimens", *Key Eng. Mater.*, c. 821, ss. 167-173, Eyl. 2019, doi: 10.4028/www.scientific.net/KEM.821.167.
[48] S. Bhandari, R. A. Lopez-Anido, ve D. J. Gardner, "Enhancing the interlayer tensile strength of 3D printed short carbon fiber reinforced PETG and PLA composites via annealing", *Addit. Manuf.*, c. 30, s. 100922, Ara. 2019, doi: 10.1016/j.addma.2019.100922.
[49] A. Özen, B. E. Abali, C. Völlmecke, J. Gerstel, ve D. Auhl, "Exploring the Role of Manufacturing Parameters on Microstructure and Mechanical Properties in Fused Deposition Modeling (FDM) Using PETG", *Appl. Compos. Mater.*, c. 28, sy 6, ss. 1799-1828, Ara. 2021, doi: 10.1007/s10443-021-09940-9.
[50] R. Srinivasan, P. Prathap, A. Raj, S. Aswinth Kannan, ve V. Deepak, "Influence of fused deposition modeling process parameters on the mechanical properties of PETG parts", *Mater. Today Proc.*, c. 27, ss. 1877-1883, 2020, doi: 10.1016/j.matpr.2020.03.809.
[51] K. Durgashyam, M. Indra Reddy, A. Balakrishna, ve K. Satyanarayana, "Experimental investigation on mechanical properties of PETG material processed by fused deposition modeling method", *Mater. Today Proc.*, c. 18, ss. 2052-2059, 2019, doi: 10.1016/j.matpr.2019.06.082.
[52] K. Sathish Kumar, R. Soundararajan, G. Shanthosh, P. Saravanakumar, ve M. Ratteesh, "Augmenting effect of infill density and annealing on mechanical properties of PETG and CFPETG composites fabricated by FDM", *Mater. Today Proc.*, c. 45, ss. 2186-2191, 2021, doi: 10.1016/j.matpr.2020.10.078.
[53] BSI, BS EN ISO 527-2:1996. Plastics- determination of tensile properties part 2: Test conditions for moulding and extrusion plasics, BSI Group (1996).
[54] ASTM International, *Standard Test Method for Tensile Properties of Plastics*, ASTM D638, (2014).
[55] A. Miller, C. Brown, ve G. Warner, "Guidance on the Use of Existing ASTM Polymer Testing Standards for ABS Parts Fabricated Using FFF", *Smart Sustain. Manuf. Syst.*, c. 3, sy 1, s. 20190051, Ara. 2019, doi: 10.1520/SSMS20190051.
[56] C. Basgul, T. Yu, D. W. MacDonald, R. Siskey, M. Marcolongo, ve S. M. Kurtz, "Does annealing improve the interlayer adhesion and structural integrity of FFF 3D printed PEEK lumbar spinal cages?", *J. Mech. Behav. Biomed. Mater.*, c. 102, s. 103455, Şub. 2020, doi: 10.1016/j.jmbbm.2019.103455.

APPENDICES

APPENDIX A: Tensile testing specimen standards

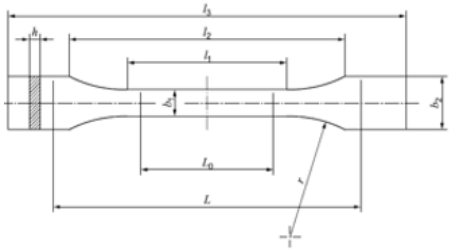

Dimensions in millimetres

	Specimen type	1A	1B
l_3	Overall length[a]	170	≥150
l_1	Length of narrow parallel-sided portion	80 ± 2	60,0 ± 0,5
r	Radius	24 ± 1	60 ± 0,5
l_2	Distance between broad parallel-sided portions [b]	109,3 ± 3,2	108 ± 1,6
b_2	Width at ends	20,0 ± 0,2	
b_1	Width at narrow portion	10,0 ± 0,2	
h	Preferred thickness	4,0 ± 0,2	
L_0	Gauge length (preferred)	75,0 ± 0,5	50,0 ± 0,5
	Gauge length (acceptable if required for quality control or when specified)	50,0 ± 0,5	
L	Initial distance between grips	115 ± 1	115 ± 1

[a] The recommended overall length of 170 mm of the type 1A is consistent with ISO 294-1 and ISO 10724-1. For some materials, the length of the tabs may need to be extended (e.g. l_3 = 200 mm) to prevent breakage or slippage in the jaws of the testing machine.

[b] $l_2 = l_1 + [4r(b_2 - b_1) - (b_2 - b_1)^2]^{1/2}$, resulting from l_1, r, b_1 and b_2, but within the indicated tolerances.

Figure A.1 : Dimensional illustrations of the specimens defined in ISO527-2 1A and 2B [ISO].

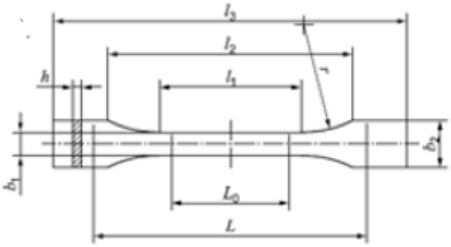

Dimensions in millimetres

	Specimen type	1BA	1BB
l_3	Overall length	≥75	≥30
l_1	Length of narrow parallel-sided portion	30,0 ± 0,5	12,0 ± 0,5
r	Radius	≥30	≥12
l_2	Distance between broad parallel-sided portions	58 ± 2	23 ± 2
b_2	Width at ends	10,0 ± 0,5	4 ± 02
b_1	Width at narrow portion	5,0 ± 0,5	2,0 ± 0,2
h	Thickness	≥2	≥2
L_0	Gauge length	25,0 ± 0,5	10,0 ± 0,2
L	Initial distance between grips	$l_2 {}^{+2}_{0}$	$l_2 {}^{+1}_{0}$

NOTE The specimen types 1BA and 1BB are proportionally scaled to type 1B with a reduction factor of 1:2 and 1:5, respectively, with the exception of thickness.

Figure A.2 : Dimensional illustrations of the specimens defined in ISO527-2 1BA and 1BB [ISO].

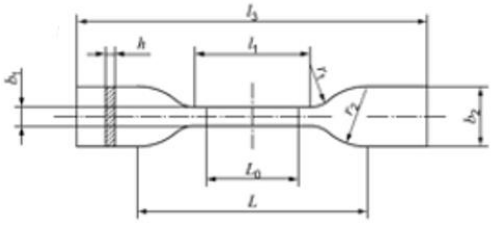

Dimensions in millimetres

	Specimen type	5A	5B
l_3	Overall length	≥75	≥35
b_2	Width at ends	12,5 ± 1	6 ± 0,5
l_1	Length of narrow parallel-sided portion	25 ± 1	12 ± 0,5
b_1	Width at narrow portion	4 ± 0,1	2 ± 0,1
r_1	Small radius	8 ± 0,5	3 ± 0,1
r_2	Large radius	12,5 ± 1	3 ± 0,1
L	Initial distance between grips	50 ± 2	20 ± 2
L_0	Gauge length	20 ± 0,5	10 ± 0,2
h	Thickness	2 ± 0,2	1 ± 0,1

NOTE The specimen types 5A and 5B are similar to type 5 of ISO 527-3 and represent types 2 and 4, respectively, of ISO 37.

Figure A.3 : Dimensional illustrations of the specimens defined in ISO527-2 1A5A and 5B [ISO].

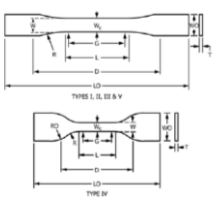

Specimen Dimensions for Thickness, *T*, mm (in.)[A]

Dimensions (see drawings)	7 (0.28) or under		Over 7 to 14 (0.28 to 0.55), incl	4 (0.16) or under		Tolerances
	Type I	Type II	Type III	Type IV[B]	Type V[C,D]	
W—Width of narrow section[E,F]	13 (0.50)	6 (0.25)	19 (0.75)	6 (0.25)	3.18 (0.125)	±0.5 (±0.02)[B,C]
L—Length of narrow section	57 (2.25)	57 (2.25)	57 (2.25)	33 (1.30)	9.53 (0.375)	±0.5 (±0.02)[C]
WO—Width overall, min[G]	19 (0.75)	19 (0.75)	29 (1.13)	19 (0.75)	...	+ 6.4 (+ 0.25)
WO—Width overall, min[G]	...	...	...	...	9.53 (0.375)	+ 3.18 (+ 0.125)
LO—Length overall, min[H]	165 (6.5)	183 (7.2)	246 (9.7)	115 (4.5)	63.5 (2.5)	no max (no max)
G—Gage length[I]	50 (2.00)	50 (2.00)	50 (2.00)	...	7.62 (0.300)	±0.25 (±0.010)[C]
G—Gage length[I]	...	...	...	25 (1.00)	...	±0.13 (±0.005)
D—Distance between grips	115 (4.5)	135 (5.3)	115 (4.5)	65 (2.5)[J]	25.4 (1.0)	±5 (±0.2)
R—Radius of fillet	76 (3.00)	76 (3.00)	76 (3.00)	14 (0.56)	12.7 (0.5)	±1 (±0.04)[C]
RO—Outer radius (Type IV)	...	...	...	25 (1.00)	...	±1 (±0.04)

Figure A.4 : Dimensional illustrations of the specimens defined in ASTM D638 TYPE IV.

APPENDIX B: Produced tensile testing specimens

CBA0	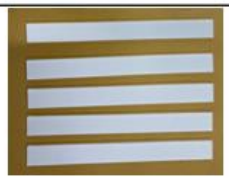	CAA0		RBA0	
CBA10	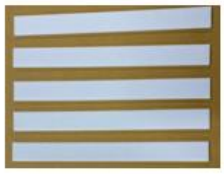	CAA10		RBA10	
CBA15		CAA15		RBA15	
CBA20		CAA20		RBA20	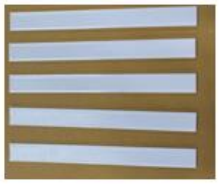

Figure B.1 : Produced tensile testing specimens (non-annealed samples).

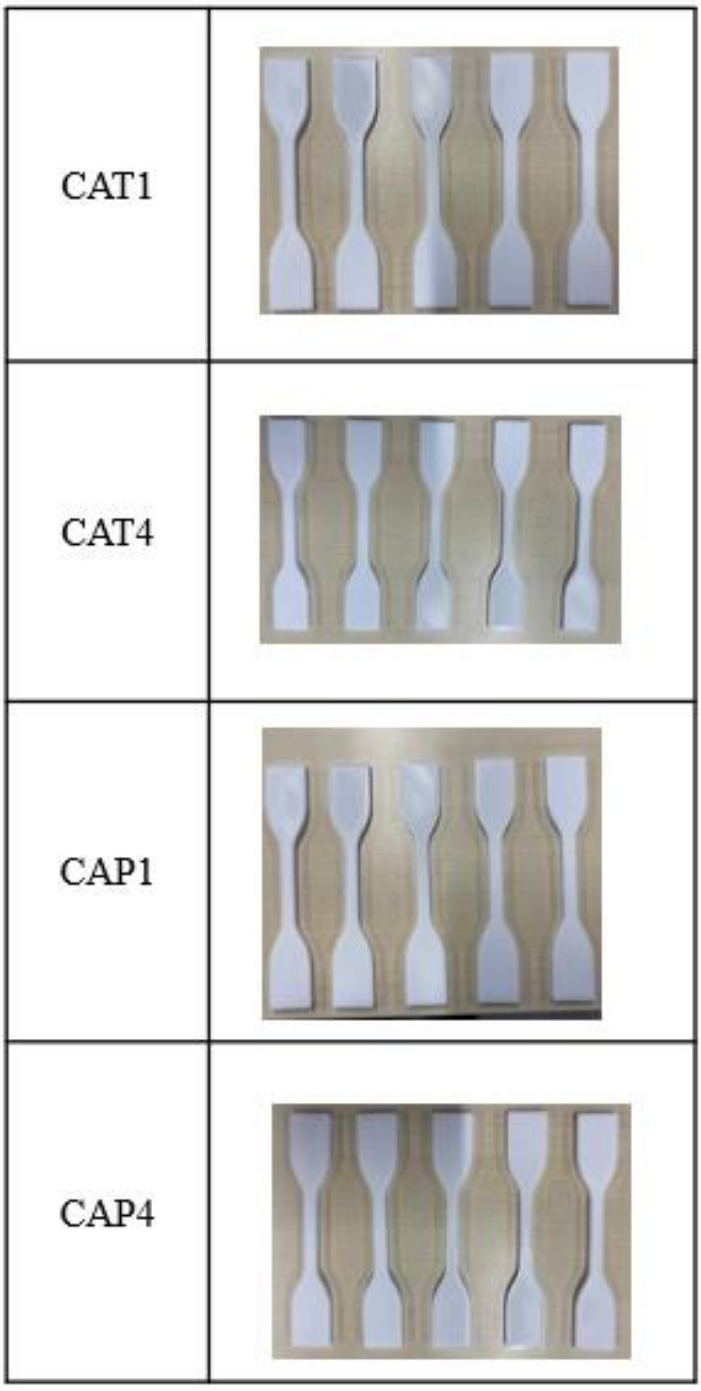

Figure B.2 : Produced tensile testing specimens (annealed samples).

APPENDIX C: Tensile testing specimens after testing

Specimen Identifications	Specimens	Fracture Locations	
CBA0		SN1	GAT
		SN2	GAT
		SN3	GAT
		SN4	GAT
		SN5	GAT
CBA10		SN1	GAT
		SN2	GAT
		SN3	LGM
		SN4	GAT
CBA15		SN1	GAT
		SN2	GAT
		SN3	GAT
		SN4	LGM
CBA20		SN1	GAT
		SN2	GAT
		SN3	GAT
		SN4	GAT
		SN5	GAT

Figure C.1 : ASTM D3039 Concentric specimens after tensile testing (non-annealed samples).

Specimen Identifications	Specimens	Fracture Locations	
CAA0		SN1	Inside Narrow Length
		SN2	Inside Narrow Length
		SN3	Inside Narrow Length
		SN4	Inside Narrow Length
CAA10		SN1	Inside Narrow Length
		SN2	Outside Narrow Length
		SN3	Inside Narrow Length
		SN4	Outside Narrow Length
CAA15		SN1	Inside Narrow Length
		SN2	Outside Narrow Length
		SN3	Outside Narrow Length
		SN4	Inside Narrow Length
CAA20		SN1	Inside Narrow Length
		SN2	Inside Narrow Length
		SN3	Inside Narrow Length
		SN4	Inside Narrow Length

Figure C.2 : ASTM D638 Type IV Concentric specimens after tensile testing (non-annealed samples).

Specimen Identifications	Specimens	Fracture Locations	
CAT1		SN1	Inside Narrow Length
		SN2	Inside Narrow Length
		SN3	Inside Narrow Length
		SN4	Inside Narrow Length
CAT4		SN1	Inside Narrow Length
		SN2	Inside Narrow Length
		SN3	Inside Narrow Length
		SN4	Inside Narrow Length
CAP1		SN1	Inside Narrow Length
		SN2	Inside Narrow Length
		SN3	Inside Narrow Length
		SN4	Inside Narrow Length
CAP4		SN1	Inside Narrow Length
		SN2	Inside Narrow Length
		SN3	Inside Narrow Length
		SN4	Inside Narrow Length

Figure C.3 : ASTM D638 Type IV Concentric specimens after tensile testing (annealed samples).

Specimen Identifications	Specimens	Fracture Locations	
RBA0		SN1	GAT
		SN2	GAT
		SN3	GAT
		SN4	GAT
		SN5	GAT
RBA10		SN1	GAT
		SN2	GAT
		SN3	GAT
		SN4	GAT
		SN5	GAT
RBA15		SN1	GAT
		SN2	GAT
		SN3	GAT
		SN4	GAT
		SN5	GAT
RBA20		SN1	AGM
		SN2	GAT
		SN3	GAT
		SN4	GAT
		SN5	GAT

Figure C.4 : ASTM D3039 Rectilinear specimens after tensile testing (non-annealed samples).

APPENDIX D: Examinations of the fracture surfaces

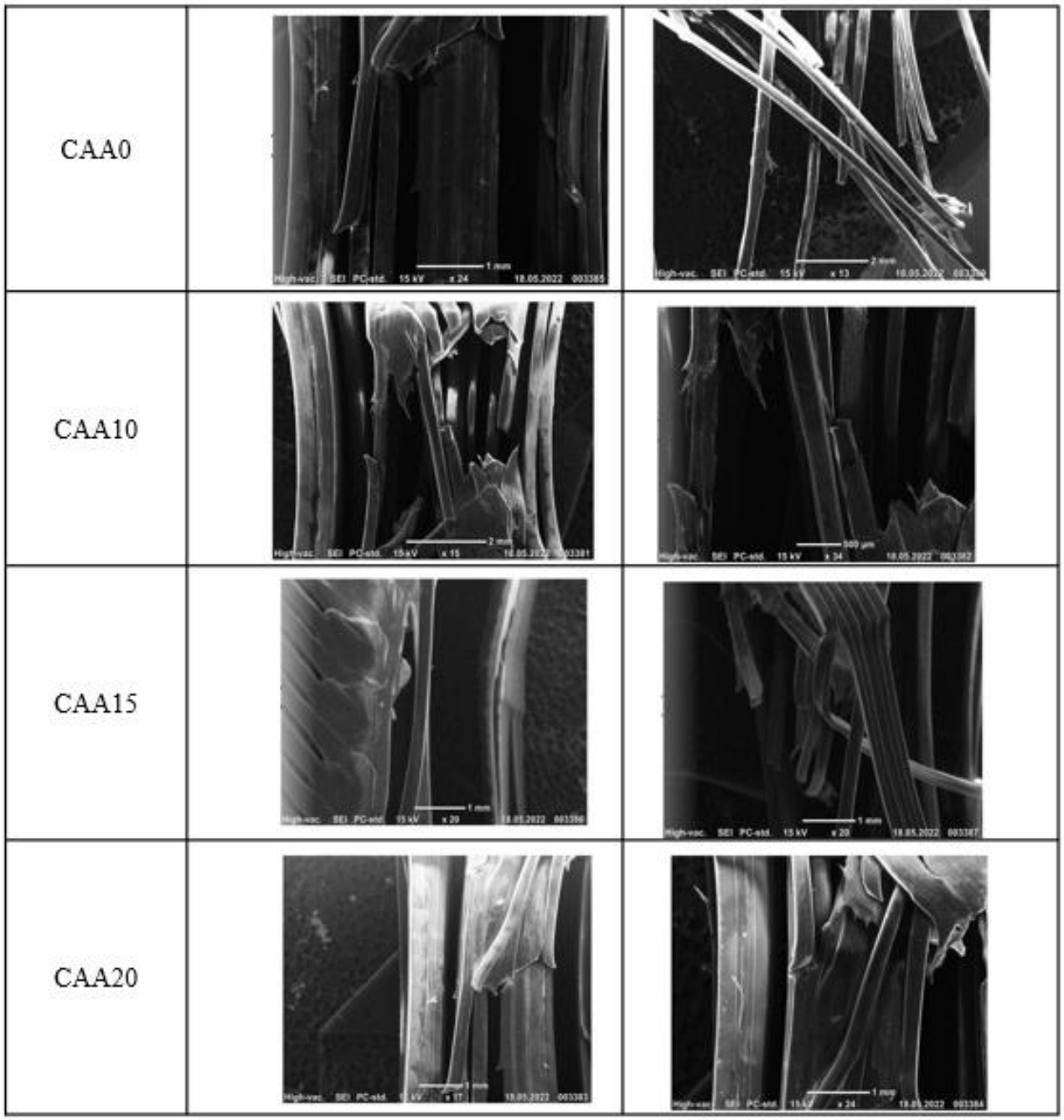

Figure D.1 : Fracture samples (concentric non-annealed samples).

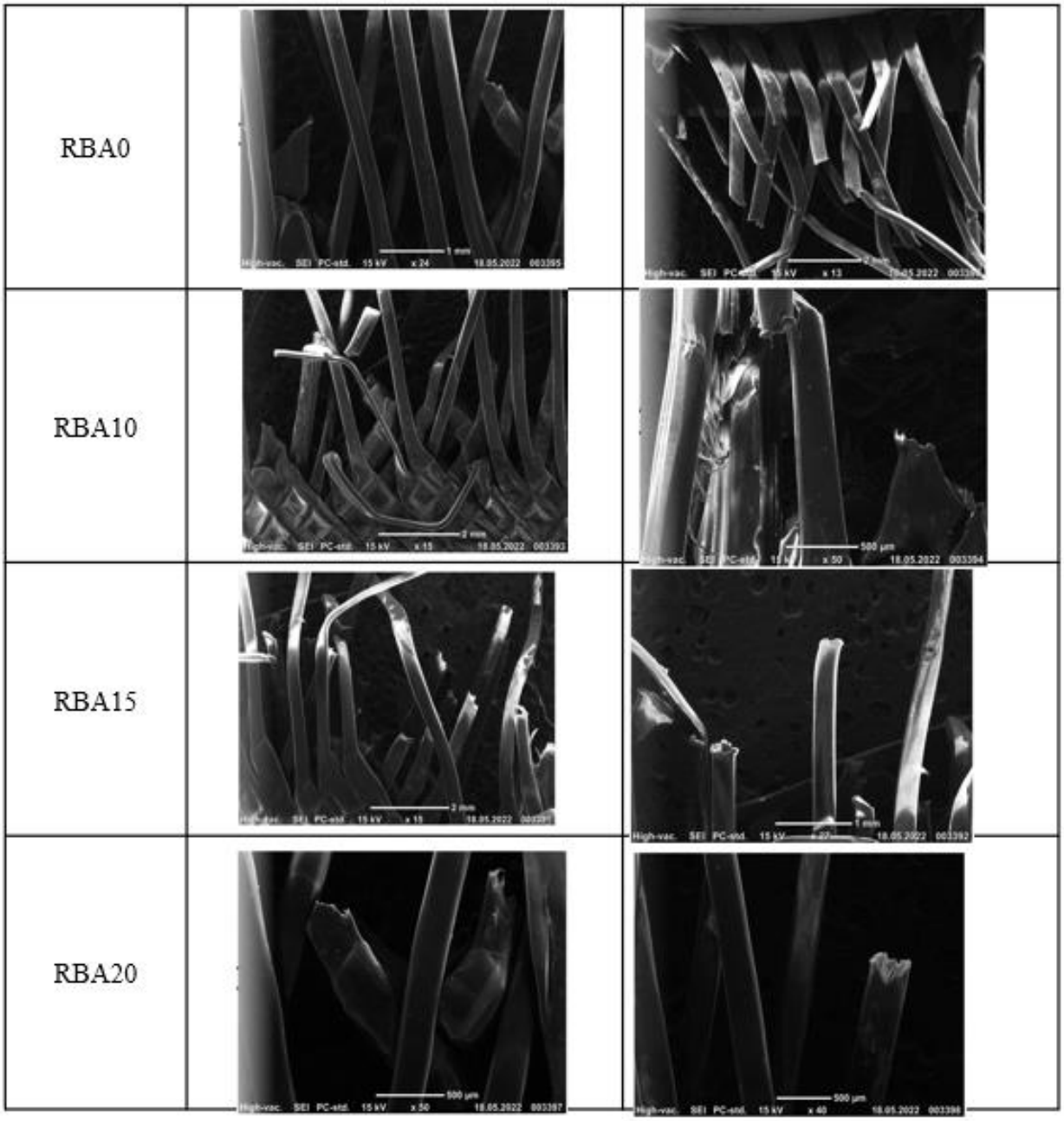

Figure D.2 : Fracture samples (rectilinear non-annealed samples).

CAT1	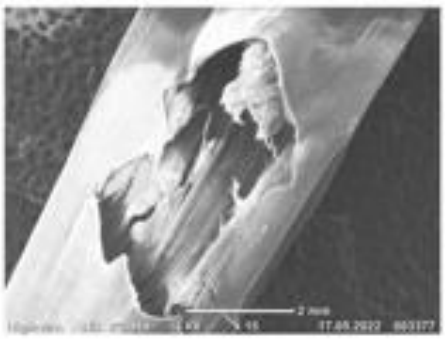
CAT4	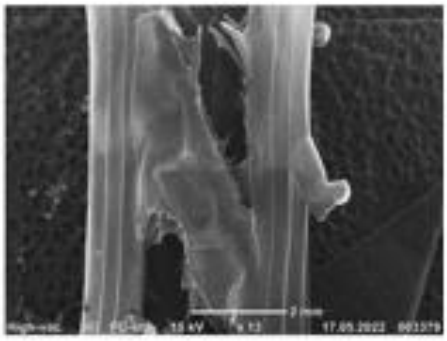
CAP1	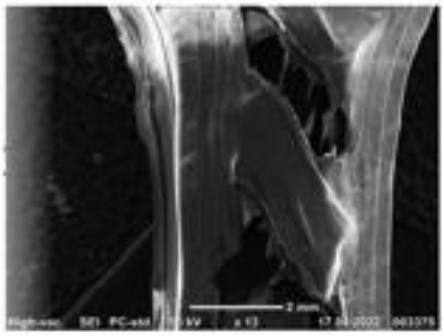
CAP4	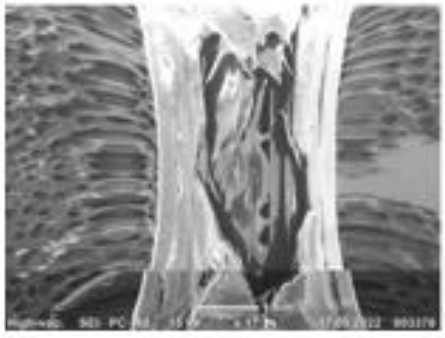

Figure D.3 : Fracture samples (concentric annealed samples).

CURRICULUM VITAE

Name- Surname : Buket PARLAK

EDUCATION:

- **B.Sc.** **:** 2015, Istanbul Technical University, Faculty of Chemical and Metallurgical Engineering, Department of Metallurgical and Materials Engineering